UNIVERSITÀ DEGLI STUDI DI PADOVA

DIPARTIMENTO DI INGEGNERIA INDUSTRIALE

CORSO DI LAUREA MAGISTRALE IN INGEGNERIA CHIMICA E DEI PROCESSI INDUSTRIALI

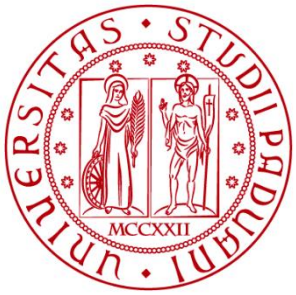

Tesi di Laurea Magistrale in Ingegneria Chimica e dei Processi Industriali

AN EXPERIMENTAL INVESTIGATION ON CO_2 METHANATION BY H_2 ON NICKEL-BASED CATALYSTS

Relatore: Prof. Paolo Canu

Laureando: DAVIDE DE FILIPPO
Matricola: 1156111

ANNO ACCADEMICO 2017-2018

Abstract

The research of the last years is mainly focused on the development of sustainable technologies that should be able to substitute all the currently adopted fossil sources.
Biogas is indeed a very attractive renewable source due to its high content in methane and it is produced via anaerobic digestion of urban waste. Unfortunately, its carbon dioxide content is too high for the biogas to be used as available and needs to be removed.

“Biogas upgrading” is a process that removes the carbon dioxide to produce biomethane, which probably will become the main competitor of natural gas in the next years. Nowadays this removal is carried out in several ways that provide for the separation of carbon dioxide through well-known techniques, such as physical or chemical absorption or water scrubbing.

This work of thesis is focused on the possibility of biogas upgrading by catalytic route: this means that the CO_2 contained in the biogas could be converted into methane by exploiting the Sabatier reaction without intermediate removal steps.

The catalytic tests were carried out from a commercial perspective, in the sense that no precious materials as catalysts and no relevant amounts of diluent were used. The process showed good performances of a commercially available nickel oxide-based catalyst and a promising prospect for a process design: in fact, sustainable biomethane could be produced by using renewable resources and a membrane separation to recycle the unreacted material.

Table of Contents

List of Figures

List of Tables

Introduction

Scopes and Goals

The European Commission, meeting in 2015 in the COP21 conference, proposed to increase the share of energy produced from renewable sources to 20% and to reduce greenhouse gas emissions by 20% by 2020 [1], [2]. It is also expected that the restrictions imposed by future COPs increase with the aim of reducing global warming: in fact, it is estimated that a major part of renewable energy will be met by bioenergy in Europe [3].
Therefore, solar and wind energy are supposed to play a fundamental role in achieving this goal, as is the search for new technologies able to make the most of resources from solid urban waste and waste from agriculture or livestock breeding.

One of the most discussed and promising technologies that use renewable resources is the exploitation of biogas. The term *biogas* indicates a mixture of various types of gas, mainly composed of methane, produced by bacterial anaerobic fermentation of organic waste from vegetable or animal residues.
The gas thus obtained is characterized by a high content of carbon dioxide and trace components such as siloxanes, hydrocarbons, ammonia, oxygen and hydrogen sulphide, which do not allow downstream uses of biogas without a preliminary purification and enhancement treatment.

Currently several techniques are used to upgrade biogas to a valuable form and differ from one another on the use of downstream flow. Some of them involve the direct use of purified biogas but are not suitable for industrial use, others include an enhancement step and all of these, in a way, provide for the *removal of carbon dioxide*.

The purpose of this work is to evaluate the possibility of upgrading biogas to biomethane by catalytic conversion of the carbon dioxide, without separating it from the biogas stream: this could allow not to use any solvent, membrane or PSA section and then have a huge impact on the global efficiency of the upgrading process. Moreover, the hydrogen necessary to produce CH_4 by methanation of CO_2 could be obtained *in situ* by electrolysis of water that exploits wind or solar energy, making the process even more sustainable.

Thesis Structure

This thesis work consists of several parts. During the first period some scientific articles were read, so that a review could be made on the biogas state of the art: this phase was fundamental to gather valuable information about the catalyst to be used. In particular, the bibliographic research shows that, to date, the possibility of biogas upgrading by catalytic route is still very little considered; moreover, many studies on this theme base their experiments on precious metals as catalysts – which make the process unattractive from an economic point of view – and under unrealistic process conditions (i.e. with a methane-free reagent mixture, even if methane is the main constituent of biogas). A summary of the current biogas exploitation routes is reported in the first chapter.

Once identified the process to be carried out, an analysis on its thermodynamic aspects was done from a realistic perspective, which means considering the real composition of biogas, and it is reported in Chapter 2.

Thanks to the precious help of the other researchers who were in the laboratory, in the following period the plant scheme was defined and implemented, then the kinds of tests to be carried out and the catalysts to be used were defined; moreover, all the parts of the plant and the methods for calculating the parameters of interest were studied and set up. In Chapter 3 the experimental setup is reported, as well as the experimental procedures and the methods used for the processing of the experimental data.

Finally, in the last chapter all the results are reported and discussed in detail: the steady state condition of the process, its dynamic behaviour, its response to lack in reagents, as well as its dependence on the quantity of catalyst and the comparison between catalysts activities.

Chapter 1

Biogas: use and upgrading

The global energy demand is rapidly growing and some research [4] showed that it will double or even triple during the current century. Furthermore, about 88% of this demand is currently met by fossil sources: this leads to high fossil fuels-derived CO_2 emissions, which are the most contributing factor to the phenomenon of global warming.
With the aim of reducing emissions below the limits imposed by the UNFCCC COPs, research is moving towards the development of high-efficiency technologies that take full advantage from renewable sources and make the energy supply safer, because most of the fossil reserves are located in regions with an unstable political situation.
With this background, *biogas* reveals a huge potential: it is produced by anaerobic digestion of organic waste and residues coming from agriculture and livestock breeding and this makes it a promising renewable source.
A great advantage of producing biogas is its high versatility since it could be used in heat and power generation, reformed to syngas (and then used for hydrogen synthesis or many other applications) or *upgraded to biomethane,* which can replace natural gas and traditional fossil fuels.

1.1 Biogas: typical composition and trace components to be purified

Methane and carbon dioxide are the main constituents of biogas [5], but it also contains some undesirable compounds such as hydrogen sulfide (H_2S), ammonia (NH_3) and siloxanes; other trace components are nitrogen (N_2), water vapor (H_2O), carbon monoxide (CO), oxygen (O_2) and hydrogen (H_2). The existence of these components and their quantities depend on the way the biogas has been produced and on the raw materials that have been used in the production process [6]. Biogas is mainly obtained by rice paddies [7], agricultural residues, municipal solid waste (MSW) [8], domestic garbage landfills [9].
Typical compositions of biogas, depending on various feedstock, are reported in **Table 1.1** [10], [11].

Table 1.1 *Biogas composition based on different feedstock*

Component	**Unit**	**POME biogas**	**Sewage Plant**	**Landfill**
CH_4	Vol%	60-70	55-65	45-55
CO_2	Vol%	30-40	35-45	30-40
N_2	Vol%	<1	<1	5-15
H_2S	ppm	10-2000	10-40	50-300
NH_3	ppm		0-100	0-5
VOC	mg m^{-3}		0-200	0-4500
Halog. HC	ppm Cl^-/F^-			20-200
Siloxanes	mg Si m^{-3}		0-40	0-50

a) POME biogas: Biogas released from palm oil mill effluent

Contaminants have great effects on the processes that use biogas [6]:

- In addition to the strong poisoning capacity of most of the commonly used catalysts, H_2S converts to SO_x and H_2SO_4 which are highly toxic and corrosive. Its concentration in biogas is variable among an interval of 10-10000ppm;
- NH_3 is toxic and corrosive. However, its combustion produces little quantities of NO_x and for this reason it is not considered as dangerous as is H_2S;
- Siloxanes are silicon-containing compounds (volatile methyl siloxanes –VMSs) and can be produced by polydimethylsiloxane (PDMS) [12] that is widely used in industrial applications and released into the environment; their concentration thus depends on the biogas source [13] (the presence of siloxanes is a problem when using biogas from landfill gases). When biogas is combusted, siloxanes can oxidize to SiO_2 and form crystalline deposits that are difficult to remove;
- Traces of water vapor may condensate in gas pipelines, engines, compressors or storage tanks and involve corrosion phenomena.

Therefore purification processes turn out to be a necessary step before any of the processes that use biogas and will not be further described in detail in this work, since they have already been widely studied [6], [14],[15].

1.2 Biogas exploitation routes

Once purification has been carried out, biogas can be used in many ways (**Figure 1.1**): as written before, some of them do not need any other particular treatment and others involve further intermediate processes.

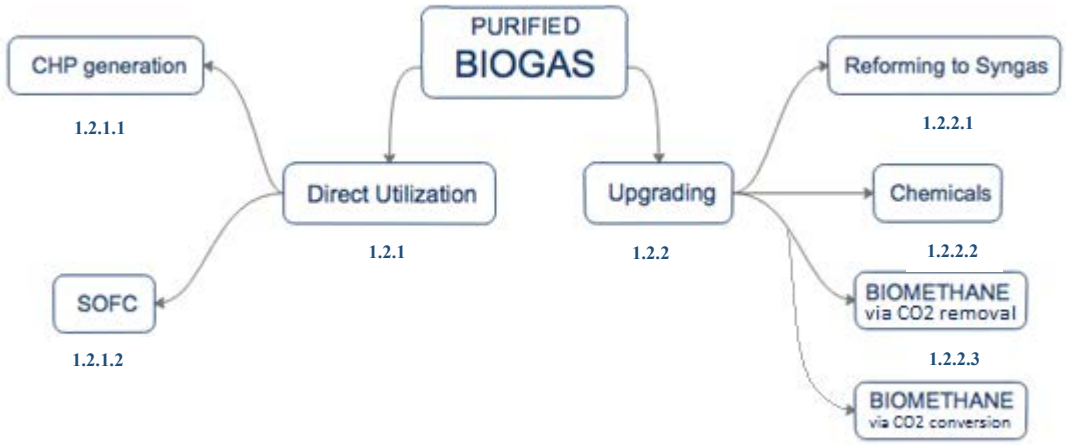

Figure 1.1 *Scheme of biogas utilization*

1.2.1 Direct utilizations of Biogas

1.2.1.1 Combined heat and power generation

Biogas can be exploited for both power and heat generation processes due to the high concentration of methane. Unfortunately, the presence of large amounts of CO_2 - and some other noncombustible trace components such as H_2O - decreases the calorific value of the biogas, which is indeed a barrier in such applications: in fact, the average calorific value of biogas is much lower than the one of natural gas (21 vs. 36 MJ/m^3, respectively)[10]. For this reason, some technologies have been already analysed to make the combustion more efficient. Upgrading technologies such as water scrubbing, cryogenic, chemical absorption and membranes processes are not economically feasible in applications of heat and power generation and are proposed for more sensitive utilizations.

Different regimes of operation have been studied for CHP (combined heat and power) generation [10]:

- Biogas conventional combustion: some analysis showed that biogas could not substitute natural gas (NG) or liquid petroleum gas (LPG) without any upgrading process or instrument changes in CHP generation system. That is due to the high concentration of CO_2 and the related issues of stability of the flame;
- Hydrogen-enriched biogas conventional combustion could of course increase the efficiency of the combustion and the stability of the flame because of the higher calorific value, anyway some pollutants (NO_x) are produced;
- Biogas flameless combustion technique turned out to be the best method for CHP generation processes and feasible even with high CO_2 concentrations. This technique requires some specific and accurate instrumentations that involve higher capital costs but at the same time are more resistant to corrosion;
- Flameless combustion of hydrogen-enriched biogas is more efficient but still problems of formation of NO_x are encountered.

1.2.1.2 Solid Oxide Fuel Cells

Some other studies have been conducted to evaluate – and then demonstrate [16], [17] – the possibility of direct feeding biogas to solid oxide fuel cells (SOFCs) to produce electricity.

Fuel cells are able to convert chemical energy of fuels – hydrogen, generally – directly into electrical energy [18]; moreover, they are able to offer higher energy efficiency and lower emissions (SO_x, NO_x, CO_2) with respect to traditional combustion engines [16]. For these reasons, energy production by biofuels has recently been considered through low temperature phosphoric acid, alkaline-based and polymer electrolyte fuel cells (PAFC, AFC, PEFC) [19]–[21]. However, any of these fuel cells needs the biogas to be hydrogen-enriched through gas processors requiring precious metals, thus resulting quite expensive.

SOFCs – so called because made of a hard ceramic material instead of a liquid electrolyte - are among the most interesting technologies of recent years because of their potential: they are less expensive than other fuel cells because of their higher tolerance to CO and resistance to impurities [17]. Their properties come from the high operating temperatures [22], [23] and provide power generation even with methane to carbon dioxide ratios with whom traditional combustion engines cannot be applicable [24].

Biogas is then a good candidate for SOFC: even with high concentrations of CO_2 it could be used for energy production instead of being harmfully wasted to the atmosphere.

If using natural gas in fuel cells, some steam is traditionally added to the gas which is then catalytically converted via steam reforming (1.1) in order to produce H_2 either externally or internally.

$$CH_4 + H_2O \leftrightarrow 3H_2 + CO \quad (1.1)$$

Some problems still exist with internal reforming, which would be preferable [17], due to loss of performances. However, some research has been done to optimise the anode formulations for internal reforming [25].
Also selective oxidation of methane (1.2) has been studied [26], but the mechanism of oxidation of methane requires higher energy and makes the process more inefficient.

$$CH_4 + \frac{1}{2}O_2 \leftrightarrow 2H_2 + CO \quad (1.2)$$

As regards the ways of the exploitation of biogas, the process that attracted much interest is dry reforming of methane (1.3) because of the inherent presence in the biogas of both the reactants, which means no addition of steam or oxygen to the biogas to produce H_2.

$$CH_4 + CO_2 \leftrightarrow 2H_2 + 2CO \quad (1.3)$$

The main drawback of direct utilization of biogas for SOFC is the variable composition of the gas stream, which of course depends on the feed stream of the production process, and the low resistance of ceramic materials to thermal shock.

1.2.2 Biogas Upgrading

As already mentioned above, some treatment steps could be necessary depending on the end use of biogas. For any application where a high energy content – which means high concentration of methane – is needed in the gas, an upgrading process has to be carried out. Therefore, each upgrading technique involve carbon dioxide *removal* to increase methane concentration.
The focus on biogas upgrading is recently rapidly growing due to an increase in traditional fuels prices [5] (**Figure 1.2**): between 2009 and 2016, the total number of biogas plants rose from 6227 to 17662, seeing Germany and Italy as the strongest countries of the industry with 10786 and 1491 plants in 2015, respectively [27].

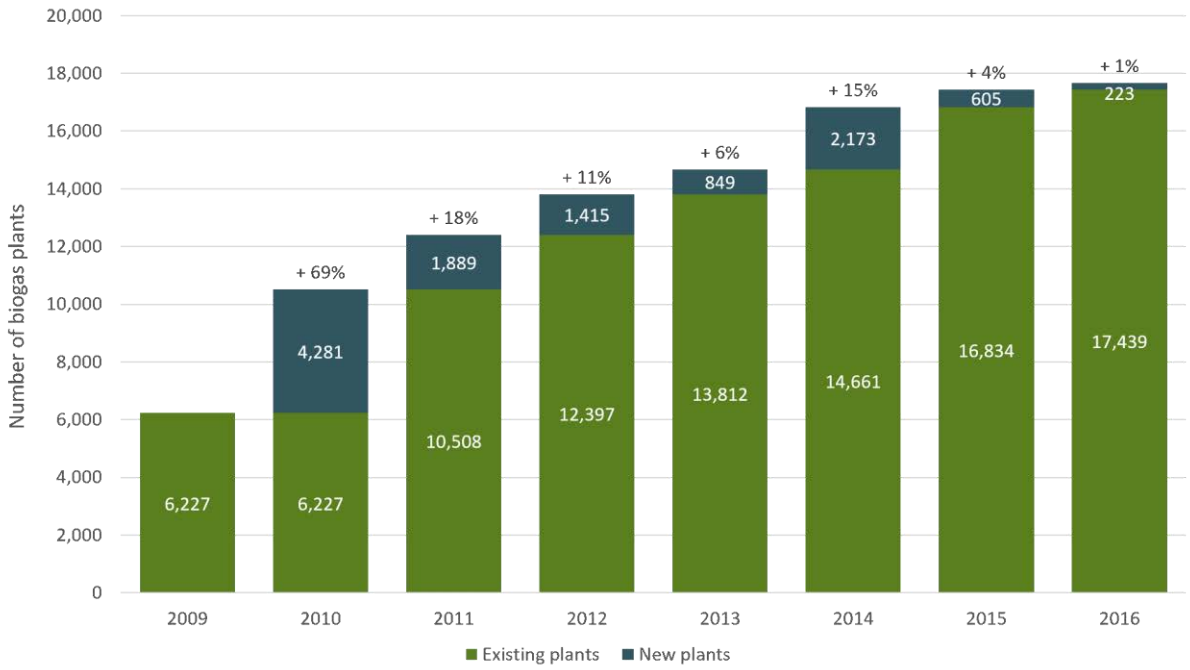

Figure 1.2 *Evolution of the number of biogas plants in Europe [EBA - European Biogas Association, 2017]*

Biogas upgrading sensitively increases the cost of the production process: it is then important to optimize the energy consumption and the methane content at the same time; a loss of methane in atmosphere, in fact, on the one hand would cause a waste of raw material and on the other would be harmful to the environment because of its GWP, that is about 20-30 times greater than that of CO_2 [28].

1.2.2.1 Steam Biogas Reforming

Traditional *steam reforming* (SR) is a process that converts any hydrocarbon into a gas mixture containing hydrogen and carbon monoxide thanks to water vapor addition (1.4).

$$C_{\mathrm{n}}\mathrm{H}_{\mathrm{m}} + \mathrm{n}H_2O \leftrightarrow \mathrm{n}CO + \left(n + \frac{m}{2}\right) H_2 \tag{1.4}$$

The mixture thus obtained is called *syngas*. It is characterized by a high energy content – depending on the hydrogen concentration – and could potentially produce any of the petrochemical industry compounds: in fact, the uses of syngas range from the production of gasolines via Fischer-Tropsch processes [29] to the feeding of fuel cells for the production of electricity. However, some secondary – and sometimes undesirable – reactions also occur and heavy hydrocarbons show more tendency to be cracked, thus causing coke formation and lower hydrogen concentration. For the latter reasons syngas is traditionally produced by steam methane reforming (SMR) (1.5) at 700°C using natural gas.

$$CH_4 + H_2O \leftrightarrow CO + 3H_2 \qquad \Delta H_r = 206.1\ \mathrm{kJ/mol} \tag{1.5}$$

As mentioned above, some other reactions occur [30]: water-gas shift (WGS) (1.6), dry reforming (DR) (1.7) and CH_4 dehydrogenation or cracking (1.8). In traditional steam reforming processes, DR is a *side* reaction because CO_2 is a product of WGS instead of being fed to the reactor.

$$CO + H_2O \leftrightarrow H_2 + CO_2 \qquad \Delta H_r = -41.2\ kJ/mol \tag{1.6}$$

$$CH_4 + CO_2 \leftrightarrow 2H_2 + 2CO \qquad \Delta H_r = 247.3\ kJ/mol \tag{1.7}$$

$$CH_4 \rightarrow 2H_2 + 2C \qquad \Delta H_r = 74.82\ kJ/mol \tag{1.8}$$

$$2CH_4 + H_2O + CO_2 \leftrightarrow 5H_2 + 3CO \qquad \Delta H_r = 453.4\ kJ/mol \tag{1.9}$$

Some research showed the possibility of feeding biogas to a Steam-Biogas-Reforming (SBR) (1.9) reactor to directly exploit the presence of both CH_4 and CO_2 on Ni [31] or Pd-Rh [32] based catalysts with positive results, thus demonstrating that hydrogen could be produced at high operating temperatures from biogas and fed to SOFC for electricity generation [33].

Other analysis [34], [35] showed that if O_2 is fed to reactor with biogas some performance enhancement could be achieved due to the Partial-Oxidation reforming (POR) (1.10), complete combustion of CH_4 (1.11), carbon oxidation (1.12) and hydrogen oxidation (1.13); moreover, all the latter reactions are exothermic and may compensate the energy consumption required by (1.7) [36], [37] and for this reason the process that combines DR and POR is known as auto-thermal reforming (ATR).

$$CH_4 + 0.5\,O_2 \rightarrow CO + 2H_2 \qquad \Delta H_r = -36\ kJ/mol \qquad (1.10)$$

$$CH_4 + 2O_2 \rightarrow CO_2 + 2H_2O \qquad \Delta H_r = -890\ kJ/mol \qquad (1.11)$$

$$C + 0.5\,O_2 \rightarrow CO_2 \qquad \Delta H_r = -110\ kJ/mol \qquad (1.12)$$

$$H_2 + 0.5\,O_2 \rightarrow H_2O \qquad \Delta H_r = -285.8\ kJ/mol \qquad (1.13)$$

However, the effects of small quantities of O_2 in the biogas are still unknown [37].
These studies also highlight the advantages that come from integrating DR (1.7), POR (1.10) and SBR (1.9) processes into one known as *trireforming* (800-900°C) [38]:

- Energy integration;
- Less water vapor required;
- Carbon black formation is hindered;
- Changing process parameters to adjust H_2/CO ratio;
- Lower CO_2 emissions.

1.2.2.2 Direct production of chemicals

Upgrading to syngas is nowadays one of the most investigated ways of exploitation of biogas, since it can be converted into formaldehyde, methanol or higher hydrocarbons; therefore, ethylene and propylene – which are the most important building blocks of chemical industry – can be produced via methanol conversion.
The huge potential of biogas is also linked to its content in components that could – theoretically – be directly converted into valuable products, thus avoiding the necessity of syngas production step and increasing the process efficiency. However, while the bond C-H is very stable the products are reactive compounds: some research on direct production of chemicals from biogas is still being carried out to bring such application at industrial scale.

Some examples are reported below:

- *Oxidative coupling of methane (OCM)* is a process that produces C_2 hydrocarbons (1.14):

$$2CH_4 + O_2 \rightarrow C_2H_4 + 2H_2O \qquad (1.14)$$

  Since 1980 a lot of studies have been conducted to evaluate the activities of different catalysts such as Li/MgO, $Mn/Na_2WO_4/SiO_2$, La_2O_3 and Fe_2O_3 [39]–[42], but they showed significantly lower performance with respect to a traditional ethane to ethylene steam cracking (yields equal to 30 and 70/80%, respectively). High temperatures (700°C) are required in order to activate some methane conversion if the currently known catalysts are used; moreover, oxidation of methane to CO and CO_2 occurs and their removal adds further costs to the process.
- *Methane dehydroaromatization (MDA)* gained a lot of attention among researchers: its high potential is linked to the possibility of converting methane to benzene. Since petroleum reserves are running out and methane is widely available in natural gas and biogas, this process is very promising for future applications and could be one of the most useful processes of the green industry. Nowadays Mo-Zeolites are used as catalysts, whose deactivation is believed to be due to carbon deposition [43]–[45]. Because of the zeolites sensibility and ease of deactivation, as well as the high temperatures required for the methane to be activated, this process is still under investigation in order to be adapted to industrial scale.
- *Direct conversion of methane to methanol (DMTM)* is a powerful process (1.15) that could substitute methanol production via syngas.

$$CH_4 + 1/2O_2 \rightarrow CH_3OH \qquad \Delta H_{298} = -30.4\ kJ/mol \qquad (1.15)$$

  The reaction of steam methane reforming to syngas (1.5) is highly endothermic and then very expensive to be carried out in terms of energy consumption; therefore, a process that exploits a widely available source, such as the methane in natural gas and biogas, in a more efficient way would be really important for chemical industry.

Several techniques have already been discussed: heterogeneous or homogeneous catalysis in gas phase, bio catalysis, plasma, photocatalysis [46]–[50]. However, none of these processes is still industrially feasible: in fact, the best compromise between methane conversion and selectivity for methanol is obtained at very low conversions (**Figure 1.3**, [51]).

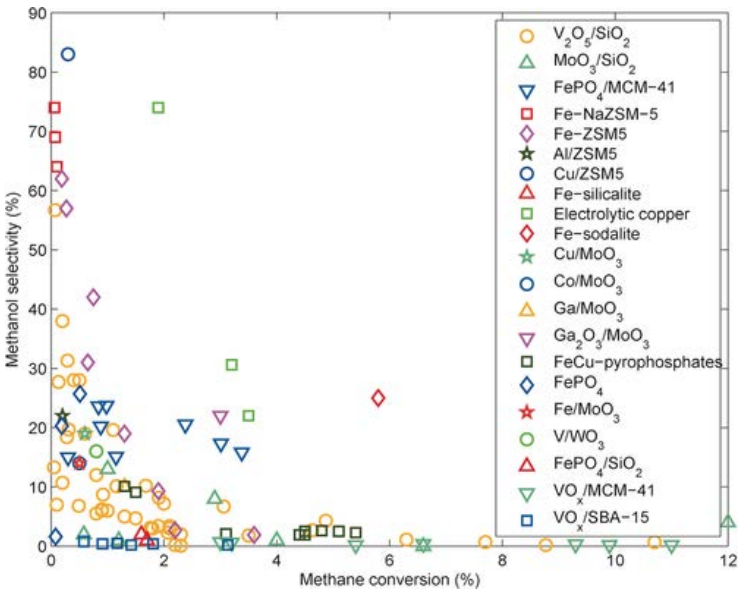

Figure 1.3 *Methanol selectivity vs. methane conversion with different catalysts*

1.2.2.3 Biomethane

Due to its high concentration in methane, biogas represents a promising renewable source which could be used for injection into natural gas grids (SNG, *substitute natural gas*) and as a vehicle fuel (CNG, *compressed natural gas*).

However, more stringent quality specifications are required with respect to those for other applications (e.g. removal of only H_2S for heat generation; H_2S, water, ammonia, siloxanes and halocarbons for CHP generation): often, CH_4 concentrations >90%vol. are necessary [11].

To reach such high methane content, the separation of CO_2 from biogas is a crucial operation and nowadays it is mainly carried out through unit operations like absorption and permeation [52].

CO_2 removal

CO_2 removal from biogas at industrial scale is currently performed via several physical or chemical technologies, depending on the costs that are related to their local availability. Biotechnologies, on the other hand, have only been validated at pilot scale but would allow bioconversion of CO_2 to more valuable products [11].

The most common process technologies are discussed below [3], [11], [52] and summarised in **Table 1.*2*** [3]:

- *Water scrubbing* is a process of physical absorption that use water as solvent for dissolving CO_2. The driving force is the difference between solubilities in water, since the one of carbon dioxide is much higher (26 times at 25°C, [53]) than the one of methane.

  It is a mature and well-known process which is considered to be the less sensitive to impurities in biogas: in fact, about 40% of biogas upgrading plants adopt this technique. The operation is carried out in a counter-current configuration at operating pressures that range from 6 to 20 bar [54], [55].

  Biogas enters at the bottom of a packed absorption column and CO_2 is absorbed in water, which flows down from the top and can be regenerated in a desorption unit (or not, if water has a negligible cost). Purified biogas (i.e. biomethane) leaves the column at the top and can have a concentration in methane up to 99%vol. If higher purity is required, water is not able to absorb non-condensable gas such as N_2 or O_2 that often are in biogas. Moreover, some CH_4 losses occur due to dissolution in water and their typical value ranges from 3% to 5%.

  The high energy consumption is mainly related to raw gas compression and water processing, but this technique is widely used since it also enables simultaneous H_2S removal, thus making pre-treatment unnecessary.
- *Physical absorption* is a technique similar to water scrubbing. Water is substituted with organic solvents – i.e. dimethyl ethers of polyethylene glycol, DMPEG [56] – because they exhibit higher affinity for CO_2 and for this reason the process can be intensified (which means same yield through smaller equipment and lower capital costs, or higher productivity with the same investment). Unlike water scrubbing, removal of H_2S is necessary since it makes the regeneration of the solvent and the CO_2 absorption more difficult. Moreover, inability in absorbing non-condensable species still exists. Regeneration step requires higher energy consumption than water scrubbing, since it is carried out at higher temperatures. The operating pressure is between 6 and 8 bar and the yield of methane is similar to water scrubbing.
- *Chemical absorption* is still similar to the previous techniques, but it involves chemical reactions between absorbed substances and solvents: therefore the bonds between molecules are much stronger than those formed during physical absorption; moreover,

the solvent can be chosen properly to selectively react – i.e. absorb – with CO_2. Alcanol amines (monoethanolamine, diethanolamine) or alkali aqueous solutions (NaOH, KOH) are widely used.

The entire absorption process is intensified due to better mass transport: consequently, smaller equipment and lower pressures are required to maintain the same yield of physical absorption and water scrubbing. For these reasons, chemical absorption is often a good choice if concentration of CO_2 is quite low and a difficult separation has to be carried out.

Very high recovery (even 99.9%) and yield (about 90%) of methane can be achieved using a counter-current configuration and quite low operating pressures, but H_2S removal is strongly recommended to avoid amine poisoning.

However, the fact that the chemical reaction is able to build strong bonds with CO_2 is the main drawback too of this technique due to the high energy demand related to regeneration step.

- *Cryogenic separation* would allow to recover high quality-liquid methane from biogas through several steps due to difference in boiling points and solidification temperatures of its constituents. The process is carried out at constant pressure (10 bar). First of all H_2O, H_2S and siloxanes can be separated at -25°C because of their higher boiling points. In the following distillation unit CH4 and CO_2 are separated by condensing most of the CO_2 at -55°C; traces of CO_2 in methane can be removed through solidification at -85°C. A further decrease in temperature between -162°C and -182°C cause methane liquefaction and separation from O_2 and N_2.

  Obviously, even if this technique has great advantages such as no pre-treatment necessity and pure liquid methane production, the great drawback is the high energy demand linked to very low temperatures. For this reason, nowadays only few plants in USA, Sweden and Netherlands use cryogenic separation.

- *Pressure Swing Adsorption* (PSA) is based on the mechanism that different molecules are selectively absorbed on a porous material depending on their dimensions. Since CH_4 is the bigger molecule in biogas, a proper material that is able to absorb all the smaller molecules is chosen; zeolites and activated carbon are widely employed. Also temperature and pressure can be varied in order to optimise the efficiency of the absorption process: in the case of PSA temperature is kept constant and pressure varied. A PSA process conventionally consists of a series of absorption columns in which absorbent material is packed and pressure cyclically changed from 4 to 10 bar. Each cycle includes some basic steps in which CO_2 is first retained and then released to the atmosphere: pressurization, absorption, depressurization, regeneration. Some techniques have already been employed to speed up each pressure cycle and intensify the process. The enriched-biomethane stream typically has a CH_4 concentration between 96 and 98%;

however, increasing purity of biomethane means higher losses of CH_4 (even 10%) making the CO_2-rich stream non-releasable to the atmosphere without any further treatment. Moreover, a pre-treatment of the biogas to remove H_2S is necessary because it can be permanently absorbed on zeolites.

- *Membrane separation* is another process that works at molecular scale. A semi-permeable membrane is used: each component has a different permeability due to molecular properties (diffusivity and absorption), thus resulting in different fluxes through the membrane. The biogas is split into two streams: CO_2 and H_2S pass through the membrane while CH_4 is retained; the streams are called *permeate* and *retentate,* respectively. A higher number of CH_4 molecules may pass through the membrane if higher purity of retentate is required: therefore, large losses of CH_4 may be involved. This technology attracted much attention thanks to ease of process and energy efficiency: in fact, lot of studies have been conducted to evaluate the performance of different materials [57], [58]; polyimide and cellulose acetate-based membranes turned out to be commercially suitable for upgrading processes. Purity of methane can reach 98% and very high recovery can be obtained if a multi-stage process is adopted.

Table 1.2 *Technical features of different upgrading technologies*

Technology	CH_4 (vol%)	CH_4 loss	Impurities (%)	Removal of O_2/N_2	Separated CO_2 (%)
Water scrubbing	96-99		CO_2 (0.5-3), O_2+N_2 (0.5-1)	No	NA
	96-98	>2	O_2 (0-0.7)	No	NA
Water scrubbing + regeneration	93-98	-	CO_2 (2-5), O_2+N_2 (0-2.5)	No	-
	97	>2	-	No	-
	98	1	-	No	-
	Up to 98	1	CO_2 (0.5-1.5)	No	CO_2 (80-90)
	98	6	-	No	-
	95-99	2	-	No	-
	96-98	1-2	-	No	-
	97-98	-	CO_2 (2-3)	No	-
Cryogenic Separation	>97	-	CO_2 (<3)	Possible	-
	98	0.65	-	Possible	-
	91	1	CO_2 (<1), N_2 (8)	Possible	CO_2 (98) + CH_4 (0.6)
	98	<0.5	-	Possible	-
	>99	-	-	Possible	-
Physical Absorption	95-98	-	CO_2 (2-5)	No	-
	97	4	-	No	-
	93-97	<2	-	No	-
	99	2-4	-	No	-
	95-99	4	-	No	-
	-	8-13	-	No	-
Chemical Absorption	-	8-10	-	No	-
	99	<1	-	No	-
	98	10	-	No	-
	97.5-99.5	<0.1	-	No	-
	>99	<0.1	-	No	-
	97-99	4-5	CO_2 (0-1)	No	CO_2 (92-93) + CH_4 (5-6)
Pressure Swing Absorption	95-98	-	CO_2 (1-4)	Possible	-
	97.5	3.5	-	Possible	-
	-	2-12	-	Possible	-
	98	9	-	Possible	-
	83-99	2-4	-	Possible	-
Membrane Separation	85	13.5	-	Possible	-
	78	10.5	-	Possible	-
	91-98	1-15	CO_2 (2-9)	Possible	-
	90-98	2	-	Possible	-

NA = not applicable.

CO_2 conversion to CH_4: the Sabatier reaction

All the techniques that have been discussed provide for the removal of contaminants. Some of them have already been developed and are widely used nowadays. However, the removal of CO_2 in any case involves some technical issues and safety problems such as solvents utilization, high operating pressures or very low temperatures; moreover, CO_2 may need some other treatments before being released to the atmosphere without any further useful exploitation.

A promising way of biogas exploitation would be the direct conversion of CO_2 into CH_4 to avoid any separation step while maximizing the methane production at the same time; as mentioned before, some biotechnologies have been evaluated for this purpose but still not validated at industrial scale.

With the aim of producing biomethane through biogas conversion, the Sabatier reaction gains much attention. As originally reported by Sabatier in 1902, it is an exothermic catalytic reaction of hydrogenation of CO_2 [59]:

$$CO_2 + 4\mathrm{H}_2 \leftrightarrow CH_4 + 2H_2O \qquad \Delta H_r = -167\ \mathrm{kJ/mol} \qquad (1.16)$$

Some studies have already been conducted to evaluate both the activity and the selectivity of several catalysts [60]. Ruthenium is known to be the most active catalyst for methanation of CO and CO_2 but its cost does not allow its use in commercial applications; nickel, instead, turned out to be the most selective methanation catalyst and still has a high activity: for these reasons, nickel-based catalysts are the most widely used in commercial applications of methanation.

Another key concept from a process design point of view is the reactor design: two-phase (gas/solid: fixed-bed, fluidized-bed, structured reactors) and three-phase (gas/liquid/solid: fluidized bed, slurry reactors) reactors have already been developed. The most interesting are reported above:

- Adiabatic fixed-bed methanation: Air Liquide, Haldor Topsoe and Johnson Matthey adopt a series of (2 - 4) fixed-bed reactors with intermediate cooling and gas recycling. Clariant and Foster Wheeler adopt three fixed-bed reactors with steam addition for temperature control. Some other concepts were proposed but never adopted: for example, ICI proposed several fixed-bed reactors in series with intermediate cooling with steam, RMP suggested a reactor concept with 4-7 adiabatic fixed-bed reactor in series with intermediate gas coolers;
- Cooled fixed-bed methanation: Linde process consisted of a cooled reactor with an integrated heat exchanger followed by a second adiabatic reactor. To control conversion and heating rate, the reacting gas mixture was added between the reactors. However, this reactor concept didn't found commercial applicability;
- Fluidized-bed two phase methanation: Bi-Gas-Process of Bituminous Coal Research Inc. and Thyssengas developed fluidized-bed reactors with internal heat exchangers for gas cooling but no industrial scale plants adopted this concept;

- Liquid-Phase Methanation (LPM) concept was developed for three-phase methanation by Chem Systems Inc. It adopted a single high pressure (70 bar) reactor in which the catalyst was suspended in an inert mineral oil that provided for simple heat removal and temperature control. Only a pilot plant was built.

Nowadays, the most commercially available reactor concepts adopt a fixed-bed configuration.
If (1.16) is exploited for biogas upgrading, an interesting and sustainable process could be designed: the hydrogen could be produced via electrolysis of water while the electricity that is required could be provided by wind or solar energy; moreover, the water to be electrolyzed is at the same time produced by the (1.16). A schematic representation of the process is reported in **Figure 1.4**.
Looking at the process globally and from a life cycle point of view, it is clear that CO_2 emissions are equal to those related to other technologies (if only a mass balance of biogas components is considered); however, producing more CH_4 in a renewable and sustainable way means increasing the efficiency of biogas upgrading.
Therefore, the focus of this work is on this possibility of catalytic biogas upgrading and it will be better discussed in the following chapters.

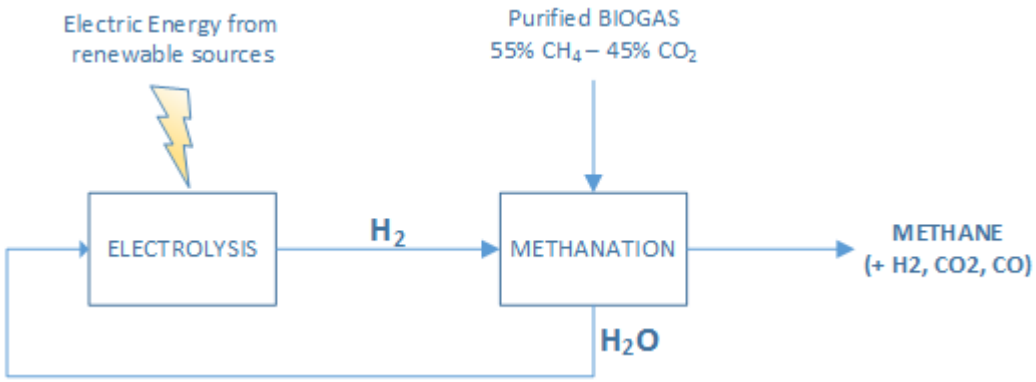

Figure 1.4 *A schematic representation of the methanation process*

Chapter 2

Thermodynamics of biogas methanation

Before undertaking the experimental tests it is useful to investigate the behavior of the system at the equilibrium condition, so as to make possible a comparison with the experimental data.
The Sabatier reaction (1.16) is exothermic and causes a decrease in the number of moles: for these reasons, the equilibrium is expected to be pushed towards the products (i.e. methane) at low temperatures and high pressures. Obviously, the composition of the gas mixture influences the equilibrium condition too: in accordance with the purpose of this work, a typical biogas composition was chosen (CH_4/CO_2 = 55% / 45% = 1.22) and a methanation stoichiometric H_2-to-CO_2 ratio was supposed.
Each calculation was implemented using *Cantera* on MATLAB®. The program allows to define a gas mixture and considers the GRI-Mech 3.0 reaction database (available on http://www.me.berkeley.edu/gri_mech/) in order to calculate the equilibrium composition. The mechanism is widely used for natural gas combustion and includes 53 species and 325 reactions: even if much less species need to be considered in this work, the accurate mechanism allows not to accidentally omit some species. The GRI-Mech thermochemistry is based upon standard databases, including the NASA-Lewis and Technion archives.
The composition of the mixture at the equilibrium condition was rearranged by removing the fraction of water, according to the experimental tests that are reported in the following chapters. The results shows that the process could be very interesting if a proper catalyst would be adopted, because of the high production of methane even at low pressures.

2.1 Effects of temperature

Figure 2.1 shows the effect of temperature on the equilibrium of the Sabatier reaction at atmospheric pressure. Since the reaction is exothermic, increasing temperature means decreasing the production of methane and consequently its molar fraction; for the same reason, an increase in the molar fraction of hydrogen and CO_2 can be observed. If the temperature is too high (500°C-700°C), CO is produced instead of CH_4: these results suggest that a catalyst that is active at low temperatures is needed. Finally, the process shows a promising behavior since the molar fraction of methane is pretty high: in fact, it is always higher than 0.5 at temperatures lower than 500°C.

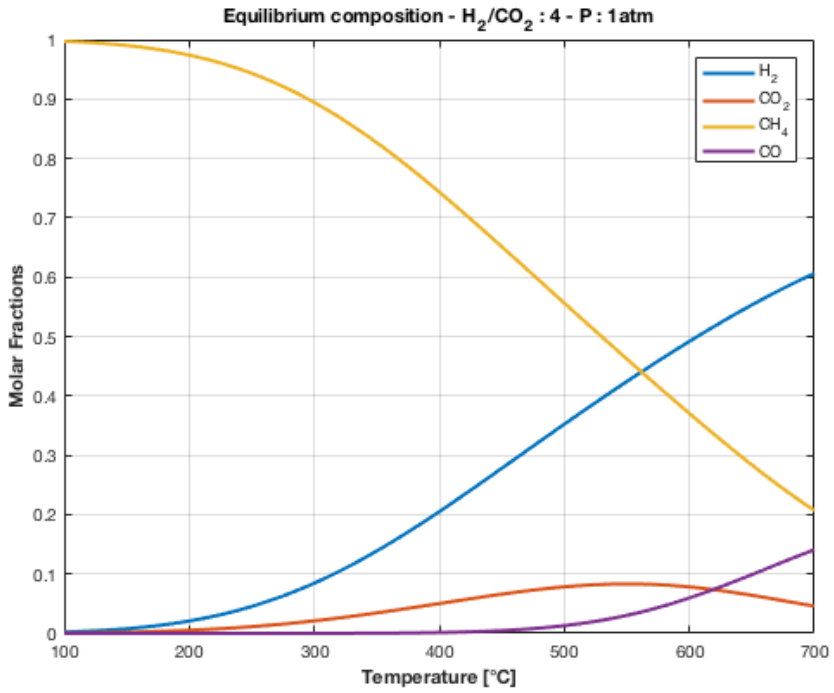

Figure 2.1 *Dry molar fractions at the equilibrium condition of a mixture reflecting both biogas composition and the Sabatier reaction stoichiometry*

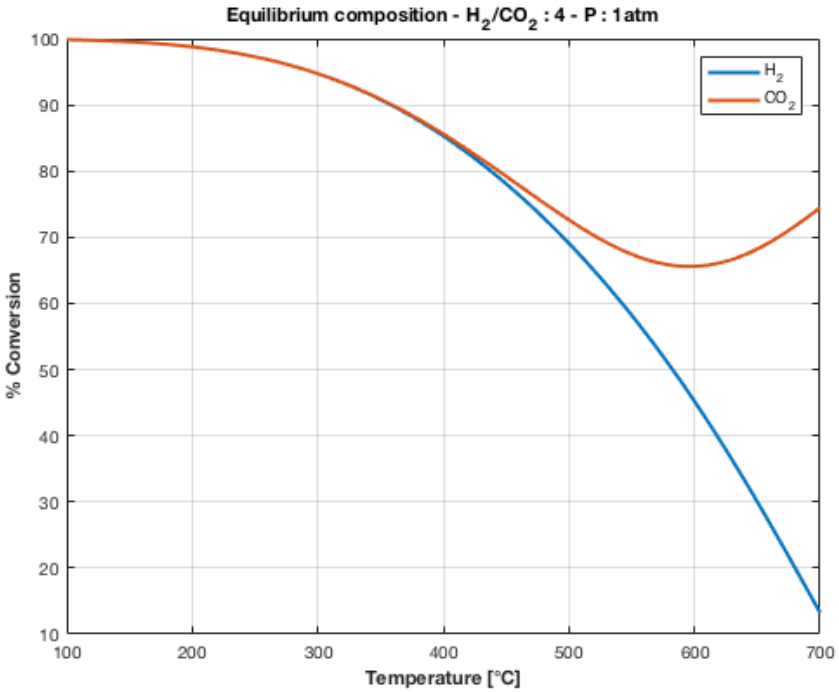

Figure 2.2 *H2 and CO2 equilibrium conversion dependence on temperature in a mixture reflecting both Biogas composition and the Sabatier reaction stoichiometry*

In **Figure 2.2** the effects of temperature on conversion are reported: low temperatures (100°C-350°C) would of course promote the thermodynamics of the Sabatier reaction, but are not actually adoptable since all the catalysts need to work at medium temperatures to favor the kinetics; at medium temperatures (350°C-450°C) equilibrium conversions of both H_2 and CO_2 remain at quite high values. Just consider that if a good catalyst would be found, both selectivity (see the molar fraction of methane in **Figure 2.1**) and conversion up to 90% could be reached at temperature ranging from 350 to 450°C. Note that the production of CO at temperatures higher than 550°C is related to the increasing in the conversion of CO_2 due to water-gas shift reaction.

2.2 Effects of pressure

The molar fraction of methane and the conversion of CO_2 were analysed at three different isobaric equilibrium conditions: 1 atm, 5 atm and 10 atm.

Figure 2.3 highlights the effects of pressure: since reaction (1.16) occurs with a decrease in the number of moles, higher operating pressures involve higher production of methane and, consequently, higher methane molar fractions with the same temperature. However, note that at relatively low temperatures the difference between molar fractions of methane becomes smaller: from a realistic point of view, this could be a huge advantage in terms of operating costs since working at atmospheric pressure would allow to avoid the expensive use of compressors and safety precautions.

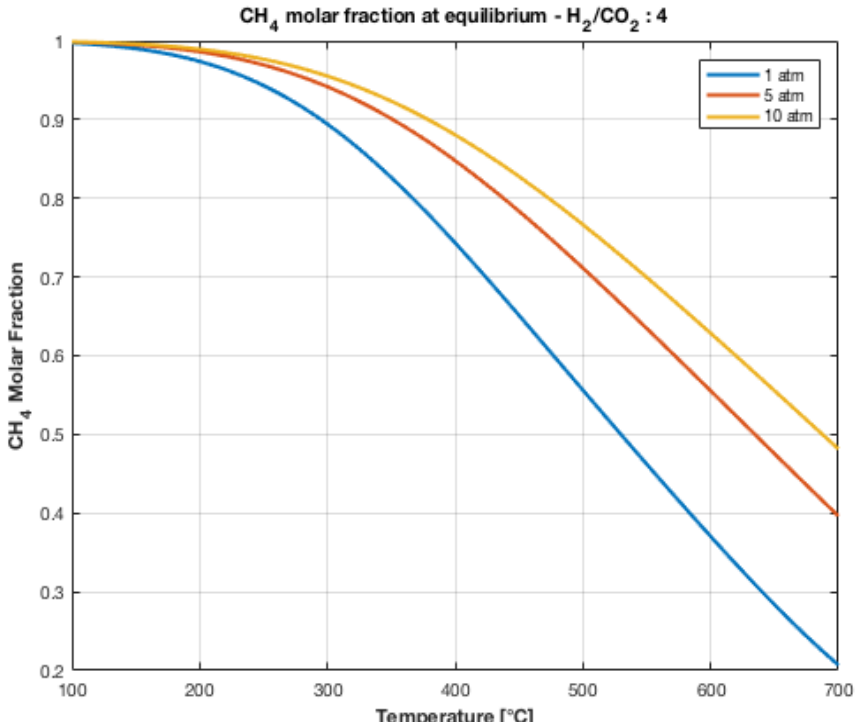

Figure 2.3 *Dependence of methane molar fraction on temperature at different isobaric conditions*

An analysis on conversion of CO_2 (**Figure 2.4**) shows that on the one hand the water-gas shift reaction is retarded if the pressure increases, but at on the other the values of conversion become comparable at low temperatures.

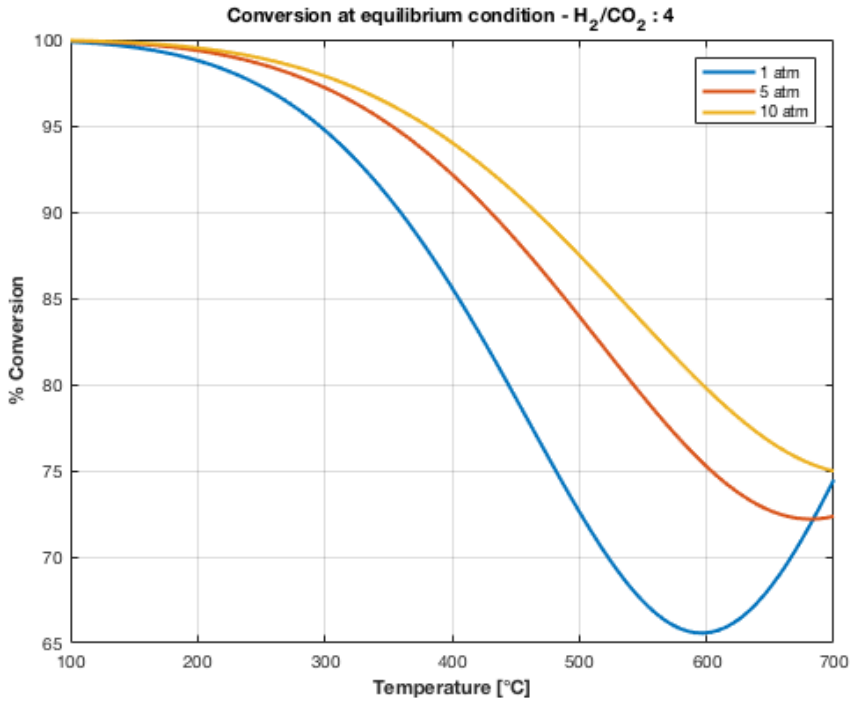

Figure 2.4 *Dependence of CO2 conversion on temperature at different isobaric conditions*

Chapter 3

Experimental Methods

In this chapter all the instruments and the methodologies that were used to conduct the experimental tests are described. All tests were carried out in a hood – for safety reasons – of the K-INN Lab in the Industrial Engineering Department of the University of Padua.

3.1 The plant scheme

First of all, a plant scheme was devised to conduct some experimental tests. Reactants were mixed and sent to a heated reactor; therefore, the product mixture was cooled to condense and remove water and then sent to the analysis instruments. A schematic representation of the plant is reported in **Figure 3.1** and each component will be described more in detail in the next paragraphs.

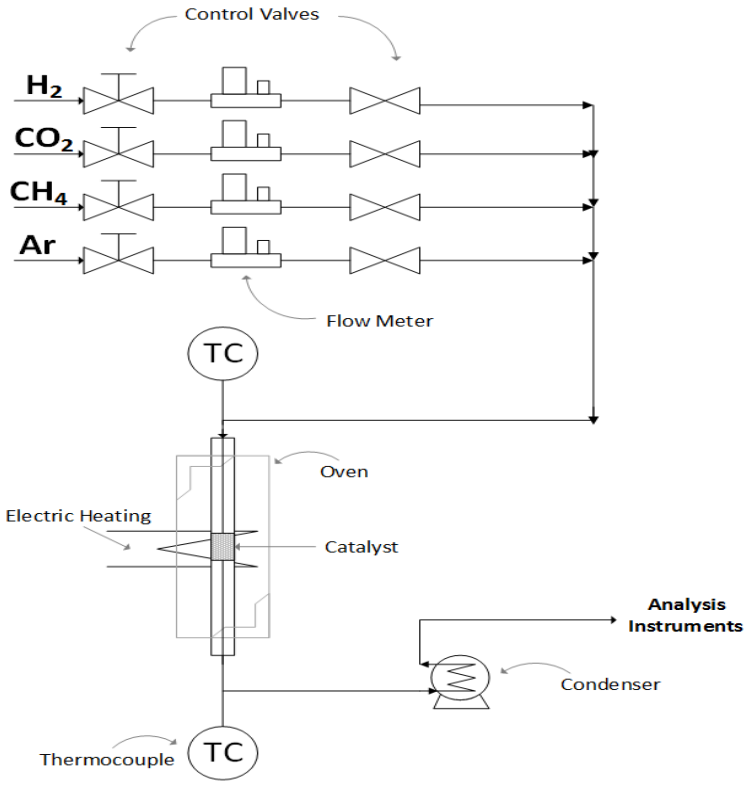

Figure 3.1 *Scheme of the laboratory plant*

3.1.1 Flowmeters

Mass flowmeters (Brooks and Bronkhorst) were used to control the flowrate of each reactant to be sent at the reactor.

These instruments are control valves equipped with a meter and a proper control law; their functioning is based on a calorimetric principle (**Figure 3.2**): the gas flow passes through a known electrical resistance and heats up; the temperature is measured upstream and downstream of the resistance and it is thus possible to obtain the volumetric flowrate of gas by

$$V = \frac{\beta \dot{Q}}{c_p \Delta T} + \gamma \quad (3.1)$$

where β and γ are empirical coefficients, $\dot{Q}$ is the exchanged heating power, $\dot{V}$ the volumetric flowrate and c_p the specific heat at constant pressure. Since γ is often negligible, (3.1) can be rearranged in the following form:

$$S = \alpha \cdot \dot{V} \quad (3.2)$$

where S is the signal and can be expressed as % of controller output or in terms of volts – depending on the type of flowmeter: digital or analogic, respectively – and α is an empirical parameter that has to be calibrated for each flowmeter. Since the equation is the same for all gases, it is possible to experimentally obtain α for a single reference gas and then rearrange it for all the other substances by dividing it by C (3.3).

$$C = \frac{c_p^{ref} \cdot \rho^{ref}}{c_p \cdot \rho} \quad (3.3)$$

where *ref* is for reference gas properties and ρ the density.

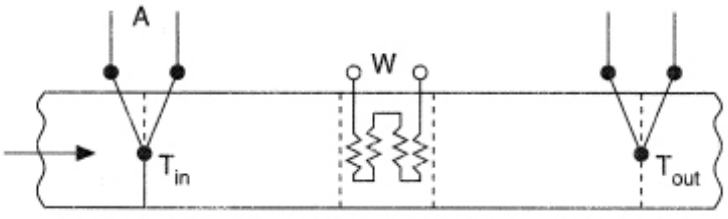

Figure 3.2 *Calorimetric mass flowmeter*

Capitolo 3

3.1.1 I flussimetri

Per la regolazione delle portate dei gas da inviare al reattore sono stati utilizzati dei flussimetri massivi. Questi non sono altro che delle valvole di regolazione accoppiate ad un misuratore di portata e ad una logica di regolazione. Il loro principio di funzionamento è calorimetrico (fig.3.2): viene misurata la temperatura prima e dopo una resistenza elettrica nota. Quest'ultima è attraversata dal flusso di gas, il quale di conseguenza si scalda. La portata è data dalla differenza di temperatura tra le due sonde e può essere calcolata come segue, secondo l'equazione

(3.1)

dove β e γ sono dei coefficienti empirici che dipendono dal flussimetro adottato. Se si trascura l'intercetta, che generalmente è molto piccola, si perviene all'equazione semplificata

(3.2)

nella quale S, ovvero il segnale, può essere espresso come % di output o in volt a seconda che il flussimetro sia analogico o digitale, mentre α è un coefficiente empirico che necessita di essere calibrato per ciascun flussimetro.

Figura 3.2. *Flussim*

Essendo questi regolatori basati su un semplice bilancio di energia, è sufficiente calibrarli con un singolo gas, generalmente azoto, e successivamente, per impiegarli con altri gas, dividere α per una costante C determinata tramite l'equazione

(3.3)

3.1.2 Reactor

The catalytic tests were carried out in a tubular plug-flow reactor consisting of a quartz tube with an internal diameter equal to 8 mm. The catalyst was loaded inside the tube in a fixed-bed configuration, while its support was given by two layers of quartz wool that avoided catalyst entrainments.
The quartz tube was arranged into a tubular furnace consisting of a ceramic heating equipment (Watlow CFH series), which is able to reach 1200°C, coated by a layer of quartz wool and an aluminum cover (**Figure 3.3**).

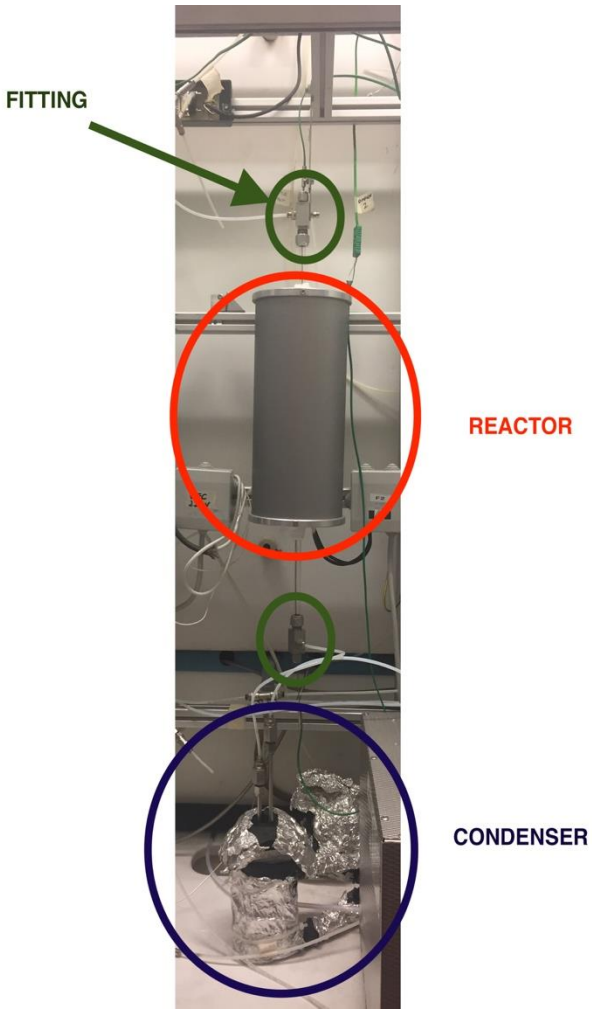

Figure 3.3 *Tubular furnace in which was placed the reactor; fittings; condenser*

An OMRON EC5N-H thermoregulator (**Figure 3.4**) – that is a relay operating via *on/off* action with PID control (the controller settings were found thanks to an automatic tuning procedure of the software CXThermo and are reported in **Table 3.1**) – was used to manipulate the electrical heating in order to establish the desired thermal profile inside the reactor.

Figure 3.4 *OMRON EC5N-H thermoregulator*

Table 3.1 *Parameters for the PID controller of the OMRON EC5N-H thermoregulator*

OMRON controller	**Value**
Proportional Band	44.5
Integral Time	120.4
Derivative Time	18.1

The temperature was measured thanks to a K-type thermocouple (**Figure 3.5**) placed inside the quartz tube in contact with the quartz wool on the gas outlet side (the quartz wool layer length was about 5mm); the software CXThermo was used in order to collect in a text file all the temperatures acquired by the thermocouple.

PA12 pipes were used to transport the gas, whose entry in the reactor was ensured by steel fittings (**Figure 3.6**). The latter are equipped with:

1) a quick connection for the pipe;
2) a hole that allows the fix of the fitting body to the hood;
3) a hole that allows the introduction of a thermocouple and a Teflon seal;
4) a thread and a perforated nut in which the quartz tube can be introduced, the seal of which is guaranteed by a Viton O-ring and a metal seal.

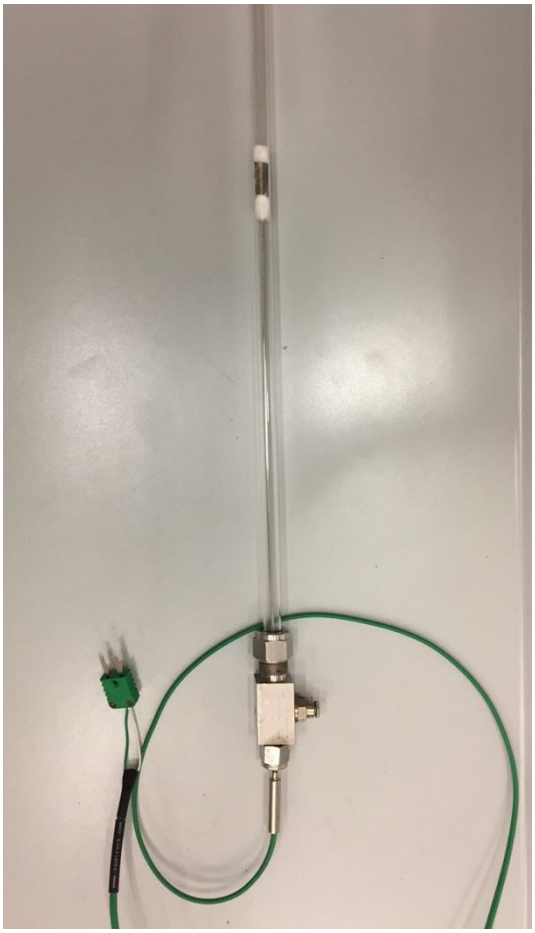

Figure 3.5 *One of the thermocouples that were used for temperature measurement: the thermocouple was placed near the quartz wool layer. In the figure also the quartz tube used as reactor and a fitting are visible*

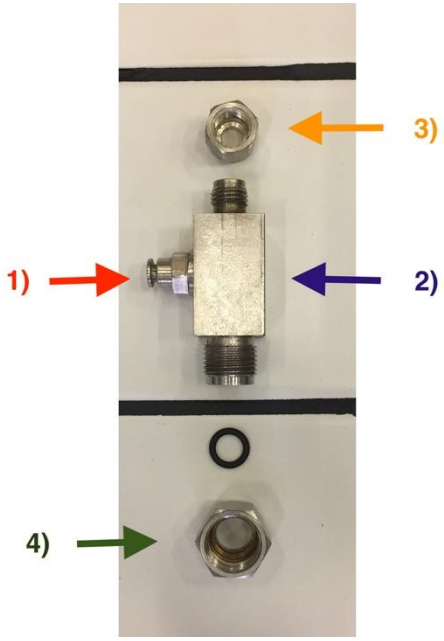

Figure 3.6 *One of the fittings that ensured the entry of the reactant mixture into the reactor. 1) a quick connection for the pipe; 2) a hole for the reactor fixing to the hood; 3) a hole for the thermocouple and for a Teflon seal; 4) perforated nut that allowed the sealing of the quartz tube with a Viton O-ring*

3.1.3 Condenser

Reaction (1.16) produces water and all the analysis instruments that were used are sensitive to it and could be irreparably compromised; moreover, stoichiometry of (1.16) suggests that the molar flowrate of produced water doubles the one of methane. Therefore, condensation of the water contained in the products mixture leaving the reactor has been done in order to protect the instruments.

The condenser was designed and built during a previous work. It works with a refrigerating liquid, that is a mixture of water and glycol, whose temperature is maintained at 3°C by a chiller (**Figure 3.7**).

Figure 3.7 *Chiller used to maintain the temperature of cooling fluid at setpoint*

The condenser consists of an aluminum body in which a glass tube (**Figure 3.8a**) with a diameter of 40 mm and a height of 115 mm is located. The top of the tube is closed by a cap with two metal tubes: a lower one, in which the gas coming out from the reactor enter and is conveyed towards the lower part of the condenser, and a higher one from which the water-free gas can exit and be sent to the analysis instruments.

The aluminum body has two connections for the inlet and the outlet of the refrigerant (**Figure 3.8b**). A previous fluid-dynamics study [61] showed that it is more convenient for the cooling fluid to enter from below.

Finally, both the condenser and the pipes connecting it to the chiller are covered with insulating material so that losses due to heat exchange can be minimized (**Figure 3.8c**).

Figure 3.8 *Details of the condenser that was used to remove water in the gas leaving the reactor: a) the aluminium body and the glass tube; b) the aluminium body with two connectors for the inlet and the outlet of the cooling fluid; c) insulating material cover that minimizes energy losses due to heat exchange.*

3.2 Analysis Instruments

Below is a description of the analysis instruments that were used during this work: a gas chromatograph and a mass spectrometer. While the first one was used during all tests, the latter was useful for few tests to give qualitative information and to compare results with those coming from the gas chromatograph; once verified that instruments gave comparable results, the mass spectrometer was left to other parallel works.

3.2.1 Gas Chromatograph Agilent GC-7820

A gas chromatograph, which is abbreviated to GC, is a widespread analysis instrument capable of separating multiple substances by means of chromatographic columns; therefore, the relative quantities of substances can be analysed and evaluated by several detectors that are placed in series with the columns.

Figure 3.9 *Gas Chromatograph Agilent GC-7820*

In this work the gas chromatograph *Agilent GC-7820* was used (**Figure 3.9**): it is equipped with two columns, Porapak Q (PPQ) and Molsieve (Molecular Sieve 5Å, which is abbreviated in MS5A), in series with two detectors (a Thermal Conductivity Detector, *TCD*, and a Flame Ionization Detector, *FID*) (**Figure 3.10**).

While PPQ is used for the separation of CO_2, H_2O and hydrocarbons, MS5A is capable in separating permanent gases. Since CO_2 and H_2O would be irreversibly absorbed on the Molsieve, thus compromising its operation, some precautions were necessary: H_2O was removed by the condenser that has been described in a previous paragraph and CO_2 was

separated by PPQ through an appropriate method implementation that provides for a valve-switching and for MS5A isolation.

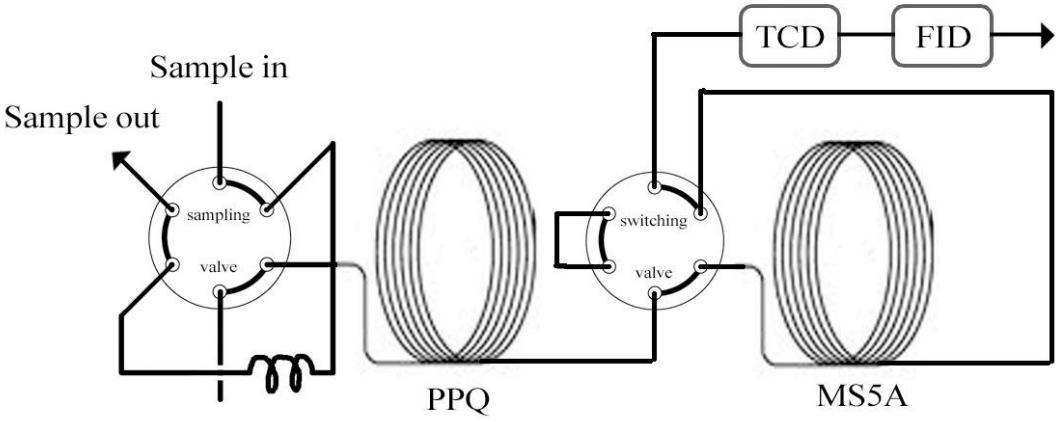

Figure 3.10 *Schematic representation of the gas chromatograph Agilent GC-7820, equipped with two chromatographic columns (PPQ, MS5A) in series with two detectors (TCD, FID).*

A "method" is the ensemble of settings adopted by the GC to perform the separation of the components, such as pressure or temperature ramps, residence times, valve-switching. After some attempts and thanks to the comparison with some other similar works, the set of parameters that allowed separation has been found and it is reported in **Table 3.*2***.

Table 3.2 *Parameters of the Agilent GC-7820 method used to separate product mixture*

Temperature	**Rate [°C/min]**	**Value [°C]**	**Hold time [min]**	**Total time [min]**
Initial		50	3	3.0
Ramp 1	50	40	2.7	5.9
Ramp 2	15	50	1.5	8.0
Pressure	**Rate [psi/min]**	**Value [psi]**	**Hold time [min]**	**Total time [min]**
Initial		47	3.2	3.2
Ramp 1	50	30		8.0
			Value	
Sampling valve temperature			120 °C	
TCD temperature			250 °C	
Internal valve switch time (ON) [min]			1.2	
Internal valve switch time (OFF) [min]			2.6	

A sample amount of gas to be analysed is injected through a six-way valve and transported by a carrier gas. Once each component has been separated, it is pushed to detectors where some physical properties are put in evidence. In this work, only the TCD signal – that is expressed in μV – was observed: therefore, each sample run shows some peaks that express the difference

in thermal conductivity between separate components and the carrier gas, which is helium in this case and corresponds to the signal baseline (**Figure 3.11**).

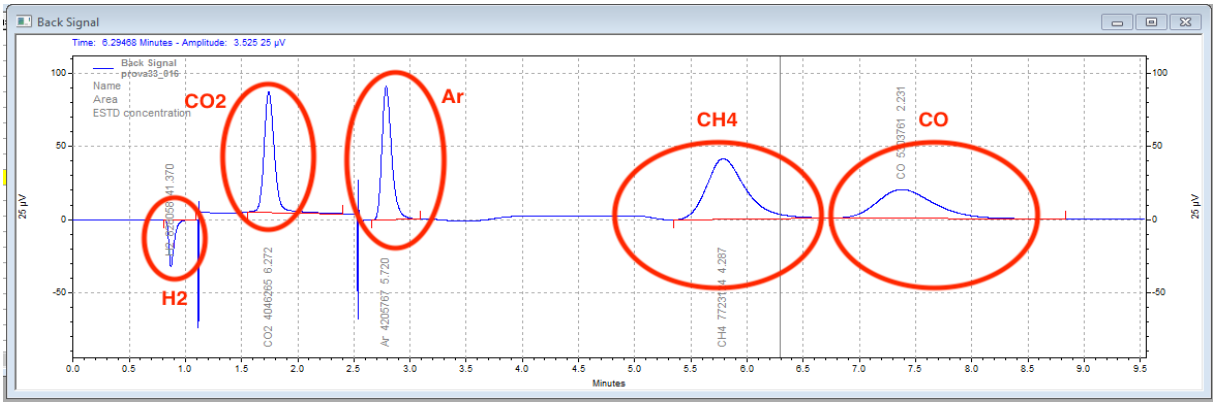

Figure 3.11 *A representation of a sample run on GC Agilent-7820 in which all peaks are visible*

The components were fed with helium one at a time to the GC to observe what moment they showed their characteristic peaks. Finally, their volumetric fractions in the sample were evaluated: each sample run generates a *.Area* file, which is a report that contains the values of all the areas subtended to the peaks; since the volumetric fractions of the components are known in non-reactive conditions, calibration lines can be extrapolated which link the areas with the mixture compositions. In particular, each calibration line showed excellent goodness of fit even in large composition ranges: for instance, just consider that the calibration for the volumetric fraction of hydrogen was almost perfect (coefficient of determination R^2=0.99) in the range 0-85%vol., which demonstrates the reliability of the gas chromatograph (**Figure 3.12**).

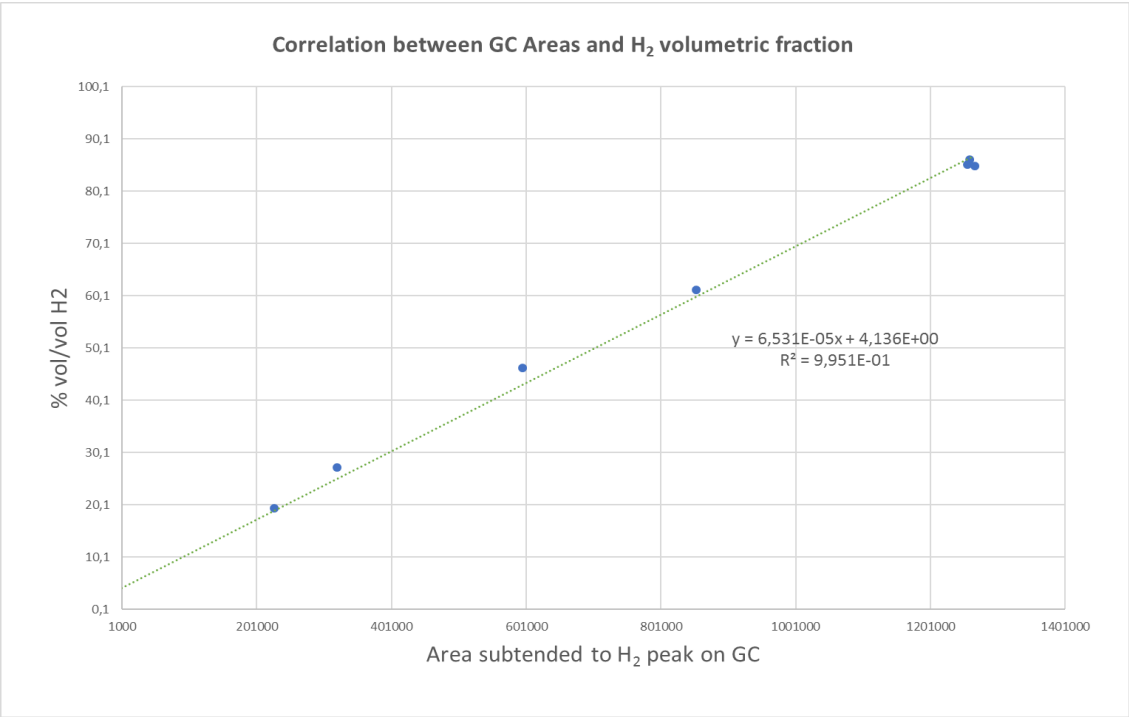

Figure 3.12 *Calibration line linking GC Areas with H2 volumetric fraction*

3.2.2 Mass Spectrometer Hiden HPR-20

A mass spectrometer is an analytic instrument that is able to separate ions having different mass-to-charge ratios. Therefore, if a gas needs to be analysed it has first to be ionised: this can occur through several techniques.

The spectrometer Hiden HPR-20 (**Figure 3.13**) was used only for few tests during this work, in a parallel configuration with the GC. The instrument showed some similarity in the calculated molar fractions with the one coming from the gas chromatograph (**Figure 3.14**) meaning that it also could be used for a good qualitative analysis.

Figure 3.13 *The mass spectrometer Hiden HPR-20 that was used during this work.*

Its working principle is based on soft ionisation technique: a known high-energy electron beam bombards the gas to be analysed in high-vacuum conditions, thus involving a phenomenon of molecules fragmentation to ions. The ions then enter a quadrupole, i.e. a device in which there are a fixed electric field and an oscillating one: the result is a sinusoidal deviation of the ions trajectories, which allows only some of them to reach the detector.

Finally, the detector is an electronic transducer able to amplify the electric current produced by the ions that have managed to reach it, the signals thus obtained are then transferred to the MASsoft calculator in order to express and represent the quantity of each relevant ion in terms of partial pressure. In **Table 3.*3*** the analysed atomic masses are reported.

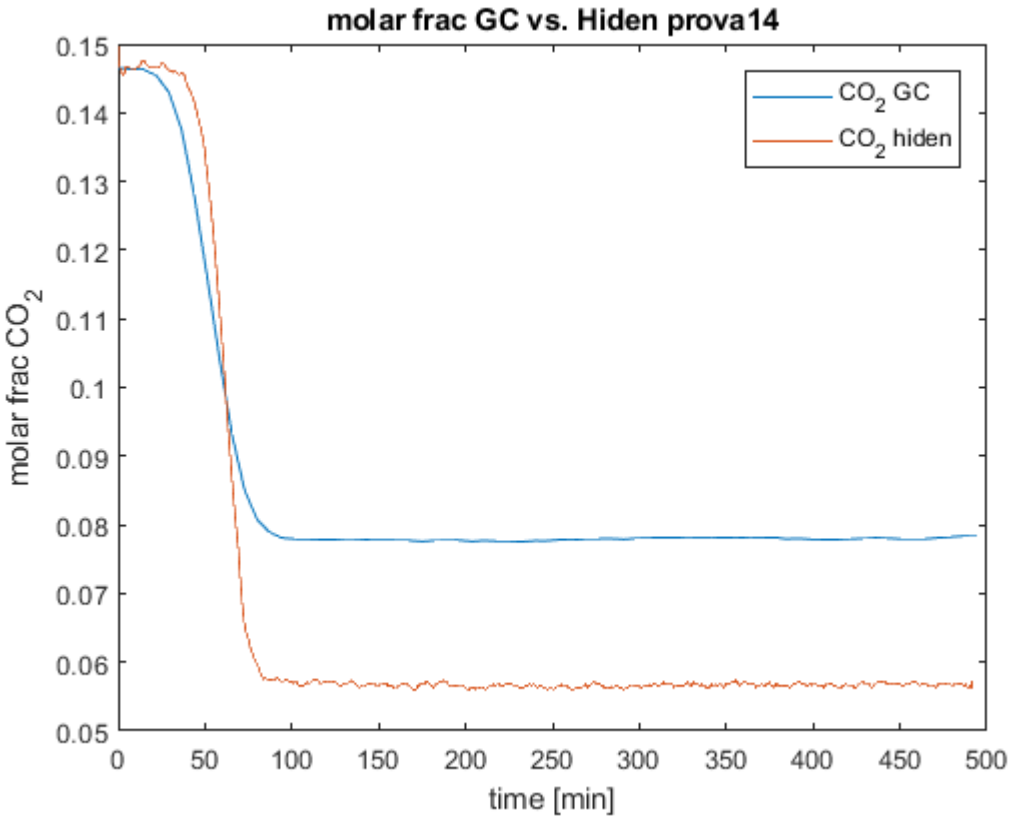

Figure 3.14 *Comparison between molar fractions of CO2 analysed by different instruments*

Table 3.3 *Atomic mass unity scanned by Hiden HPR-20 mass spectrometer*

Scanned a.m.u. (atomic mass unity)	**Corresponding Gas**
2	H_2
44	CO_2
40	Ar
28	CO
16	CH_4

3.3 Experimental procedures

In this paragraph the parameters that were used for the processing of experimental data are defined: conversion, yield, selectivity, GHSV, atomic balances; moreover, all the procedures that were adopted are explained, from the thermal politics to the methods implemented for the calculation of parameters and processing of experimental data.

3.3.1 Experimental setup

Operating conditions and composition of the reacting mixture

Thanks to its huge potential, catalytic biogas upgrading could easily be integrated into livestock and agricultural farms. Since the aim of this work is to simulate an upgrading process as realistic as possible in a commercial context, experimental tests were conducted at atmospheric pressure so as to verify if it would be possible to exploit biogas without using a too complex plant.
For the same reason, the tests were performed with an inlet gas mixture representing on the one hand the real composition of biogas ($CH_4/CO_2 = 0.55/0.45$) and on the other the stoichiometric molar ratio of the Sabatier reaction (1.16) ($H_2/CO_2 = 4$); no inert was used as diluent but a small fraction of Argon in order to trace the potential variation in the volumetric flow due to the change of the total number of moles (**Table 3.*4***). The mixing of reactants in the gaseous phase was supposed to be spontaneous at the junction points between the pipes.

Table 3.4 *Composition of the reaction mixture used for the experimental tests*

Component	**H_2**	**CO_2**	**CH_4**	**Ar**
%	61	15.3	18.7	5

From the thermal point of view, different kinds of tests were performed in order to evaluate the activity of catalysts: ramp up / ramp down and isothermal. While the latter kind of tests allowed to observe the behavior of the system at steady-state conditions, temperature ramps were useful to evaluate the dynamic response of the reactant mixture to thermal cycles. In any case the temperature was controlled in a way that the rate of heating and cooling was always set equal to 5°C/min.
As already mentioned in the previous chapter, the gas leaving the reactor was first fed to a condenser to remove water and then to the gas chromatograph. During some tests the signals of the mass spectrometer were also analysed and compared to those of the chromatograph.

Catalysts and flowrate

Different catalysts were tested: a commercial nickel-based catalyst (provided by Johnson Matthey, **Figure 3.15**) in grains, that was accurately sieved to obtain the fraction with dimensions within the range 710 - 850 μm; a 500 mg Nickel gauze (provided by AlfaAesar, **Figure 3.16**) which was rolled up so it could be inserted into the quartz tube; a self-made NiO/Al_2O_3 (**Figure 3.17**). The latter was prepared through the wet impregnation technique following the suggestions that were found in literature [62], [63]:

1) Al_2O_3 (provided by CTS) with an average diameter dimension equal to 260 μm was stirred in an aqueous solution (1 mL H_2O / 1 mg Al_2O_3) for few hours with Nickel (II) nitrate hexahydrate ($Ni(NO_3)_2 \cdot 6H_2O$);
2) The solution was dried for about 5 hours at 90°C;
3) Finally, the solid compound was calcined at 700°C for 5 hours.

The self-made catalyst had a Ni content of 16% by weight, defined as the ratio between the nickel mass and the alumina mass.

Catalyst was always loaded into the reactor in a fixed-bed configuration and supported by quartz wool to avoid entrainments. In any case, catalyst was pre-reduced with the reactant mixture (containing 61% of H_2) at temperatures higher or equal to 600°C in order to be activated.

From a realistic point of view, the quantities of catalyst to be used assume an important role: in fact, with the same conversion, a process with lower residence times (i.e. smaller quantities of catalyst at the same flow rate or greater flow rate with the same quantity of catalyst) is economically more advantageous. For this reason, always a Gas Hourly Space Velocity (*GHSV*, Eq. 3.4) higher than 15000h^{-1} was used in the experimental tests.

$$GHSV = \frac{\dot{V}}{V_{reactor} * porosity} = \frac{\dot{V} * \rho_{catalyst}}{W_{catalyst}}, \tag{3.4}$$

where $\dot{V}$ is the volumetric flow rate, V, W, ρ are volume, weight and density, respectively; the density of the JM catalyst was assumed equal to 1000 mg/mL (however, since the nickel-oxide density is about 7mg/mL, the apparent density was probably higher than that assumed) while the one of the nickel gauze was provided by AlfaAesar and equal to 8.908 mg/mL.

The flowrate was always changed in accordance to the objective of the tests, but never was set at too low values in order to guarantee some pressure at the inlet of the gas chromatograph: for this reason, its value was always higher than 50 ml/min.

In order to make a proper comparison between catalysts, it was useful to give an estimation of the surface area per mass unit (A/M): to do this 200 mg of the JM catalyst were used and put into the reactor and a bed with 5mm height was obtained. A porosity of the bed equal to 60% was assumed.

$$\frac{A_{JM}}{M} = N_{particles} * \frac{A_{particle}}{M} = V_{reactor} * \frac{porosity}{V_{particle}} * \frac{A_{particle}}{M} \quad (3.5)$$

$$\frac{A_{gauze}}{M} = N_{wires} * \frac{A_{wire}}{M} = \frac{A_{tot}}{M} * \frac{\frac{100 - \%_{open}}{100}}{d_{wire} * length_{wire}} * \pi * d_{wire} * length_{wire} \quad (3.6)$$

A_{JM}/M and A_{gauze}/M were calculated using the equations above and were equal to 6 and 6.7 mm^2/mg, respectively: these values suggested that the catalysts provided similar surface area per mass unit.

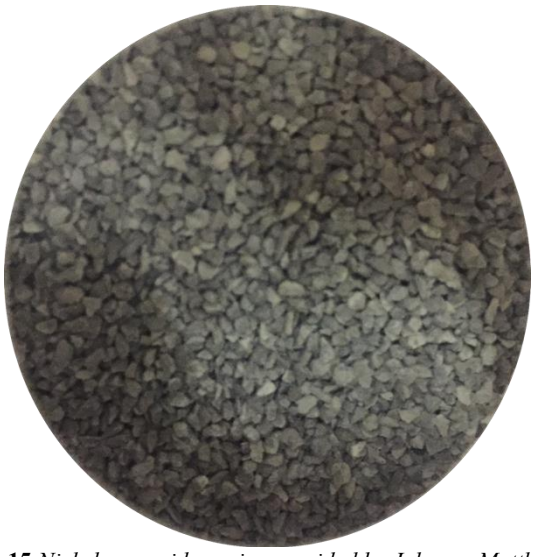

Figure 3.15 *Nickel monoxide grains provided by Johnson Matthey. Particle diameters ranging from 750µm to 810 µm.*

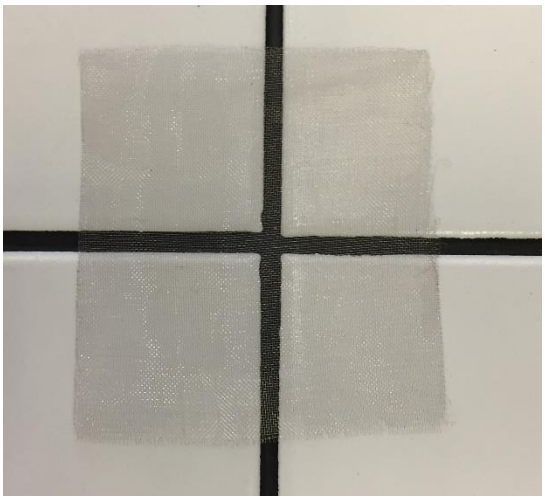

Figure 3.16 *Nickel gauze provided by AlfaAesar. It was rolled up and inserted into the quartz tube to be used as catalyst*

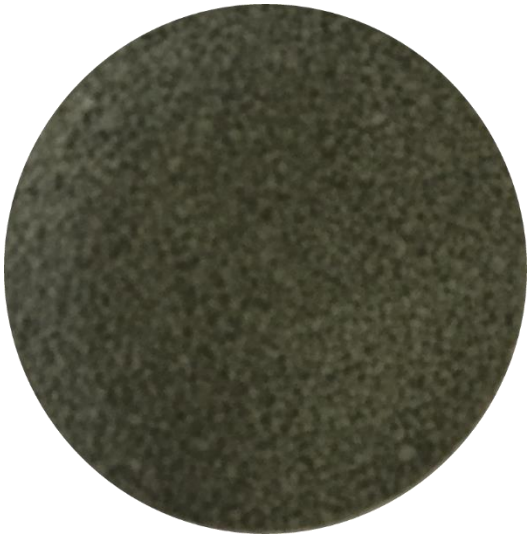

Figure 3.17 *Nickel-based self-made catalyst with Ni content equal to 16% by weight*

3.3.2 Processing of experimental data

The experimental data coming from the analysis instruments were processed on MATLAB® to quantify the relative variations in the reactants and products concentrations. Therefore, it was possible to give an estimation of H_2 and CO_2 conversions as well as yield and selectivity for CH_4 and CO as functions of temperature and time.
The script used on MATLAB® is able to open the files *.Area* coming from the GC and read the values of each area associated to a single component; moreover, it also allows to load all the temperatures that were collected by CXThermo and calculate all the parameters that were considered in this work.

Conversion calculation

Since the process occurs with a decrease in the number of moles, the total molar flowrate is decreasing if reagents are converted. If the conversion of species *i* is defined as in Eq. 3.7, where *y* is the molar fraction (that is equal to the volumetric one because of the low operating pressure) and *N* the total molar flowrate, both the molar fraction and the total flowrate are known at the inlet, while the molar fraction in the outlet is calculated through the GC areas. The total molar flowrate in the product mixture is not known and need to be calculated: for this reason, a small amount of inert was added in the reacting mixture (that is Argon, **Table 3.*4***). Thanks to the molar balance of Argon (3.8), Eq. 3.7 can be rearranged into Eq. 3.9 and the conversion can be calculated through the experimental data.

$$\chi_i = 1 - \frac{y_i^{out}\,\dot{N}^{out}}{y_i^{in}\,\dot{N}_{in}} = 1 - \frac{\dot{n}_i^{out}}{\dot{n}_i^{in}} \tag{3.7}$$

$$y_{Ar}^{in}\;\dot{N}^{in} = y_{Ar}^{out}\;\dot{N}^{out} \tag{3.8}$$

$$\chi_i = 1 - \frac{y_i^{out}}{y_i^{in}}\frac{y_{Ar}^{in}}{y_{Ar}^{out}} \tag{3.9}$$

The same script was also used to calculate both the composition of the mixture and the conversion of CO_2 and H_2 at the equilibrium condition through the *Cantera* libraries and functions that were already described in Chapter 2.

Yield and atomic balances

The yield was defined as the ratio between the produced methane and the entering CO_2 (Eq. 3.10), so that it was equal to 100% if all the entering CO_2 was converted into methane.

$$Y_{CH_4} = \frac{molar\ flowrate\ of\ produced\ CH_4}{molar\ flowrate\ of\ CO_2\ in\ the\ inlet\ mixture} x100\% \quad (3.10)$$

Moreover, the script is also able to calculate the atomic balance of all the species involved in the process, so as to evaluate the errors coming from the calculation while processing the experimental data. In particular, each atomic balance was evaluated as follow:

$$err_C = \frac{\dot{n}_{CO_2}^{in} + \dot{n}_{CO}^{in} + \dot{n}_{CH_4}^{in} - (\dot{n}_{CO_2}^{out} + \dot{n}_{CO}^{out} + \dot{n}_{CH_4}^{out})}{\dot{n}_{CO_2}^{in} + \dot{n}_{CO}^{in} + \dot{n}_{CH_4}^{in}} x100\% \quad (3.11)$$

$$err_{Ar} = \frac{\dot{n}_{Ar}^{in} - \dot{n}_{Ar}^{out}}{\dot{n}_{Ar}^{in}} x100\% \quad (3.12)$$

$$err_{H_2} = \frac{\dot{n}_{H_2}^{in} + 2\dot{n}_{CH_4}^{in} - (\dot{n}_{H_2}^{out} + 2\dot{n}_{CH_4}^{out})}{\dot{n}_{H_2}^{in} + 2\dot{n}_{CH_4}^{in}} x100\% \quad (3.13)$$

where *err* represents the relative error with respect to the inlet molar flowrate of a given species. In some cases it was useful to evaluate the molar flowrate of produced water. Since it was condensed before being sent to the analysis instruments, it was impossible to directly measure its flowrate. Even if it was collected into the condenser, measuring the water quantity would not be useful at all because it would be an integral quantity and could not give any information about the flowrate. For this reasons, the molar flowrate of water was calculated thanks to a hydrogen atomic balance (3.14): since the hydrogen fed to the reactor must be equal to the one leaving it, all the atoms that were not analysed by the instruments were collected in the condensed water.

Finally, the selectivity was defined as in Eq. 3.15 in a way that it could range between 0 and 1 for a more intuitive understanding of the process yield.

$$\dot{n}_{H_2O}^{out} = \dot{n}_{H_2}^{in} + 2\dot{n}_{CH_4}^{in} - \dot{n}_{H_2}^{out} - 2\dot{n}_{CH_4}^{out} \quad (3.14)$$

$$S = \frac{\dot{n}_{CH_4}^{prod}}{\dot{n}_{CH_4}^{prod} + \dot{n}_{CO}^{prod}} \quad (3.15)$$

Chapter 4

Results and Discussion

4.1 Blank test

Before analyzing the reacting system behavior on different catalysts, it was certainly useful to observe if some activity would occur at high temperatures in the absence of any catalytic material. For this reason, the reacting mixture was heated at 800°C and:

- Some CO production occurred (**Figure 4.1**);
- Only at temperatures higher than 550°C some CO_2 conversion was observed (**Figure 4.2**a)
- No hydrogen conversion occurred.

Dry reforming was supposed to be the only reaction occurring in the absence of catalyst at temperatures higher than 550°C: in fact, if only dry reforming occurs, the balance equation 4.1 (where Δi is the difference in the molar flowrate of component i between the outlet and the inlet section) must be verified as can be observed in **Figure 4.3**.

$$\Delta CO + \Delta CO_2 = 0 \qquad (4.1)$$

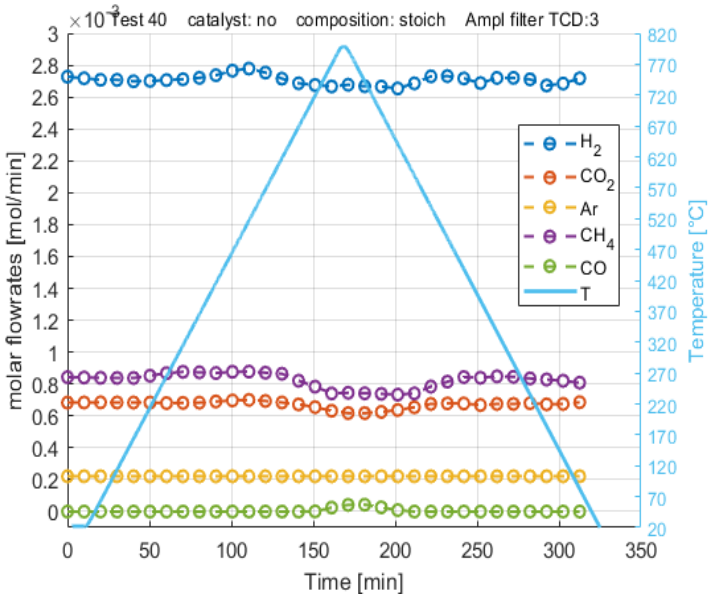

Figure 4.1 *Molar flowrates of all components in the reacting mixture heated to 800°C in the absence of catalyst*

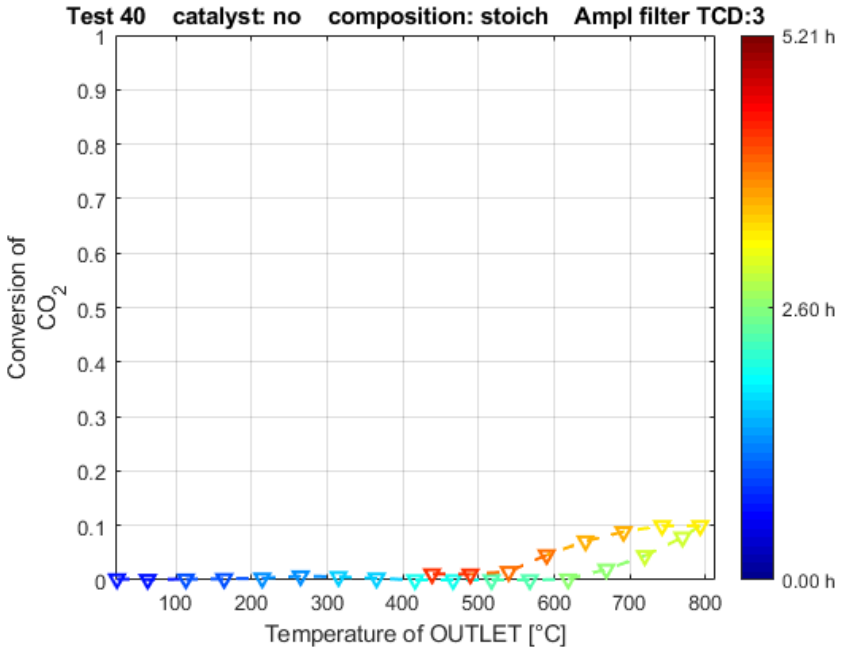

Figure 4.2 *CO2 (a) and H2 (b) fractional conversion dependence on temperature in the absence of any catalytic material*

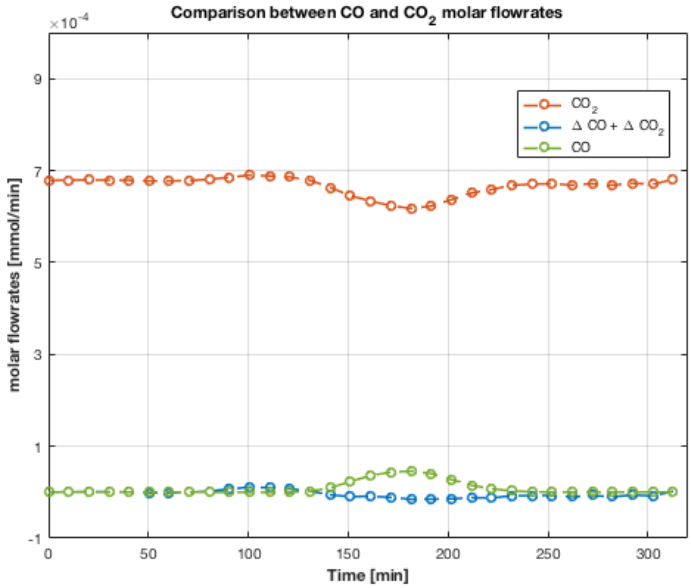

Figure 4.3 *Comparison between CO2 and CO molar flowrates leaving the reactor*

4.2 Nickel gauze by AlfaAesar

Thanks to the cues taken from the available literature, it was decided to carry out some tests with nickel as catalyst since the most used catalysts for biogas upgrading are nickel-based. For this purpose, we opted for the purchase of a nickel gauze, supplied by AlfaAesar, to investigate its activity towards the Sabatier reaction.

The gauze measured 75mmx75mm and weighed 500mg, with an open area of 81% and a width of opening equal to 0.46mm. As already described before, the gauze was rolled up to be loaded into the reactor in a fixed-bed configuration (the gauze before being rolled up was reported in **Figure 3.16**, while in **Figure 3.5** the reactor in which the rolled up gauze was placed is visible).

4.2.1 Ramp up / ramp down tests

In order to evaluate the effects of flowrate and temperature, ramp up / ramp down tests were carried out.

Even if flowrate as low as possible was used and pre-reduction at 600°C of the catalyst was performed, the results were not as successful as expected maybe due to too high values of GHSV, meaning that higher quantity of catalyst would be needed. The conversion of CO_2 was very low and always under 10% even at high temperatures and similar results were obtained by decreasing the total molar flowrate (**Figure 4.4**): this result suggested that catalyst as a gauze had very weak activity and maybe higher temperatures (or lower GHSV) were needed to involve some catalyst activation.

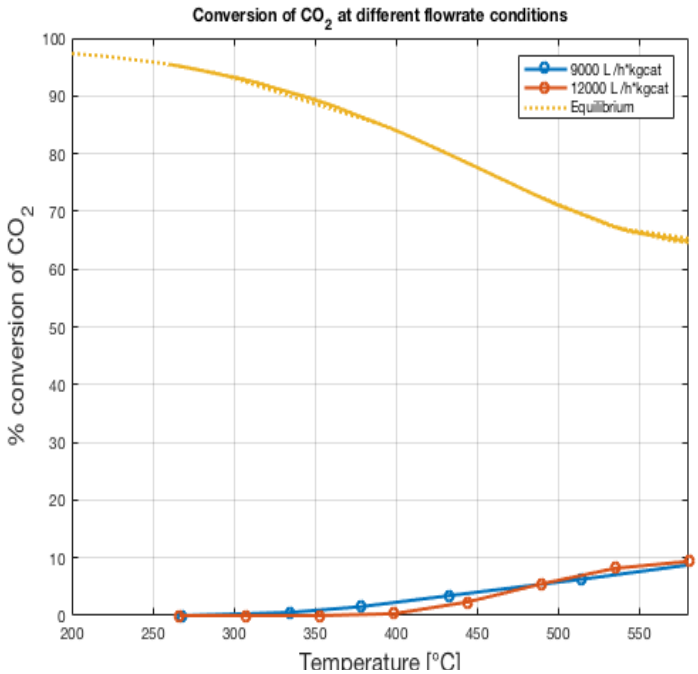

Figure 4.4 *Conversion of CO2 on Nickel gauze as catalyst at different flowrate conditions.*

4.2.2 Isothermal test

For a better understanding of what happened during reactant conversion, another test was carried out during which the temperature was first increased to even higher values (700°C) in order to search for catalyst activation, then maintained for few hours at 650°C and finally at 500°C. As reported in **Figure 4.5**, conversion of H_2 reached the equilibrium value (10%) at 700°C while the one of CO_2 was much higher than that observed at lower temperatures (**Figure 4.4**) and was 4 times bigger than the one of hydrogen.

Looking at the molar flowrates (**Figure 4.7**) instead, it can be noticed that no methane was produced nor consumed even with some CO_2 and H_2 conversion, while some production of CO occurred: this suggests that the only active reaction was reverse water-gas shift (i.e. the opposite reaction of 1.6). In fact, this evidence can also be verified through an observation to the reagents conversion because only ¼ of the fed hydrogen was converted, thus reflecting the stoichiometric molar ratio $H_2/CO_2 = 1/1$ of the reverse WGS, or by comparing the molar flowrates of produced water and CO that must be equal if only reverse WGS occurs (**Figure 4.6**).

$$CO + H_2O \leftrightarrow H_2 + CO_2 \qquad \Delta H_r = -41.2\ kJ/mol \qquad (1.6)$$

The latter observation could also be based on the ratio between the net variations of the molar flowrates: if only reverse WGS occurs $\Delta CO/\Delta CO_2$, $\Delta H_2/\Delta CO_2$ and $\Delta H_2/\Delta CO$ must all be equal to 1 (absolute value) (**Figure 4.8**). These tests showed that the Nickel gauze could not be used for catalytic biogas upgrading since even pre-reducing it at high temperatures no production of methane occurs: probably this is due to very low surface area of the gauze, which would maybe require very high residence times to show activity towards the Sabatier reaction thus losing interest from a commercial perspective.

For the latter reasons, no more catalytic tests on the nickel gauze were carried out.

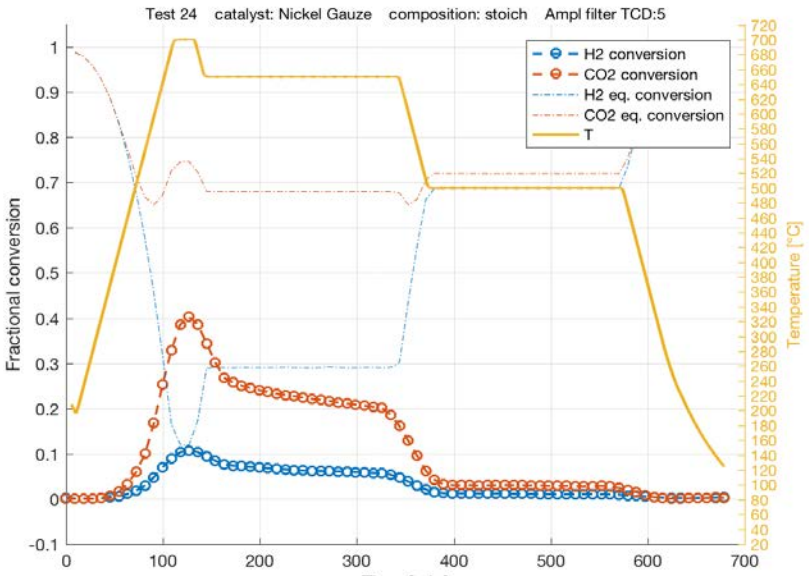

Figure 4.5 *Equilibrium and actual conversion of both H2 and CO2 at different steady state conditions*

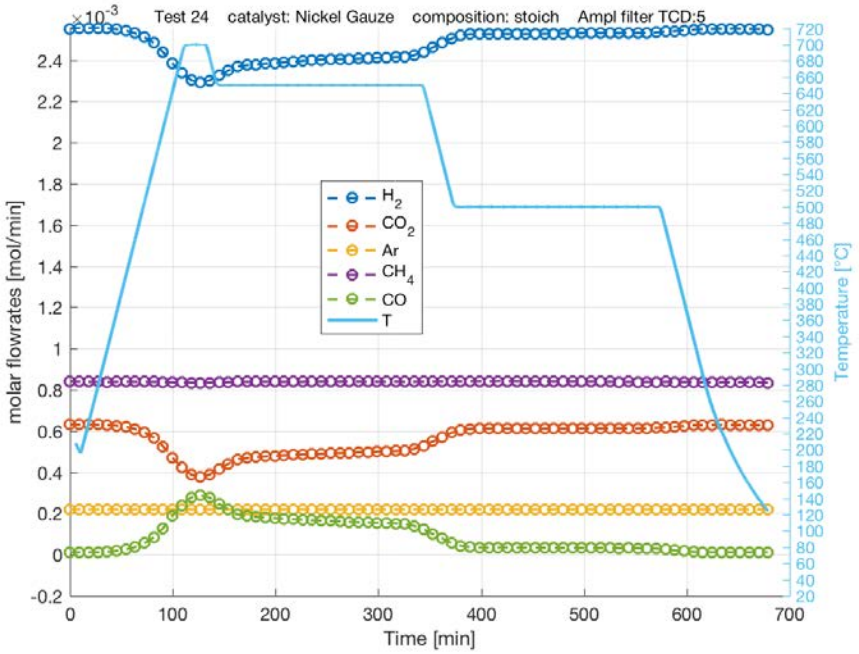

Figure 4.7 *Molar flowrates of all components at different steady state conditions on Nickel gauze as catalyst*

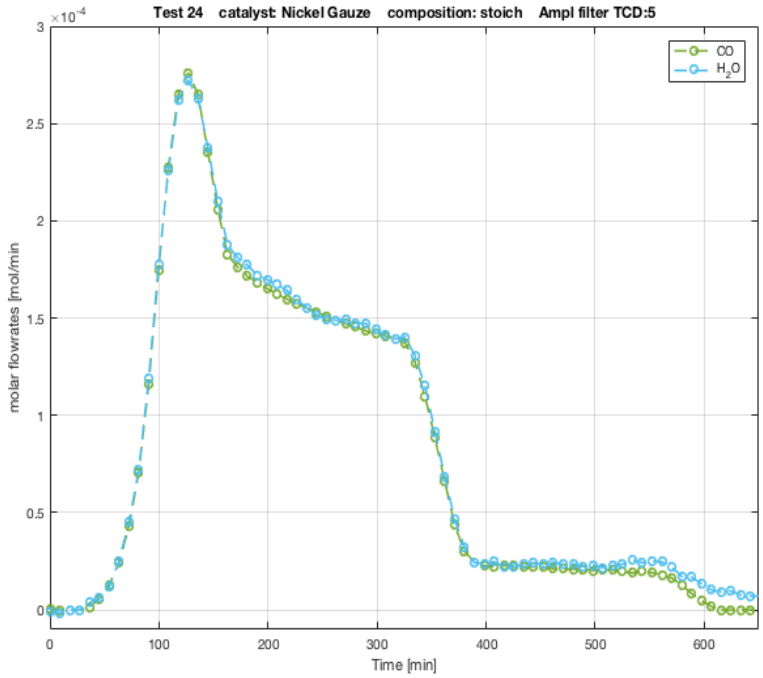

Figure 4.6 *Comparison between water and CO molar flowrates during an isothermal test on Nickel gauze*

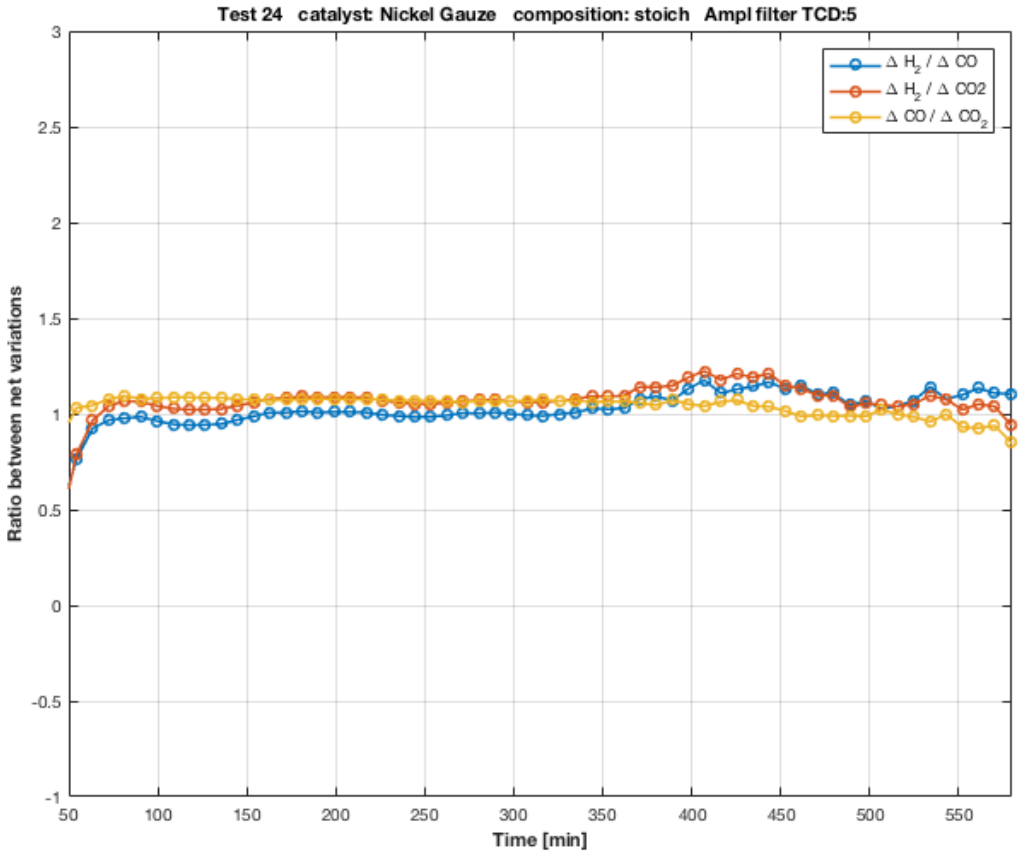

Figure 4.8 *Ratios between net variations are all equal to one, meaning that only reverse WGS occurred*

4.3 Nickel-based catalyst by Johnson Matthey

A catalyst provided by JM was tested: it is a catalyst usually adopted for steam reforming processes, but suitable for the purpose of this work since it is nickel monoxide-based and commercially available.

4.3.1 First tests with one thermocouple at the reactor outlet

The first tests on the JM catalyst were carried out with just one thermocouple (with a diameter d = 1/8") at the reactor outlet. This configuration was then changed for a better analysis of the temperature profile inside the reactor.

4.3.1.1 Preliminary tests with SiC

Due to the exothermicity of the Sabatier reaction, the first tests were performed with silicon carbide (SiC) as diluent to decrease the contact area between the catalyst and the reactant mixture in order to avoid hot spot in the reactor.

With the aim of evaluating if SiC was actually an inert, a test with no catalyst was performed and, as expected, no conversion of reactants was observed (**Figure 4.9**) up to 600 °C.

Once verified that SiC was an inert, it was loaded into the reactor with the catalyst. Both SiC and the catalyst were sieved to obtain comparable particle size within the range 710-850 µm; SiC was loaded at 25% by weight.

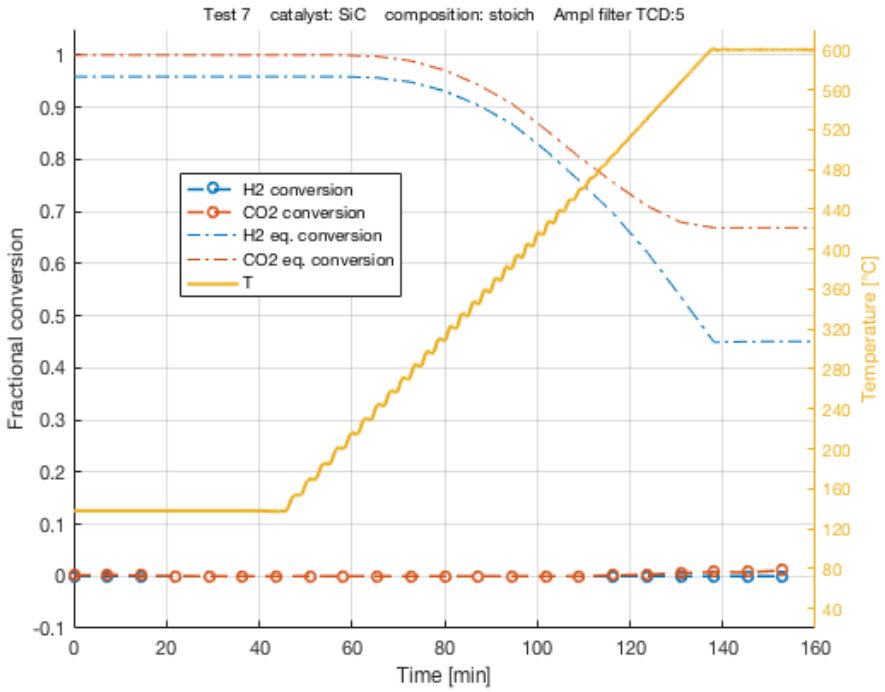

Figure 4.9 *Preliminary test performed to verify that SiC is an inert*

4.3.1.2 Isothermal preliminary tests

Some isothermal preliminary tests were performed in order to evaluate conversion of reactants at different temperatures in steady state conditions. However, as reported in **Figure 4.10**, **Figure 4.11** and **Figure 4.12**, no significant conversion was observed in any test. Only at 400°C (**Figure 4.12**) conversion began to be visible but still very low.

The oscillating behavior of the measured temperature that is visible in the following plots is linked to an incorrect controller tuning, which was further tuned with the parameters reported in **Table 3.1**.

These results suggested that the catalyst needed to be previously reduced in order to be activated and, for this reason, in all the tests that were performed in isothermal conditions the catalyst was first pre-heated at high temperature.

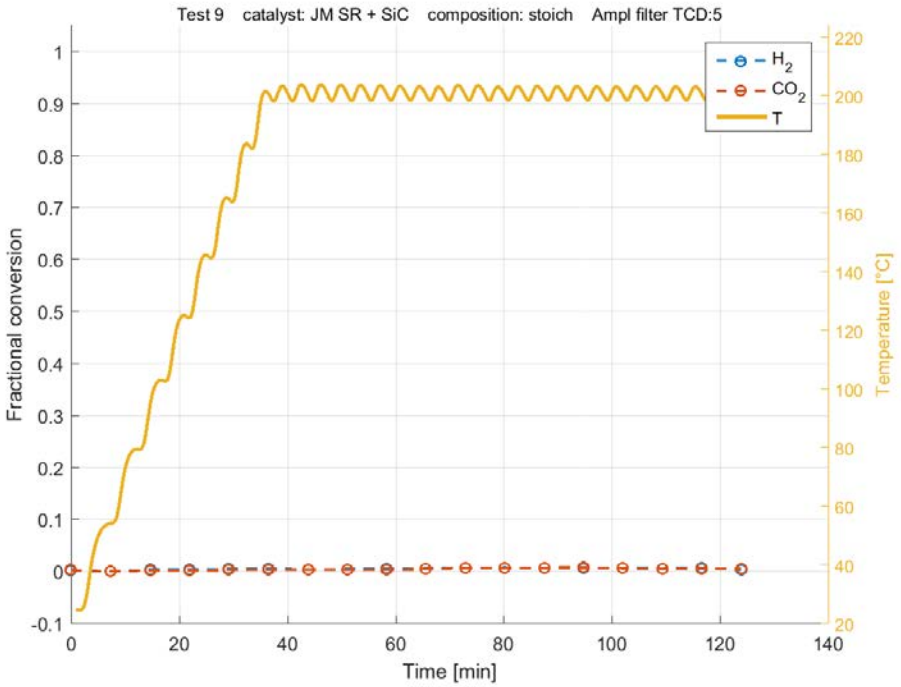

Figure 4.10 *Isothermal test performed at 200°C to evaluate conversion at steady state conditions*

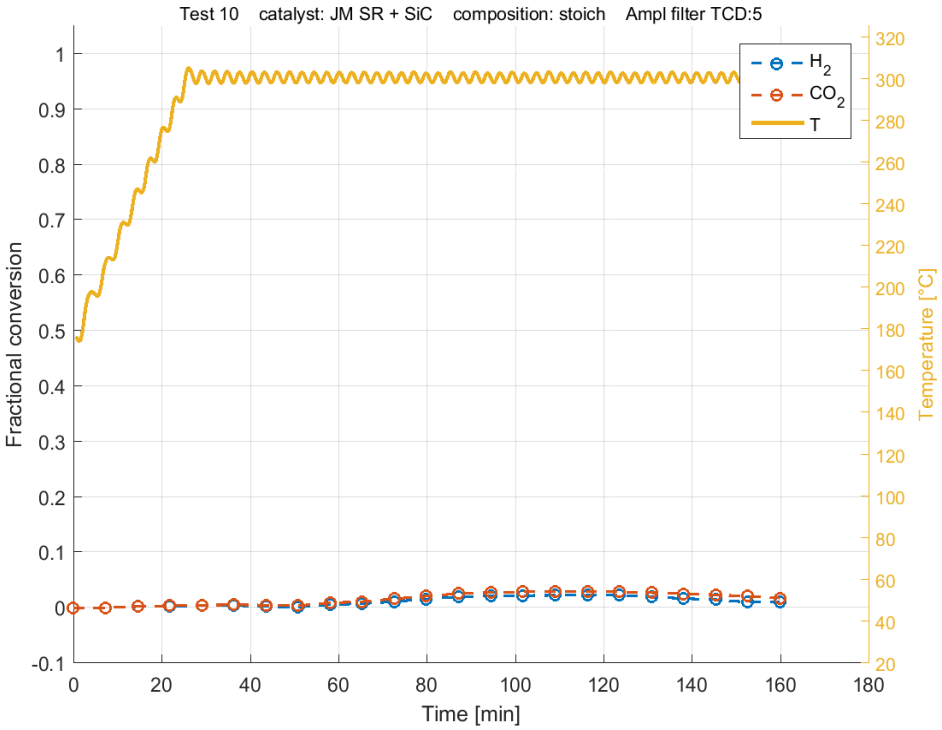

Figure 4.11 *Isothermal test performed at 300°C to evaluate conversion at steady state conditions*

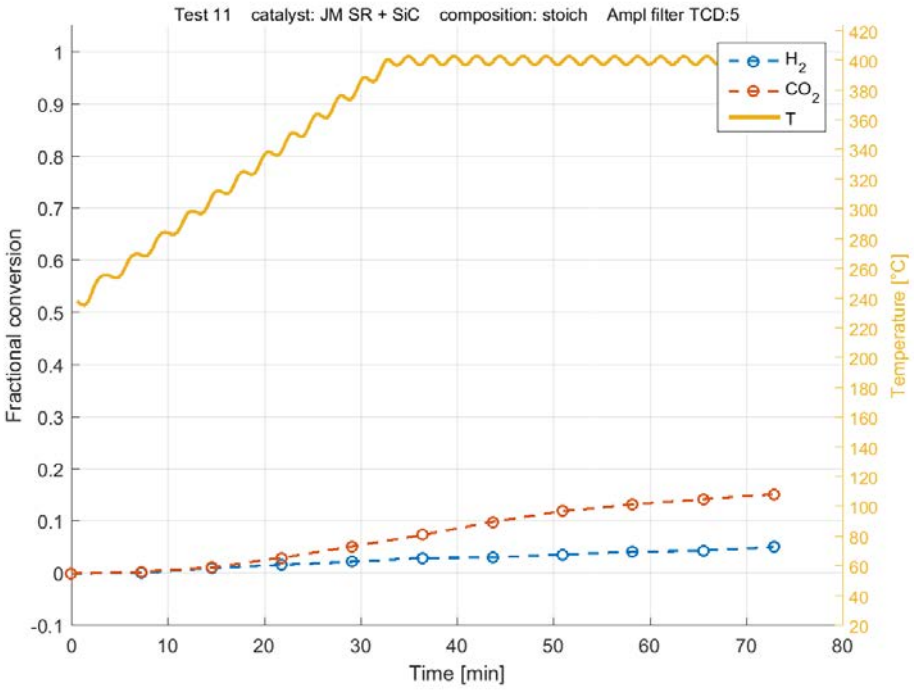

Figure 4.12 *Isothermal test performed at 400°C to evaluate conversion at steady state conditions*

4.3.1.3 Ramp up / ramp down tests: the effects of temperature and flowrate

Some thermal cycles were performed at different flowrates in which high temperatures were reached in order to evaluate the dynamic response of the reactant mixture to changes in temperature. The fresh catalyst was pre-reduced in the first cycles because of the high content of hydrogen in the reactant mixture.

In particular, **Figure 4.13** shows the conversion of hydrogen and CO_2 with a value of GHSV equal to 50000 h^{-1}: looking at the second cycle, it is quite evident how far is the conversion of the heating phase from that of the first cycle and how similar it is to the conversion during the cooling of first cycle; the latter effect is due to the catalyst activation by reduction and is clearly visible also in **Figure 4.14**.

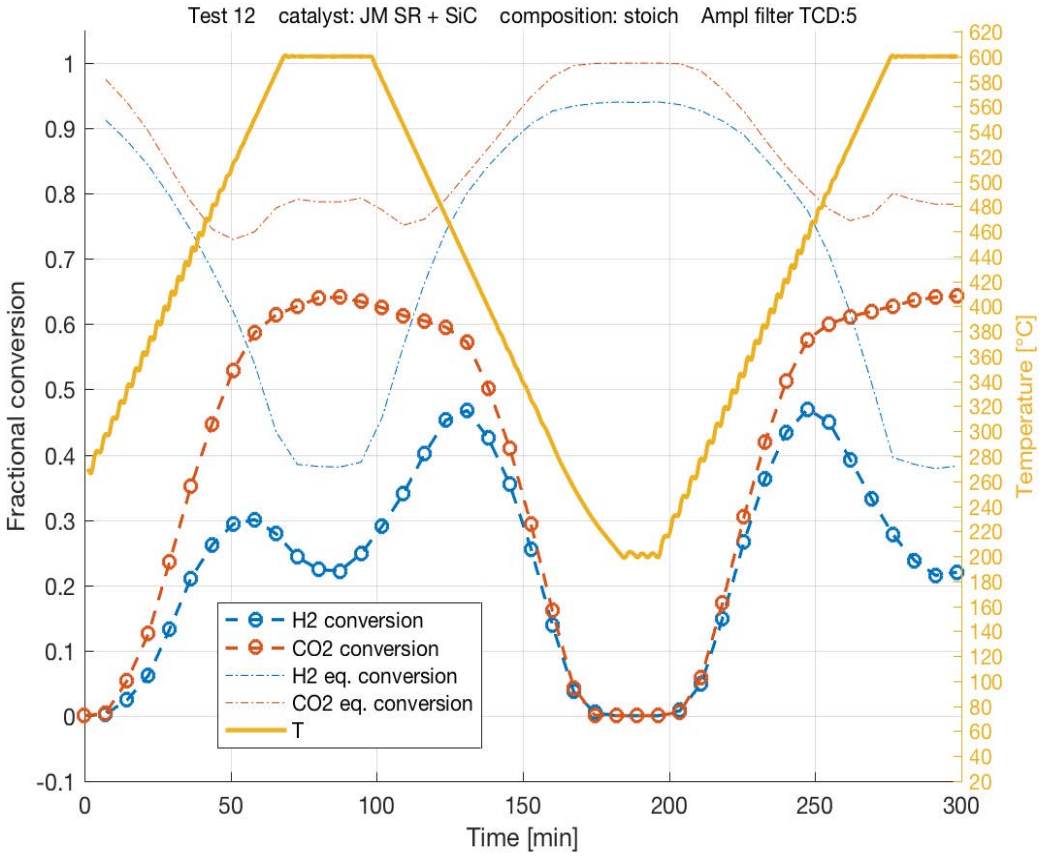

Figure 4.13 *Conversion of hydrogen and CO2 during thermal cycles with GHSV=50000 h-1*

Figure 4.13 also highlights that at high temperatures the conversion of hydrogen decreases, while the one of CO_2 still increases: this is assumed to be due to dry reforming reaction (1.7) that is endothermic and involves the reaction of methane and CO_2 to produce H_2 and CO.

$$CH_4 + CO_2 \leftrightarrow 2H_2 + 2CO \qquad \Delta H_r = 247.3\ kJ/mol \qquad (1.7)$$

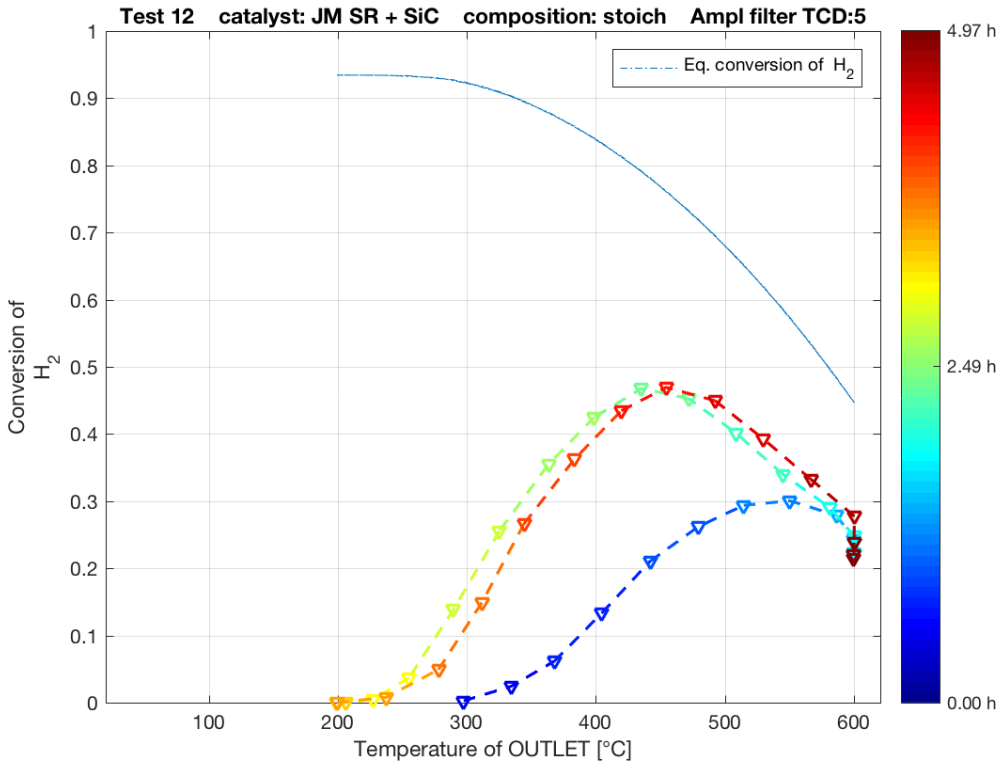

Figure 4.14 *Dependence of hydrogen conversion on temperature in which the first activation phase is visible*

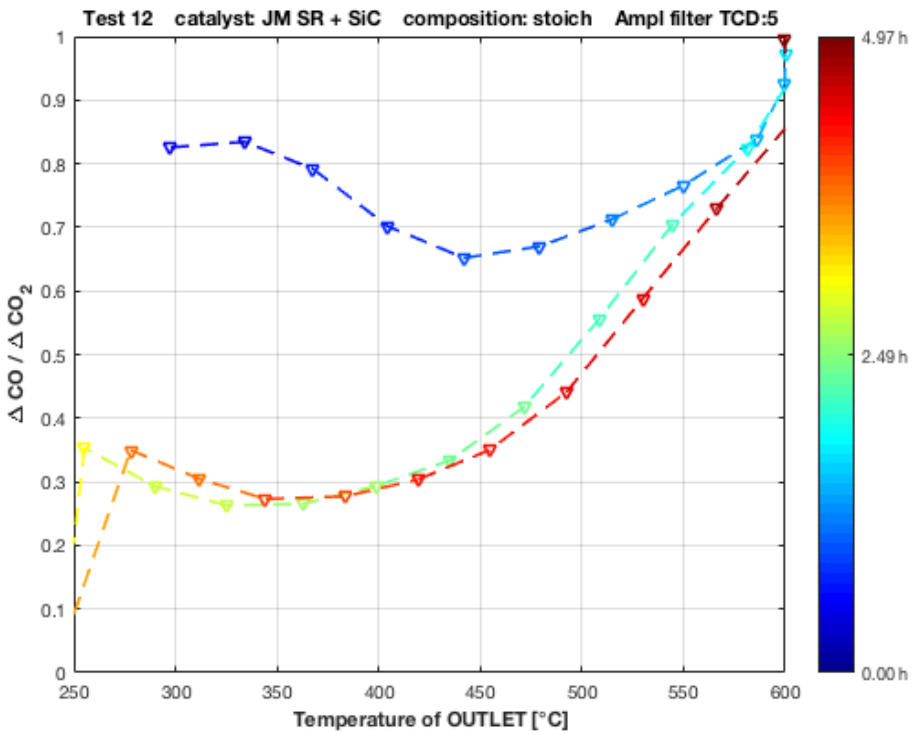

Figure 4.15 *comparison between net variations of CO and CO2, Test 12 - GHSV = 50000h-1*

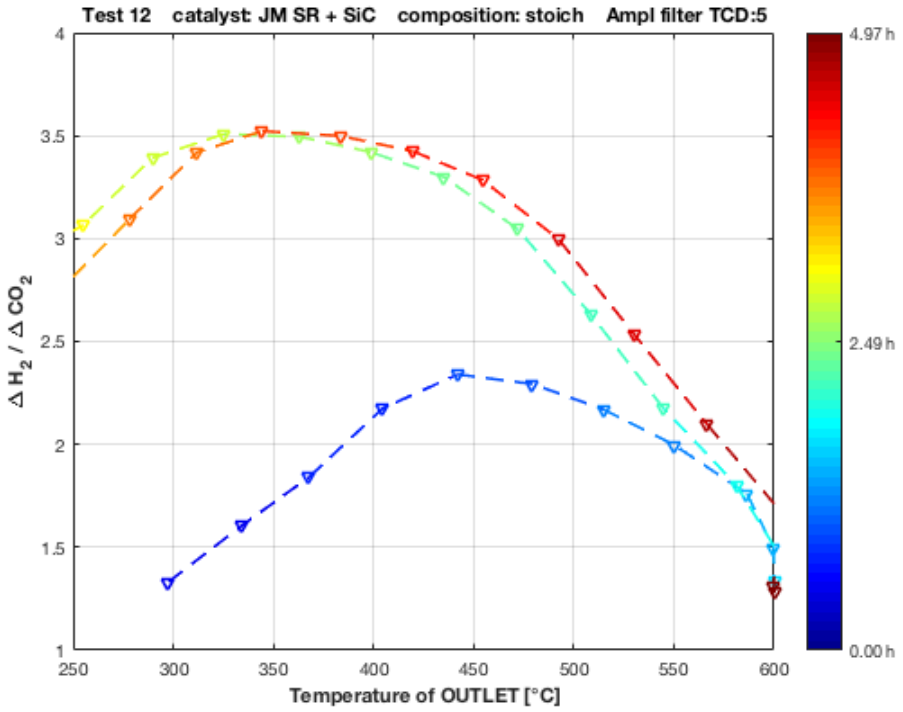

Figure 4.16 *comparison between net variations of H2 and CO2, Test 12 - GHSV = 50000h-1*

Figure 4.15 and **Figure 4.16** report the ratios between net variations of the species that were considered significant. In fact, the variations of hydrogen and CO with respect to that of CO_2 can provide an idea of how much the methanation reaction is predominant compared to the side reactions:

- if the ratio $\Delta H_2/\Delta CO_2$ tends to 4 – that is the stoichiometric ratio of the Sabatier reaction – the methanation is predominant, if the ratio tends to 1 instead the reverse WGS mainly occurs;
- if the ratio $\Delta CO/\Delta CO_2$ increases, then side reactions are occurring (because both DR and reverse WGS produce CO) and the higher is its value the more predominant DR and reverse WGS are with respect to methanation.

Both the figures highlight that while at 350°C the Sabatier reaction is predominant, if temperature increases its contribution dramatically decreases and at 600°C $\Delta H_2/\Delta CO_2$ is almost equal to 1, meaning that the hydrogen consumption almost was only related to reverse WGS. In the temperature range 450°C-600°C the ratio $\Delta CO/\Delta CO_2$ rapidly increase, meaning that the contribution of the side reactions was predominant (at 450°C the 35% of reacted CO_2 produced CO and the same happened with the 70% of reacted CO_2 at 550°C and almost 100% at 600°C).

Figure 4.17 shows all the effects of dry reforming in terms of molar flowrates: at about 600°C both methane and CO_2 are consumed, while molar flowrates of hydrogen and CO increase. Looking at these evidences from a realistic point of view, these results highlight the fact that the process has to be carried out at temperatures always lower than 500°C because high T causes a methane consumption and, consequently, a decreasing in the global efficiency of the process.

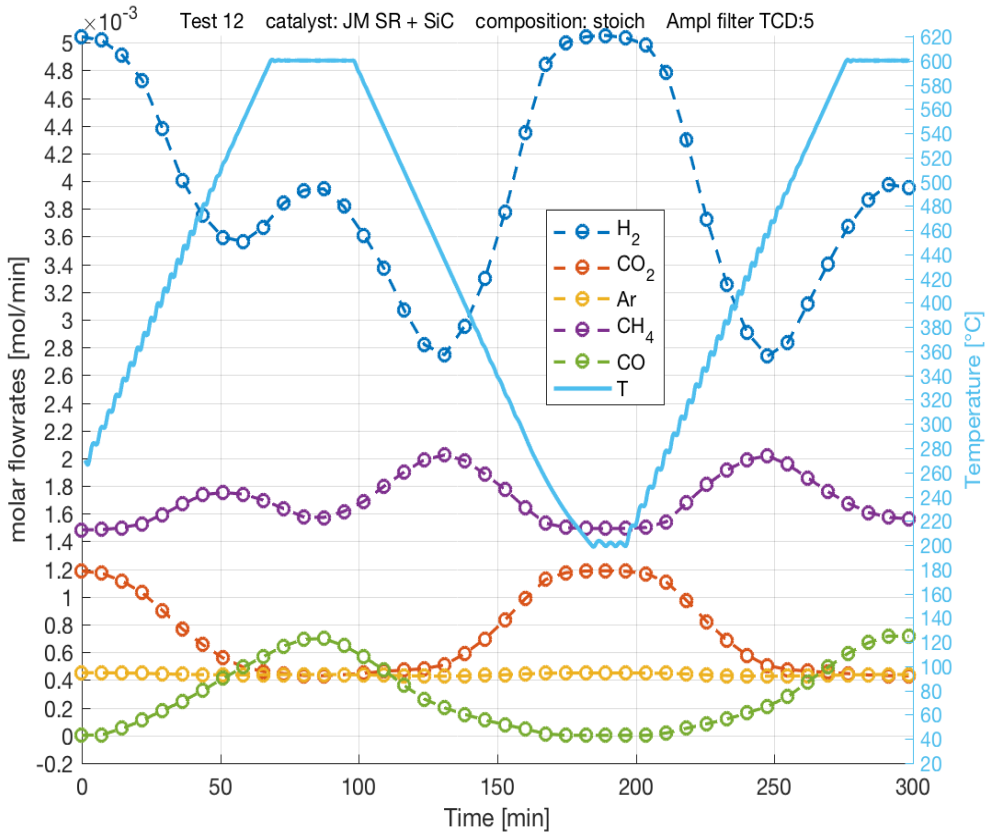

Figure 4.17 *Molar flowrates of all components in a thermal cycle on the Johnson Matthey catalyst. GHSV=50000h-1*

Ramp up / ramp down tests were also useful to verify if changing the residence times (i.e. GHSV) of the reagent mixture in the reactor would change the dependence of the conversion of CO_2 on temperature and, consequently, the efficiency of the process from a realistic perspective. Obviously, in the presence of a fixed amount of catalyst, if residence times increases (i.e. the flowrate decreases) then the time available for contact between reagents and catalyst increases. However, no tests were carried out with too low values of GHSV because too high amounts of catalyst or too low flowrates would decrease the applicability of the process at industrial scale. Therefore, the effect of flowrate was observed through a little decrease in the total molar flowrate, without changing the composition of the inlet mixture, in order to compare conversion of CO_2 with GHSV=50000 and 30000 h^{-1}.

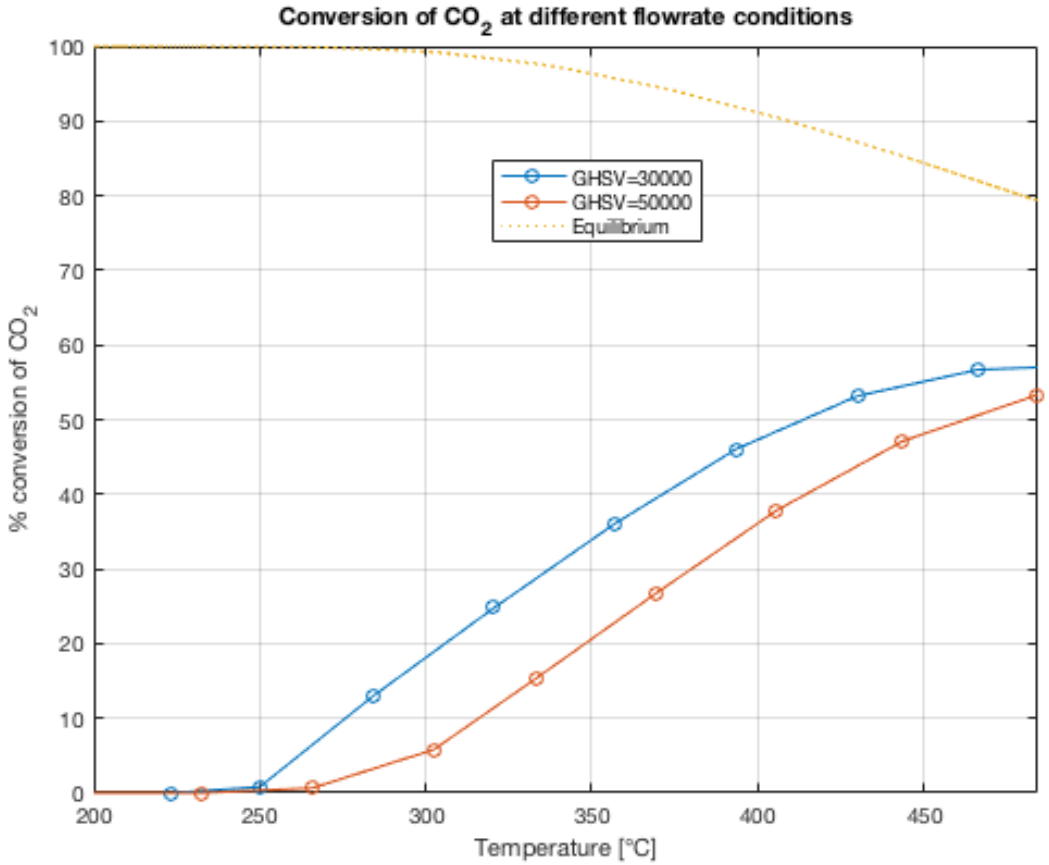

Figure 4.18 *Conversion of CO2 under different flowrate conditions. Tests 13 and 16*

Figure 4.18 shows that a decrease in the molar flowrate causes an increase in the conversion, as expected. However, under these conditions, conversion always remains below 60%: a good result, if we consider that both the presence of methane in the inlet mixture and the low operating pressure are going to decrease conversion, but still not applicable at industrial scale without any other separation process. In fact, a maximum value of the methane molar fraction equal to 35% was observed by converting the molar flowrates of **Figure 4.17** into fractions, vs. 18.7% in the inlet mixture (**Table 3.*4***): even if the molar fraction is almost doubled, it is still not sufficient to be injected into the gas grid and, in particular, it is even smaller than the one in biogas before upgrading. However, note that if the molar fraction of hydrogen is not considered – assuming a downstream hydrogen separation – the methane molar fraction could rise up to 75%: this was indeed a big upgrade in terms of molar fraction too. In **Table 4.*1*** a comparison between methane molar fractions is reported, in which the fractions were rearranged in order to neglect the Argon amount.

Table 4.1 *Comparison between volumetric percentages of methane*

CH_4 volumetric composition	In biogas	In the inlet mixture	After upgrading	Upgraded, no H2	For gas grid
%	55	~20	**~40**	**~75**	>90

The repeatability of the experimental tests

Since comparisons were done between different tests in non-stationary conditions, it was important to verify that the tests were repeatable, which means that the system always responds in the same way to some changes in the input variables.

Both conversions of H_2 and CO_2 were observed during some thermal cycles in which the reactor temperature was continuously changed from 250 to 500°C with a rate of 5°C/min.

As shown in **Figure 4.20** and **Figure 4.19**, conversion always shows the same dependence on temperature after the first heating cycle in which the activation of the catalyst occurs, and completes at T=500°C.

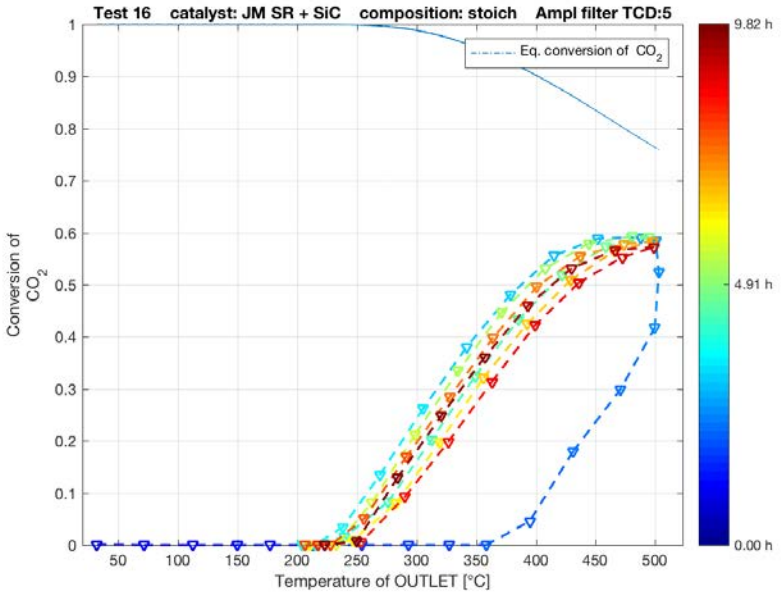

Figure 4.20 *Repeatability of CO2 conversion during thermal cycles between 250 and 500°C, GHSV=30000h^{-1}*

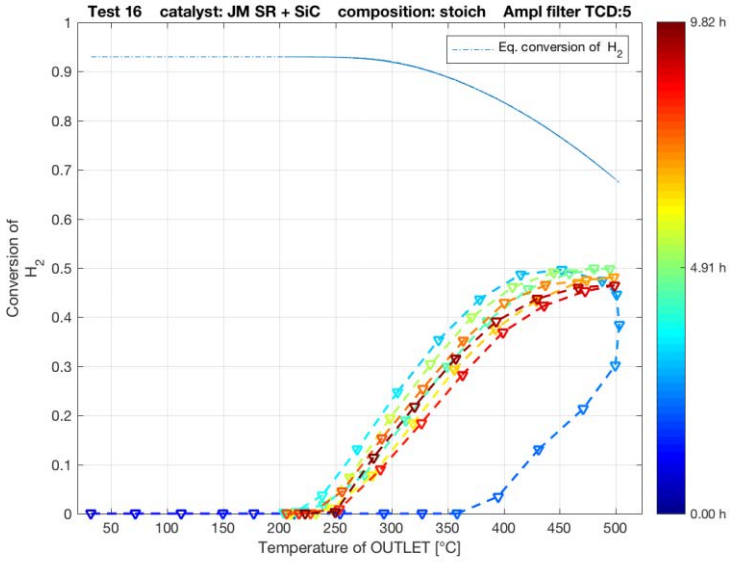

Figure 4.19 *Repeatability of H2 conversion during thermal cycles between 250 and 500°C GHSV=30000h^{-1}*

4.3.1.4 Isothermal tests on pre-reduced catalyst: yield and thermal considerations

Once verified that pre-reduction of catalyst was necessary, isothermal tests were carried out in order to evaluate the yield of the process at steady state.

The following tests were all carried out with GHSV=30000 h^{-1}, since it was considered to be still quite high with respect to the experimental tests already available in literature and more industrially interesting at the same time.

A good starting point for operating temperature was thought to be 450°C since it showed good performances in ramp up / ramp down tests.

The tests showed interesting results, since both the molar fraction of methane (**Figure 4.21**) and consequently its yield (**Figure 4.22**) are near to the equilibrium condition (the yield reached the 80% of the equilibrium value, **Figure 4.23**) at relatively low temperatures (450°C); moreover, while conversion of CO_2 remained quite constant among the temperature range between 450 and 600°C, H_2 conversion reached its highest value (50%) at 450°C (**Figure 4.24**). The same test was carried out without methane in the inlet mixture too, but keeping all the other operating parameters unvaried: the result was very interesting, since it was identical in terms of yield to

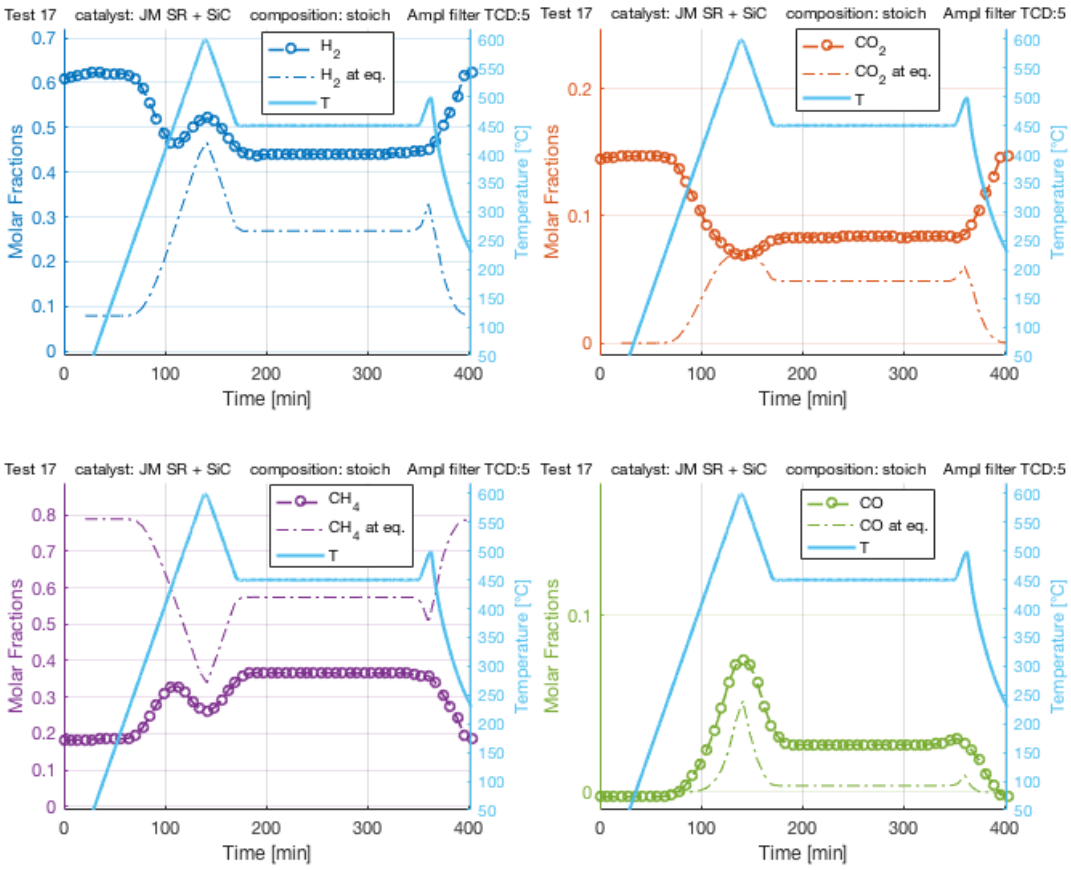

Figure 4.21 *Molar fractions of all species compared to those at the equilibrium conditions in an isothermal test at 450 °C with GHSV=30000 h-1*

that containing methane in the reacting mixture and demonstrated the possibility of directly upgrading biogas with no yield losses (**Figure 4.25**).

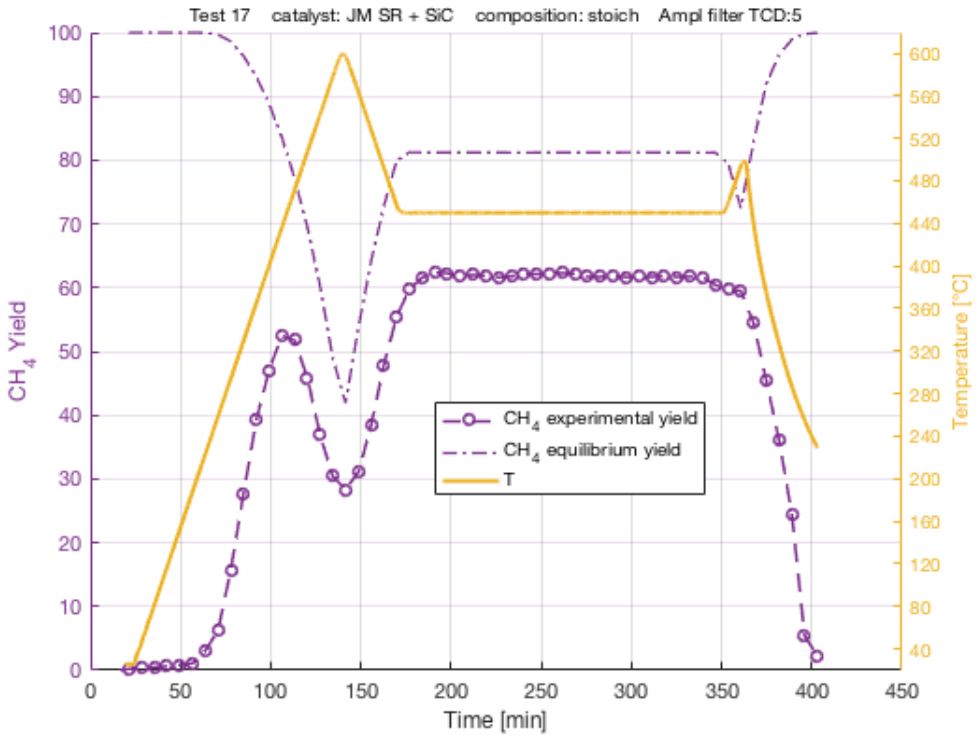

Figure 4.22 *Yield of methane compared to the equilibrium one during an isothermal test at 450 °C*

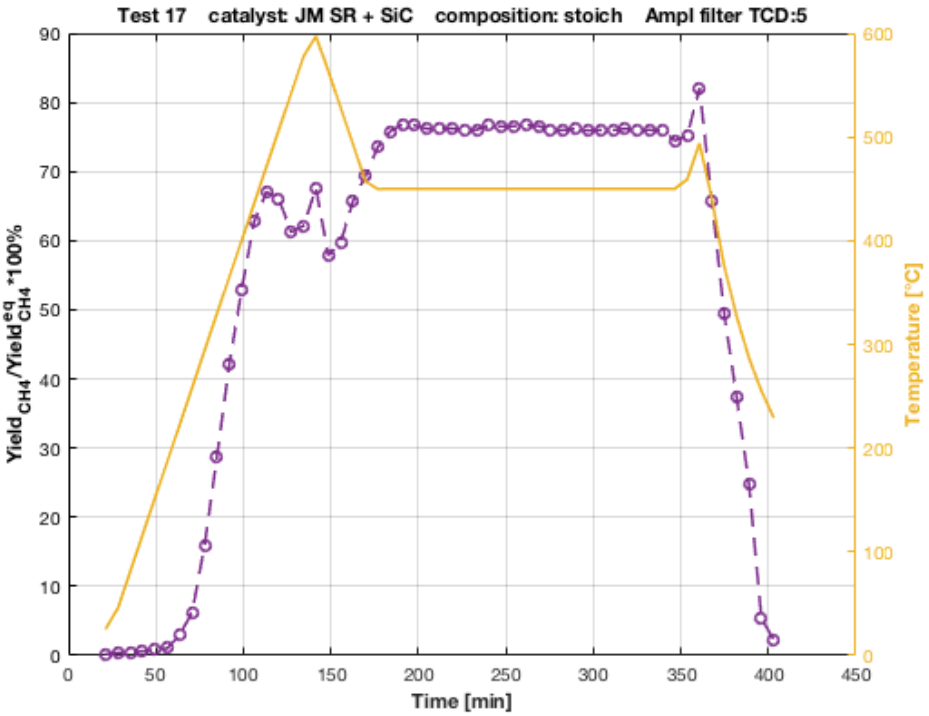

Figure 4.23 *Ratio CH4 yield to CH4 yield at equilibrium at 450°C*

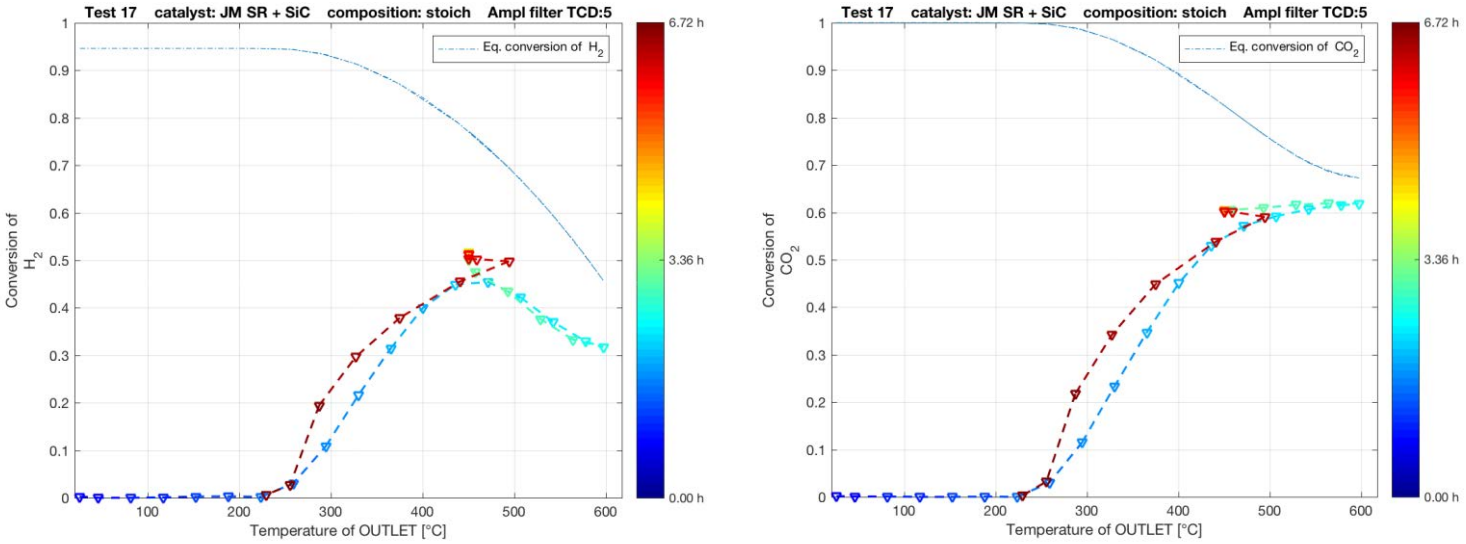

Figure 4.24 *H2 (on the left) and CO2 (on the right) conversions behaviour with temperature compared to the ones at equilibrium during an isothermal test at 450°C*

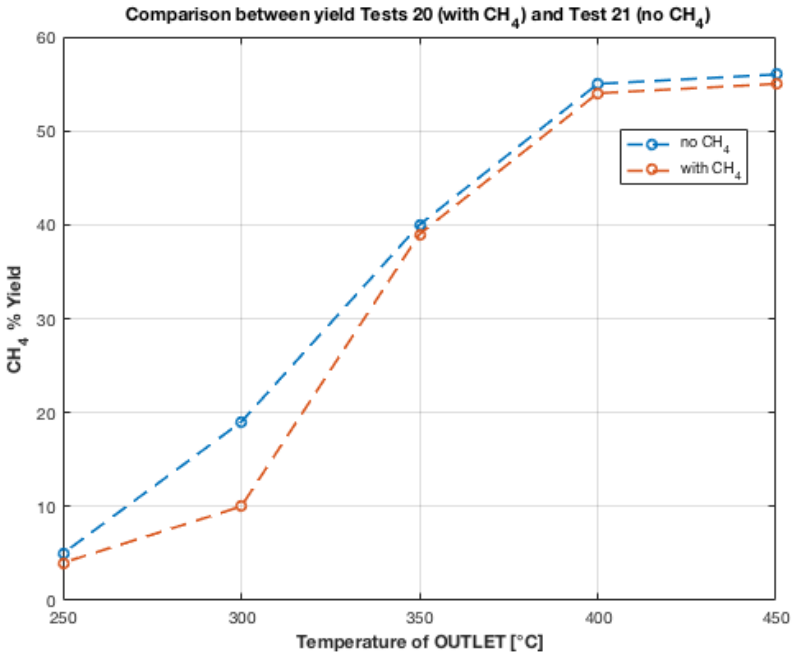

Figure 4.25 *Difference in methane yield between an inlet mixture reflecting biogas composition and a mixture with no methane but Sabatier stoichiometric H2/CO2 ratio*

In **Figure 4.26** the convergence between kinetics and thermodynamics – calculated as the difference between the equilibrium and the experimental conversions – is reported:

- the difference is going to rapidly decrease if temperature increases, meaning that while kinetics favors the conversion of reagents the equilibrium conversion is limited by the thermodynamics;
- after the first heating phase the difference is even 15% smaller;
- the difference ranges from 50% to 20% in the temperature interval between 350°C and 450°C.

These evidences highlight the necessity to find a catalyst (or better operating conditions) that shows higher activity at lower temperatures in order to increase the velocity of convergence between kinetics and thermodynamics.

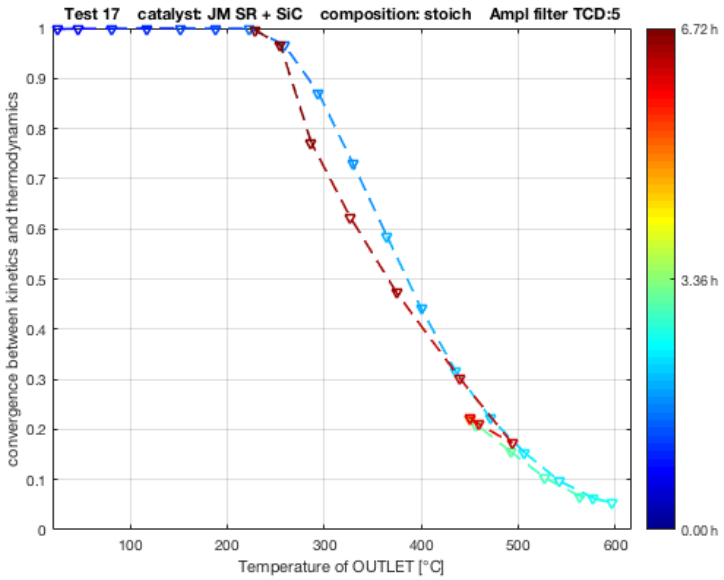

Figure 4.26 *Convergence between kinetics and thermodynamics, GHSV=30000h-1*

From a realistic perspective, the electrical heating supplied to the reactor plays a fundamental role since it involves an increase in the operating costs. However, since the methanation reaction is exothermic, this contribution to the global costs of the process could be minimized even if both water vapor (that is produced by the Sabatier reaction) and methane (that is fed to the reactor and produced at the same time) act as thermal flywheels.

For this reason, the electrical heating of the furnace was observed in order to analyze the effect of the heat provided by the conversion of the reagents: the OMRON controller generates a text file in which not only all temperatures are collected, but also other parameters such as the internal setpoint of the controller or the manipulated variable (MV), which can give an idea of how much electricity is supplied to the furnace and is expressed as a percentage.

Theoretically, MV should be 0 if the heat provided by the reaction is equal to that necessary for keeping the gas mixture at the operating temperature: as shown in **Figure 4.27**, the electrical heating was never turned off even if some conversion occurred in isothermal conditions.

This suggested that perhaps the presence of SiC was redundant since H_2O and CH_4 act as thermal flywheels and their contribution could be sufficient for avoiding hotspot in the reactor even without using SiC. For this reason, another test was carried out with identical operating conditions but no SiC was used as diluent and no relevant differences were observed in the methane yield (**Figure 4.28**) nor in the manipulated variable (**Figure 4.29**).

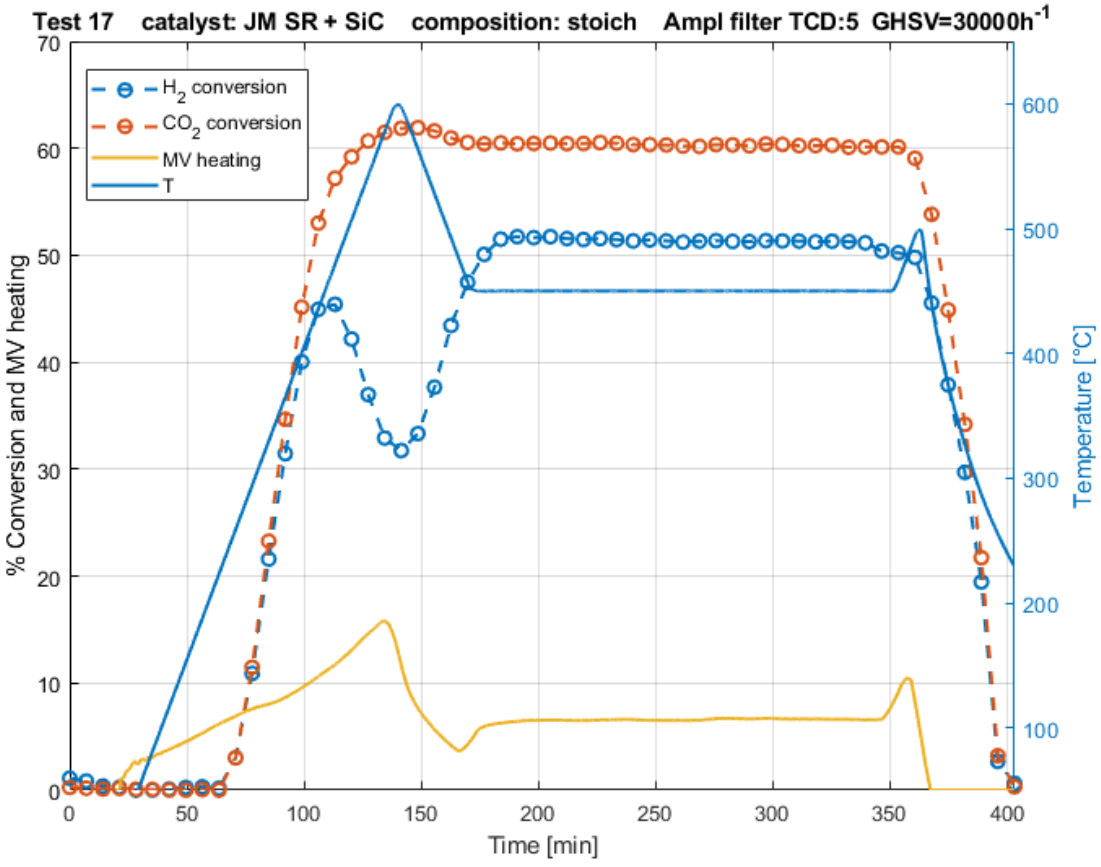

Figure 4.27 *Conversion of H2 and CO2 and electrical heating provided by the furnace during an isothermal test at 450°C*

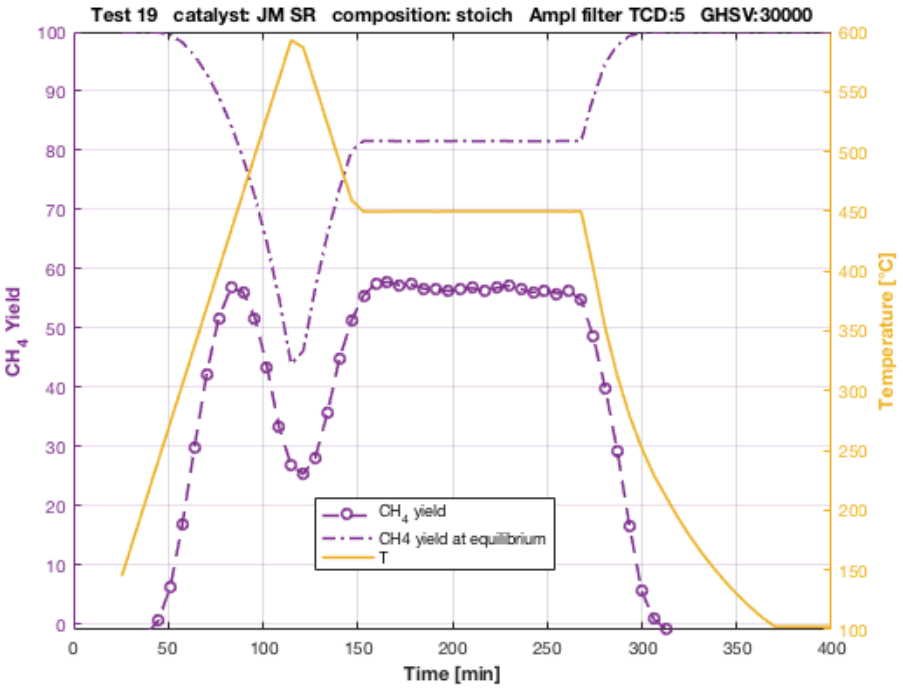

Figure 4.28 *CH4 Yield in a repetition of Test 17 with no SiC as inert*

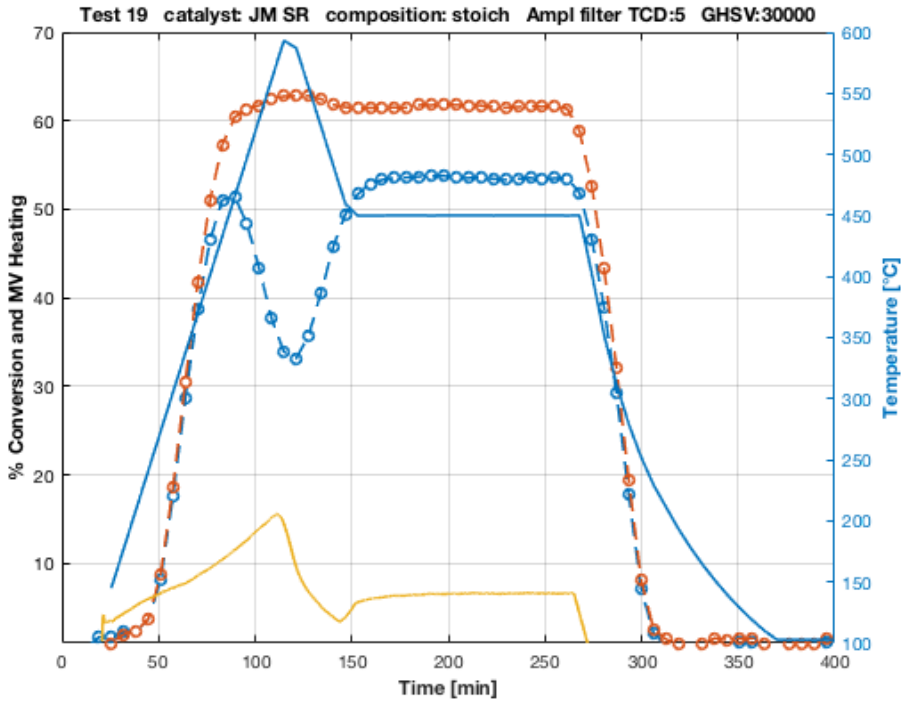

Figure 4.29 *Conversions and MV in a repetition of Test 17 with no SiC as inert*

4.3.2 Tests with two thermocouples

The unnecessity of using SiC is indeed an advantage, since it allows to use less material with the same GHSV. However, no changes in the electrical heating were observed even if SiC was removed. A more detailed study was then needed on the temperature profile in the reactor in order to understand the extent of the heat delivered by the reaction.

Another thermocouple (with diameter d=1/8'') was placed into the reactor so as to ensure the measurement of the temperature at the inlet (the thermocouple was put inside the reactor in contact with a quartz wool layer with the height of 5mm): since the reaction is exothermic, some difference in the measured temperatures was expected and, in particular, the outlet temperature was expected to be higher than the inlet one. However, as shown in **Figure 4.30**, no difference was observed even if CO_2 was converted: this was probably linked to the large diameter of the thermocouples with respect to the one of the reactor; for this reason the temperatures were most likely measured in the area adjacent to the reactor wall, which being heated by the furnace was at a higher temperature and uniform along the wall.

The latter motivations led to replace both the thermocouples with two K-type thermocouples having smaller diameter (1/16'') that were used in all the following tests.

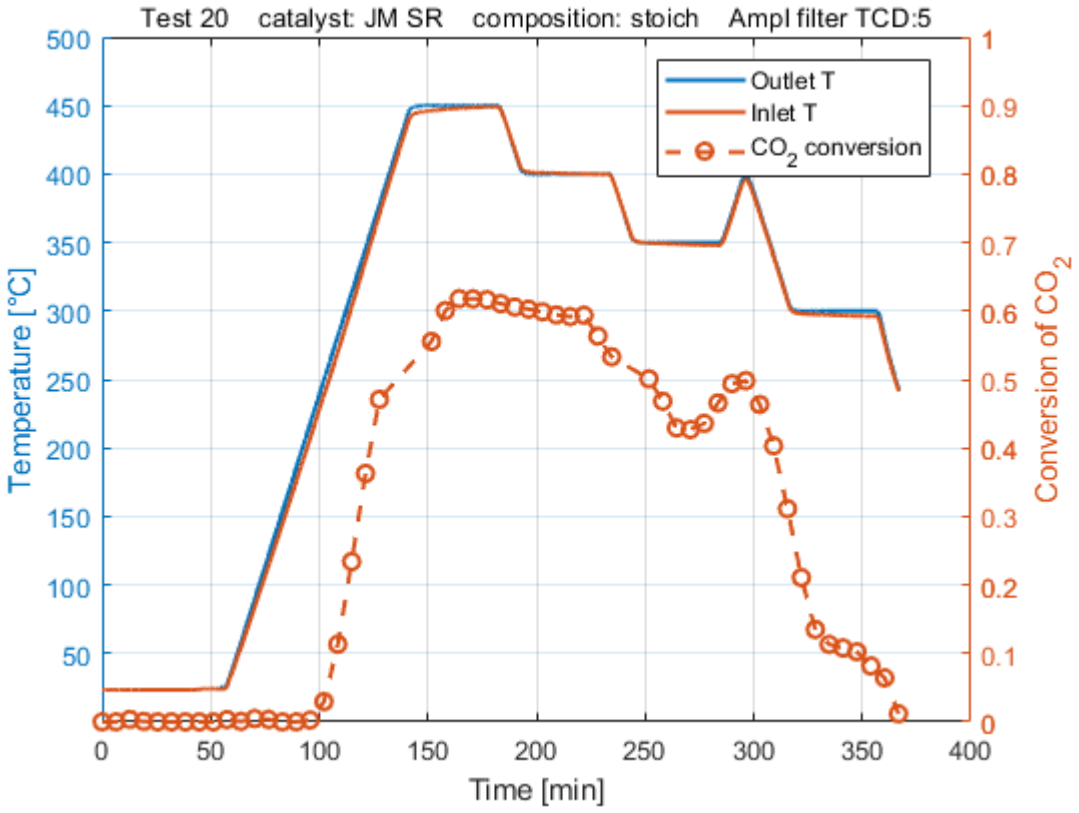

Figure 4.30 *Outlet and inlet temperature during an experimental test on Johnson Matthey catalyst*

4.3.2.1 Ramp up / ramp down test

Since the previous observations could be compromised by this change in the experimental setup due to possible errors in temperature trends, a test was needed to verify the reliability of the tests that were already carried out. For this purpose a ramp up / ramp down test was carried out and, as expected, some temperature difference between the inlet and the outlet sections could be observed when conversion began to rise (**Figure 4.31**) and it was maximum (~20°C) at temperatures ranging from 350°C to 400°C.

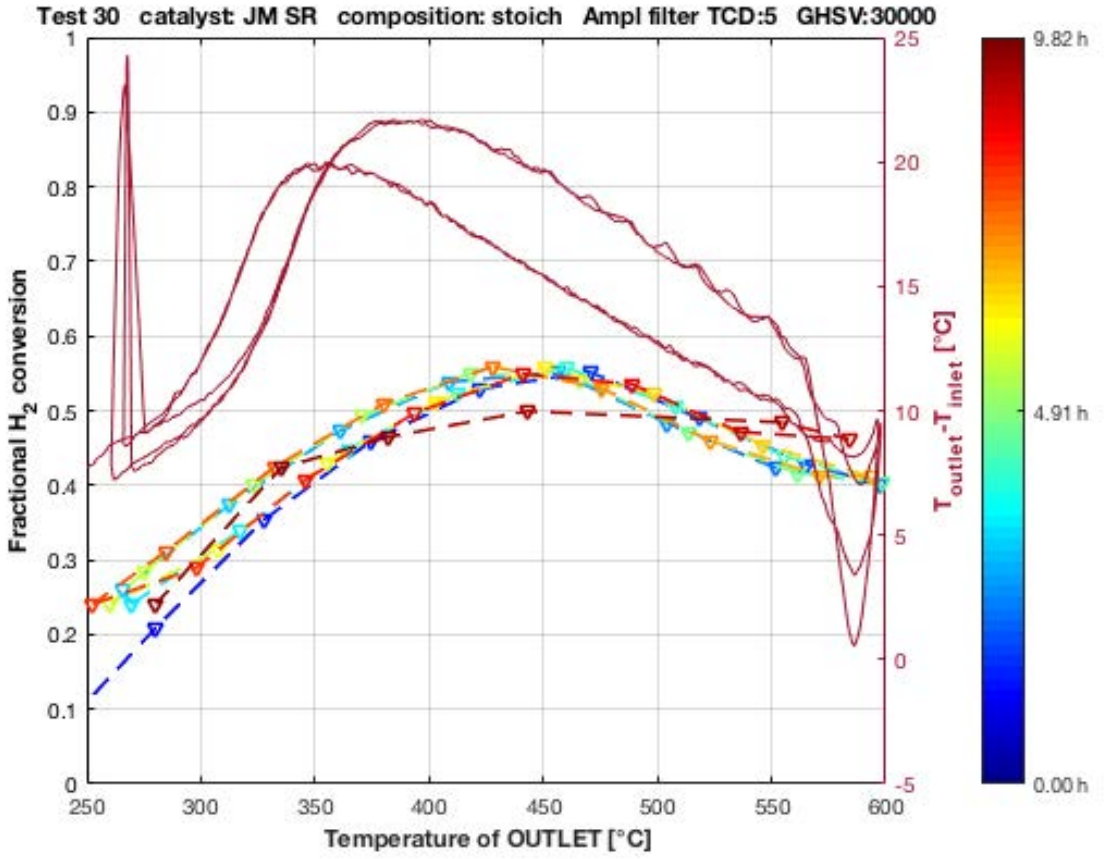

Figure 4.31 *Difference in temperature between the inlet section and the outlet one during a ramp up / ramp down test*

Moreover, the test showed very similar behavior to the previous tests: the conversion dependence on temperature, the methane production and the effects of dry reforming at 600°C (visible in the decreasing of hydrogen conversion, **Figure 4.31**): in fact, at temperatures higher than 400°C the difference in temperatures between the outlet and the inlet section decreases because of the endothermic side reactions. This was verified by observing the ratio between the net variations of CO and CO_2: if side reactions occur (i.e. dry reforming, reverse WGS), then the ratio had to increase due to CO production (**Figure 4.32**).

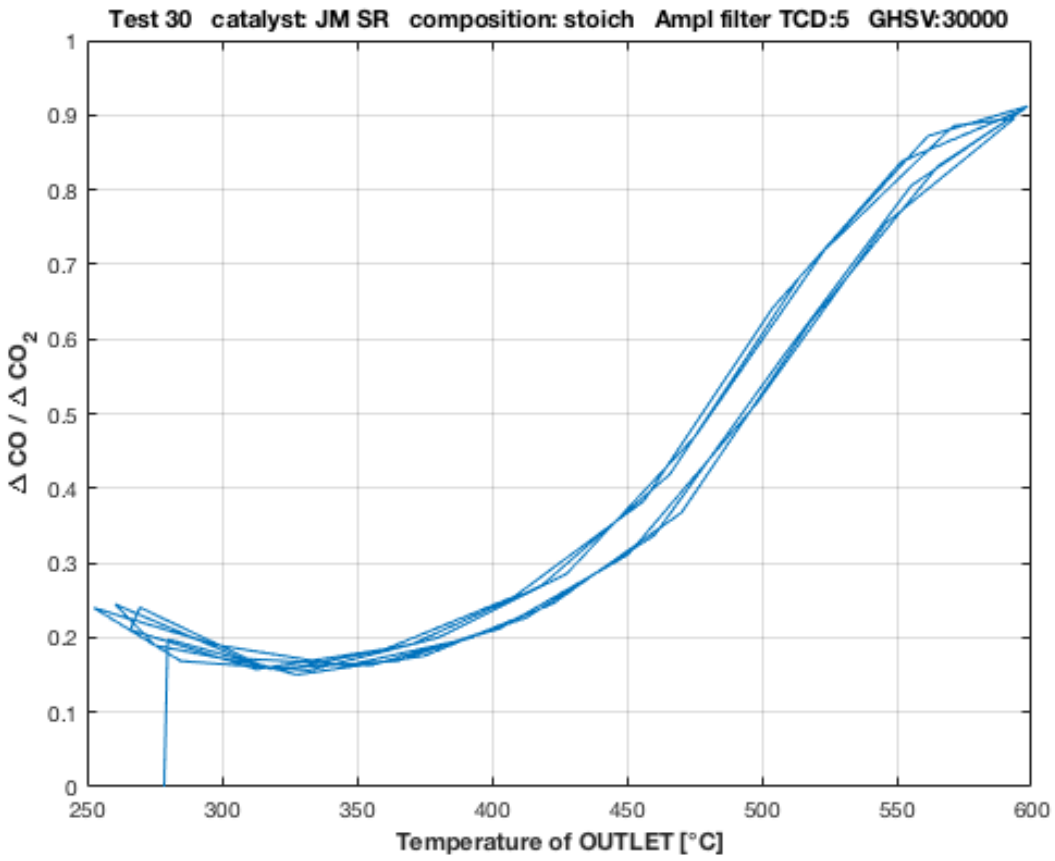

Figure 4.32 *The ratio between net variations of CO and CO2 increases with temperature due to side reactions (DR, reverse WGS)*

4.3.2.2 Isothermal tests

Some isothermal tests were carried out with GHSV=30000 h^{-1} to evaluate the steady-state performance and the power provided to the reactor under this new configuration for thermal control.

Even if results were slightly different, they were still very similar to the previous tests and in no case the heat provided by the reaction was sufficient to maintain the set point temperature.

Moreover, with such high value of GHSV the methane yield was high but still to improve and this means that a high fraction of hydrogen was still present in the product mixture: in fact, these results showed that the methane molar fraction was never really "upgraded" (**Table 4.2**). The better results were obtained at 400°C, with a good methane yield (60%) and high methane content (49%), in fact it was the only operating condition that allowed the methane molar fraction to be very near to the typical one of biogas. However, consider that if hydrogen was separated from the outlet mixture than the CH_4 molar fraction would have resulted much higher than the one in biogas (84.5% vs 55%, by 400°C methanation).

Table 4.2 *Results obtained in isothermal tests with stoichiometric inlet mixture and GHSV=30000 h^{-1}*

Temp.	Yield	% H_2	% CO_2	MV	Molar %			Molar %, no H_2	
°C	CH_4 %	conversion	conversion	%	H_2	CO_2	CH_4	CO_2	CH_4
350	60	55	55	4	46	12	41	22	77
400	60	65	65	5	40	9	49	15	**84.5**
450	50	60	65	6.5	43	9	45	16	83

Even if a better thermal control was expected and some difference in the temperatures could clearly be observed (**Figure 4.33**) in isothermal conditions, in no case MV was null and its values was very similar to those of the previous tests: this was probably linked to the heat dispersion, that provided for a temperature decrease of the product mixture in the quartz wool layer. The latter observation can certainly explain why the energy supply was never null even if the reaction is exothermic and, at the same time, could demonstrate the feasibility of the process: at industrial scale, in the absence of the quartz wool, it would be simply necessary to measure the temperature in the zone very close to the catalyst with no heat-dispersion layers.

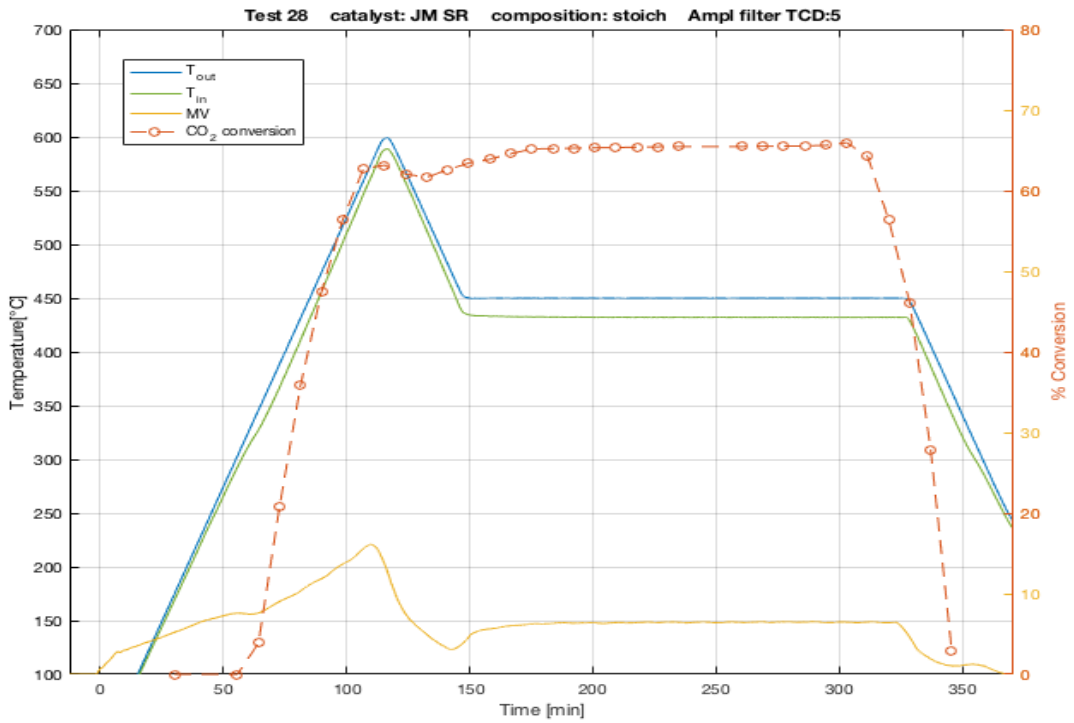

Figure 4.33 *Difference in temperature between the inlet section and the outlet one during an isothermal test, GHSV=30000*

Isothermal test with GHSV = 15000 h^{-1}

Another isothermal test at 400°C was carried out with a lower value of GHSV, set equal to 15000h^{-1}, since it was supposed to be still applicable at industrial scale because the real density of the catalyst was probably higher than that assumed. The result was interesting since conversion of both hydrogen and CO_2 reached 70%, which was very near the equilibrium one (80%), but still similar to the results obtained with GHSV=30000h^{-1}. In particular, the observed methane selectivity was very near the maximum value of 1 (**Figure 4.34**) while that of CO only was high (0.55) during the catalyst activation phase in which 650°C were reached (**Figure 4.35**). A comparison of the molar fraction of all components between the two operating conditions is reported in **Table 4.3**. In the table the upgrading efficiency U.E. (4.2) is reported too: it was defined so as it can provide an idea of how much the methane-to-carbon dioxide molar ratio has been upgraded.

In these conditions, the methane-to-carbon dioxide molar ratio was almost five times higher than that in biogas and if the hydrogen fraction is not considered the molar fraction of methane rises to 85%, (i.e. 1.5 times higher than that in biogas).

$$U.E. = \frac{x_{CH_4}^{out}}{x_{CO_2}^{out}} * \frac{x_{CO_2}^{biogas}}{x_{CH_4}^{biogas}} = \frac{x_{CH_4}^{out}}{x_{CO_2}^{out}} * \frac{0.45}{0.55} \qquad (4.2)$$

Table 4.3 *Comparison between U.F. and molar composition in different temperature and flowrate conditions*

GHSV [h^{-1}]	T °C	% H_2 conversion	% CO_2 conversion	Molar %			U.E.	Molar %, no H_2
				H_2	CO_2	CH_4		CH_4
30000	400	65	65	40	9	49	4.46	84.5
15000	400	70	70	37	9	53	**4.83**	**85**

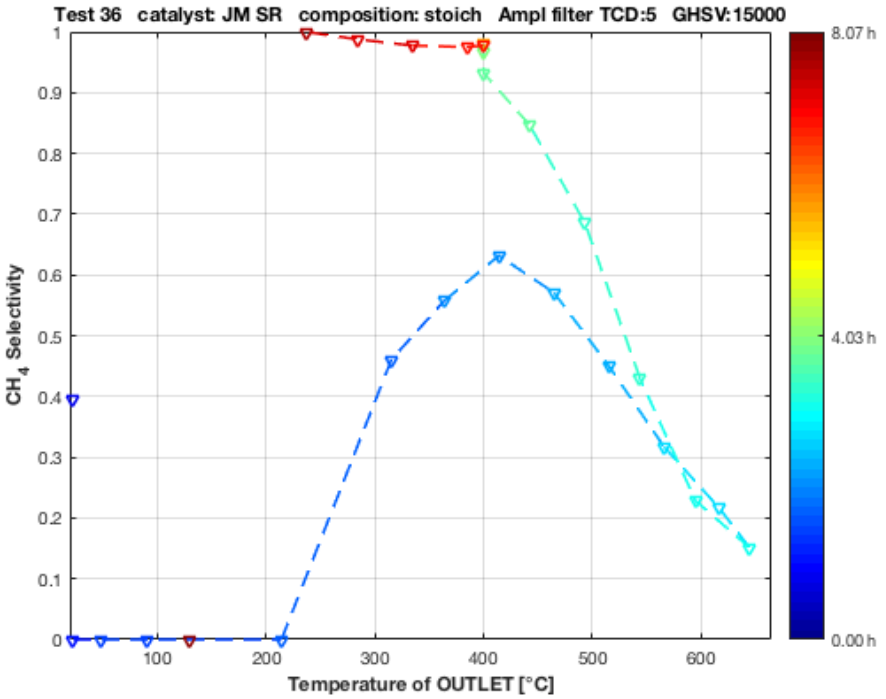

Figure 4.34 *Methane Selectivity during an isothermal test at 400°C in which the catalyst activation phase and the cooling phase are visible too*

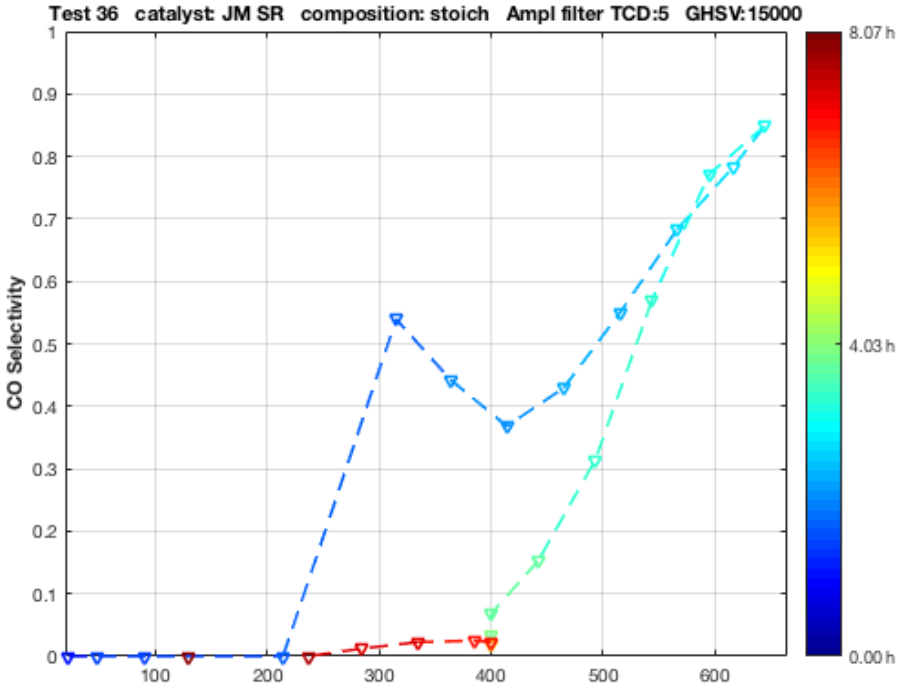

Figure 4.35 *CO Selectivity during an isothermal test at 400°C in which the catalyst activation phase and the cooling phase are visible too*

Dependence on temperature and flowrate

The last tests (37 at 450°C, 38 at 400°C, 39 at 350°C) on this catalyst were carried out to evaluate its performance dependence on the residence time τ (4.3) by simply varying the total flowrate and keeping unvaried the molar composition in different isothermal conditions. The tests were carried out in a fixed-bed configuration with 400 mg of JM catalyst and the flowrates reported in **Table 4.*4***.

$$\tau = 60 * GHSV^{-1}\ [min] \tag{4.3}$$

Table 4.4 *Flowrates used in Tests 37, 38, 39 to evaluate yield and selectivity in different isothermal conditions*

Flowrate [ml/min]	75	100	133	200	260
τ*10^3 [min]	5.3	4	3	2	1.5

The results showed that the system has a very similar behaviour in a temperature interval ranging from 350 to 400°C: even if lower temperatures would favour the thermodynamics – and consequently the methane yield – under these conditions the kinetics were penalized (**Figure 4.36**). The latter result is indeed very interesting: in fact, operating at 350°C would on the one hand imply minor costs related to the pre-heating phase and, on the other, would even increase the methane yield in the presence of a hot-spot with a temperature increase of up to 400°C.

At higher temperatures (450°C) instead the equilibrium would strongly penalize the yield, making it even smaller than the experimental one observed at lower temperatures (350°C-400°C). This is certainly linked to some loss in the selectivity: while at low temperatures the selectivity was always very high (up to 99%) and near the equilibrium one, at 450°C it rapidly decreased when the residence time decreased (**Figure 4.37**).

As expected, the lower was the temperature, the nearest was the selectivity to the equilibrium value (**Figure 4.39**). Moreover, the highest temperature allowed the experimental yield to be the nearest to the equilibrium while as temperature decreased the kinetic contribution was predominant (**Figure 4.38**). The best results were obtained at 400°C and $\tau = 5.3 * 10^{-3}$ min, since the yield almost was equal to 70% and reached the 90% of the equilibrium value: in these conditions, the molar composition of methane in the outlet mixture was 87,5% if hydrogen and argon are not considered, with an upgrading efficiency equal to 5,7 that is indeed a huge upgrade of the biogas methane content.

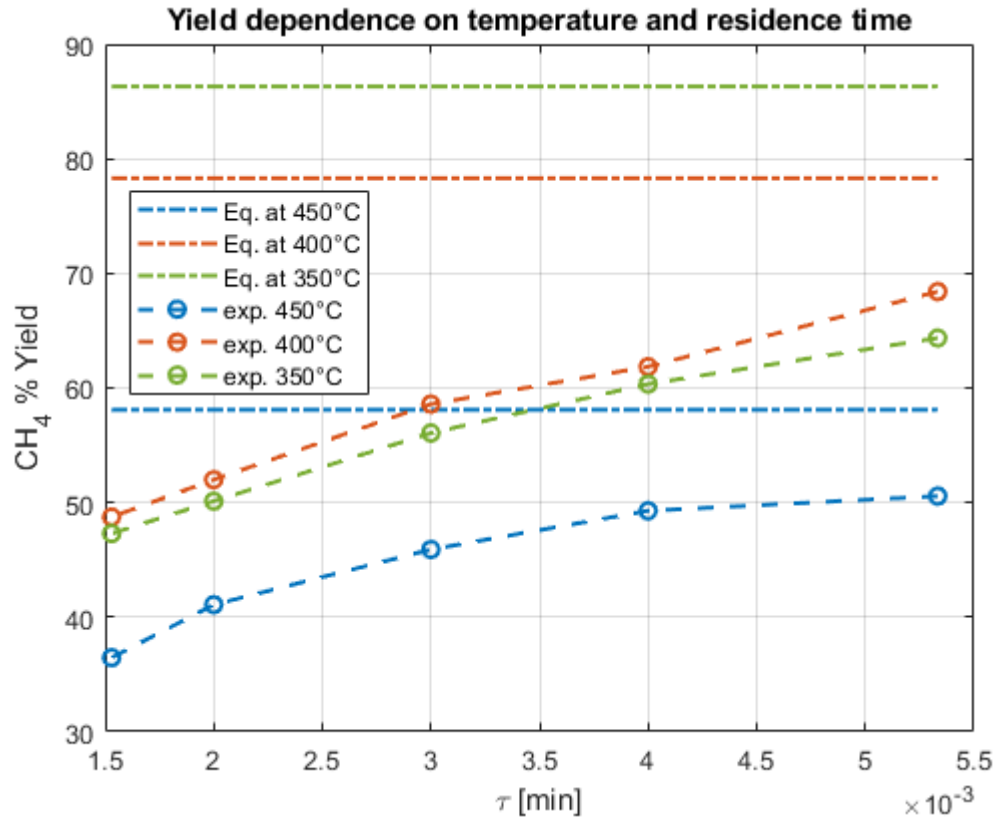

Figure 4.36 *Methane yield dependence on temperature and residence times*

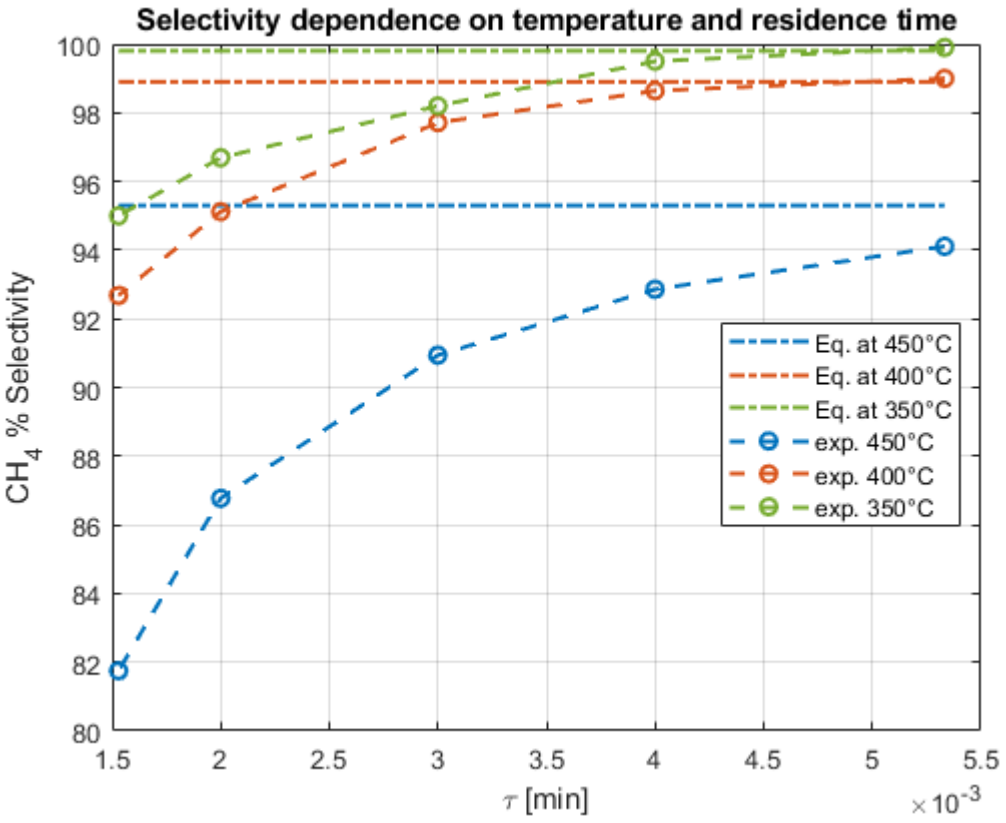

Figure 4.37 *Methane selectivity dependence on temperature and residence times*

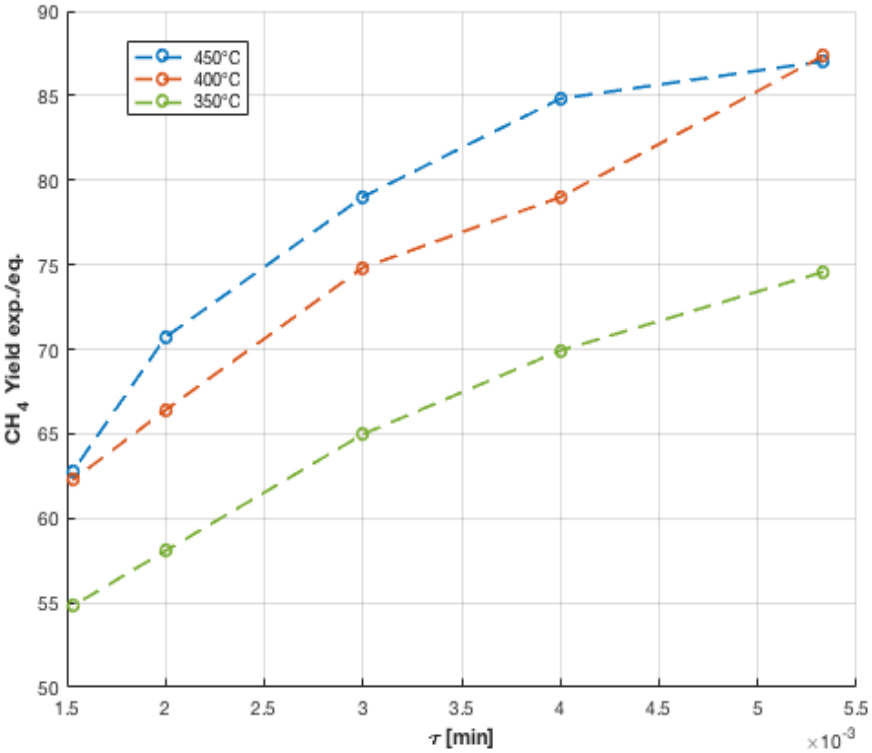

Figure 4.38 *Ratio between experimental and equilibrium methane yield*

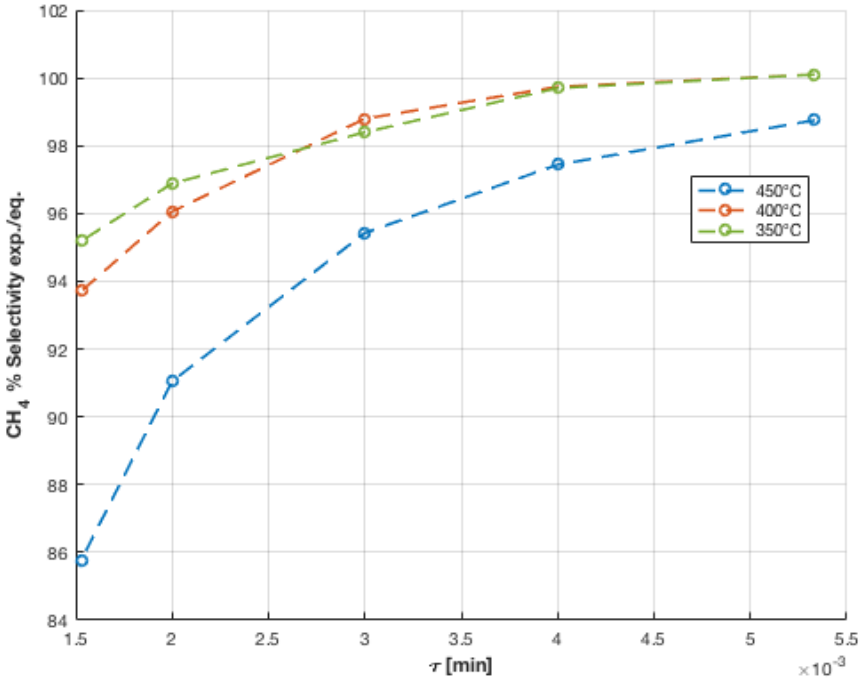

Figure 4.39 *Ratio between experimental and equilibrium methane selectivity*

4.4 Self-made NiO/Al_2O_3

Since a cheap and easy process was desired in order to simulate a realistic perspective of applicability, an experimental investigation was carried out on a self-made catalyst that should be simple to produce and as cheap as possible. For this purpose, Al_2O_3 grains provided by CTS were used for the preparation of the nickel-based catalyst through the wet impregnation technique.

However, the catalyst showed weak performance and was poisoned during its activation phase, thus demonstrating the strong dependence of the catalyst on the presence of impurities.

4.4.1 Ramp up / ramp down test

A preliminary ramp up / ramp down test showed different behaviour with respect to the previous tests: in fact, in the very first heating phase it showed some catalytic activity towards the methanation reaction that rapidly decreased when temperature increased (**Figure 4.40**); during the following thermal cycles not only no methane production was observed, but it seemed to be even consumed (**Figure 4.41**): for this reason, both reverse water gas shift and dry reforming were probably occurring.

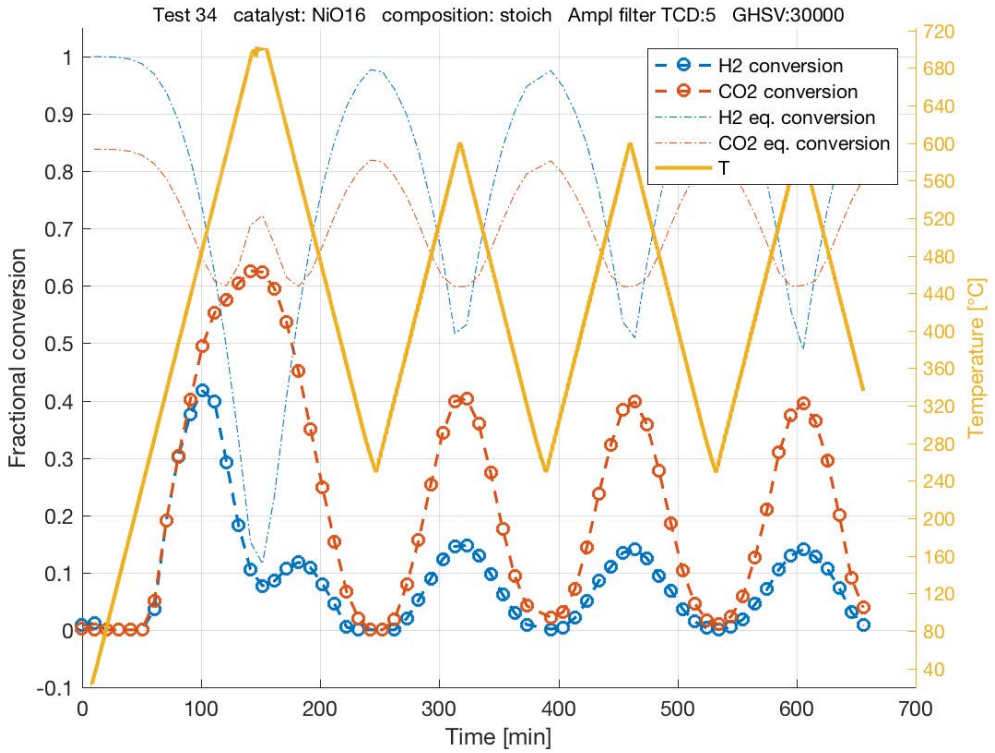

Figure 4.40 *Hydrogen and CO2 conversion dependence on temperature during a ramp up / ramp down test on NiO16*

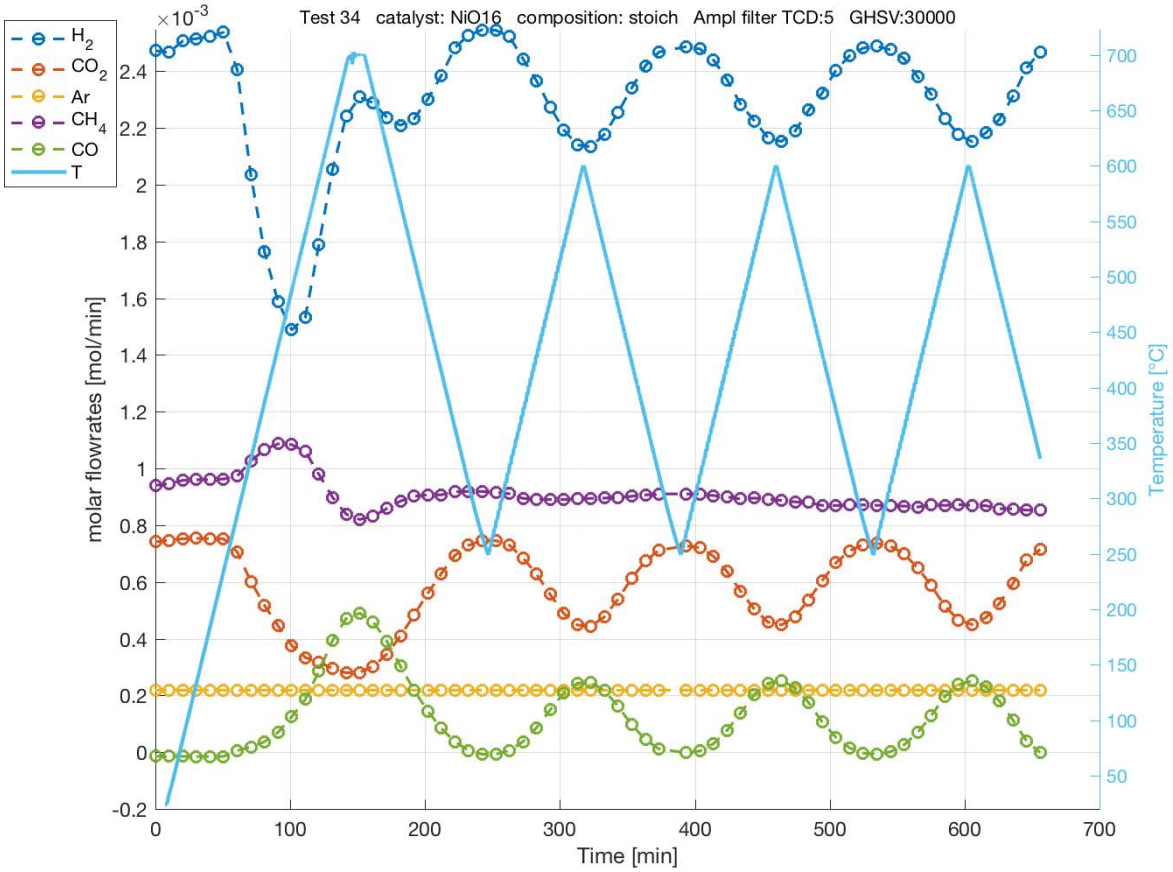

Figure 4.41 *Molar flowrates of all components in the product mixture leaving the reactor in a ramp up / ramp down test on NiO16*

4.4.2 Isothermal test

An isothermal test was carried out in which the catalyst was first pre-heated to higher temperatures: as the ramp up / ramp down test already showed, no methane was produced but some consumption occurred instead (**Figure 4.42**). For this reason, the catalyst was supposed to be poisoned in the previous ramp up / ramp down test and no further tests were carried out.

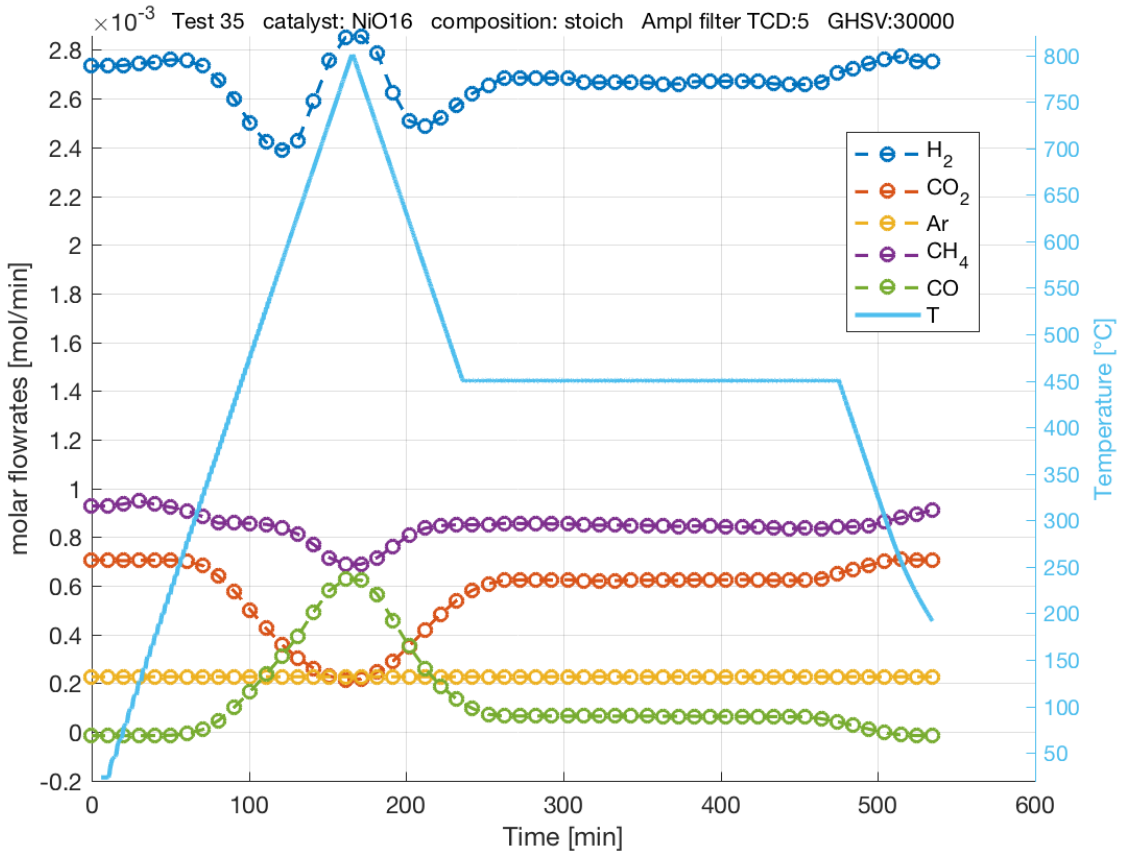

Figure 4.42 *Molar flowrates of all components during an isothermal test at 450°C on NiO/Al2O3*

CONCLUSIONS

During this work different tests at atmospheric pressure were carried out to evaluate the performances of different catalysts towards the Sabatier reaction, with the aim of exploiting a well-known reaction to enhance the methane content in biogas.

The effects of residence times and temperatures on methane yield and selectivity, as well as on CO_2 and hydrogen conversions, were observed.

The catalyst showing the most promising activity was the JM nickel-monoxide: after an activation phase at high temperature of the catalyst – always performed with the reacting mixture containing 60%vol. hydrogen – the catalyst showed the possibility of converting the 70% of the biogas CO_2 to methane, without the necessity of a preliminary separation of the reagents.

A preliminary observation on the composition of the mixture leaving the reactor led to think that – although good results were obtained in terms of conversion and yield – in no case seemed to be the methane molar fraction high enough for the product mixture to be directly injected into the gas grid. This effect was certainly related to the decrease in the total number of moles, causing the contribution of the unreacted H_2 and CO_2 molecules to be non-negligible in the final composition.

However, in all the tests a very promising result could be observed: the molar methane-to-carbon dioxide ratio in the product mixture was higher with respect to the one in biogas and in particular it was almost 6 times greater in the case of a proper temperature and residence time combination.

The latter observation could lead to design an ad-hoc process which should use a membrane for the hydrogen separation from the product mixture:

- The hydrogen could be recycled back to the inlet section;
- The hydrogen supply for the steady-state operation could be minimized thanks to the recycle;
- Methane molar fractions up to 0.9 would be obtained, compared to 0.55 of biogas.

It is important to highlight that a membrane requires a certain ΔP between the product mixture side and the separated components one as driving force to perform a separation. Therefore, the operating pressure should be higher than 1atm to allow hydrogen downstream separation: even if this would involve higher capital and operating costs related to recompression, it would be an advantage at the same time since higher pressure favours the thermodynamics of the Sabatier reaction.

The process described above would be very attractive, since the technologies on membrane processes are evolving very quickly due to their sustainability. For example, polymeric hollow fibers would have good selectivity for hydrogen [64] but should operate at low temperatures due to mechanical resistance problems of polymeric materials: however, the hot product mixture

could be cooled to recover some energy (e.g. for the feed pre-heating) before being sent to the separation section. The main drawback of hollow fibers would be the high ΔP required for their functioning, but Pd-based porous membranes could also be used: stainless steel support showed good performances with only 3 atm pressure difference and ceramic supports have been developed with comparable performances and ΔP=2-3atm [65].

Bibliography

[1] C. Stevens, "Environmental degradation pathways for the breakdown of polydimethylsiloxanes," *J. Inorg. Biochem.*, vol. 69, no. 3, pp. 203–207, Feb. 1998.

[2] N. Höhne *et al.*, "The Paris Agreement: resolving the inconsistency between global goals and national contributions," *Clim. Policy*, vol. 17, no. 1, pp. 16–32, Jan. 2017.

[3] Q. Sun, H. Li, J. Yan, L. Liu, Z. Yu, and X. Yu, "Selection of appropriate biogas upgrading technology-a review of biogas cleaning, upgrading and utilisation," *Renew. Sustain. Energy Rev.*, vol. 51, pp. 521–532, Nov. 2015.

[4] P. Weiland, "Biogas production: Current state and perspectives," *Applied Microbiology and Biotechnology*, vol. 85, no. 4. pp. 849–860, 2010.

[5] A. Petersson and A. Wellinger, "Biogas upgrading technologies-developments and innovations," *IEA Bioenergy*, no. Task 37-Energy from biogas and landfill gas, 2009.

[6] N. Abatzoglou and S. Boivin, "A review of biogas purification processes," *Biofuels, Bioproducts and Biorefining*, vol. 3, no. 1. pp. 42–71, 2009.

[7] G. K. Kafle and S. H. Kim, "Effects of chemical compositions and ensiling on the biogas productivity and degradation rates of agricultural and food processing by-products," *Bioresour. Technol.*, vol. 142, pp. 553–561, Aug. 2013.

[8] M. L. de Souza-Santos and K. Ceribeli, "Technical evaluation of a power generation process consuming municipal solid waste," *Fuel*, vol. 108, pp. 578–585, Jun. 2013.

[9] S. Rasi, J. Läntelä, and J. Rintala, "Upgrading landfill gas using a high pressure water absorption process," *Fuel*, vol. 115, pp. 539–543, Jan. 2014.

[10] S. E. Hosseini and M. A. Wahid, "Development of biogas combustion in combined heat and power generation," *Renew. Sustain. Energy Rev.*, vol. 40, pp. 868–875, Dec. 2014.

[11] R. Muñoz, L. Meier, I. Diaz, and D. Jeison, "A review on the state-of-the-art of physical/chemical and biological technologies for biogas upgrading," *Rev. Environ. Sci. Bio/Technology*, vol. 14, no. 4, pp. 727–759, Dec. 2015.

[12] G. (Grish) Chandra and R. B. Allen, *Organosilicon materials*. .

[13] M. Schweigkofler and R. Niessner, "Removal of siloxanes in biogases," *J. Hazard. Mater.*, vol. 83, no. 3, pp. 183–196, May 2001.

[14] Q. Zhao, E. Leonhardt, C. Macconnell, C. Frear, and S. Chen, "Purification Technologies for Biogas Generated by Anaerobic Digestion," 2010.

[15] W. Yuan and T. J. Bandosz, "Removal of hydrogen sulfide from biogas on sludge-derived adsorbents," *Fuel*, vol. 86, no. 17–18, pp. 2736–2746, Dec. 2007.

[16] Y. Shiratori, T. Oshima, and K. Sasaki, "Feasibility of direct-biogas SOFC," *Int. J. Hydrogen Energy*, vol. 33, no. 21, pp. 6316–6321, Nov. 2008.

[17] "News and Views," *Green Chem.*, vol. 3, no. 5, pp. 2–12, Oct. 2001.

[18] B. C. H. Steele and A. Heinzel, "Materials for fuel-cell technologies," *Nature*, vol. 414, no. 6861, pp. 345–352, Nov. 2001.

[19] M. Duerr, S. Gair, A. Cruden, and J. McDonald, "Hydrogen and electrical energy from organic waste treatment," *Int. J. Hydrogen Energy*, vol. 32, no. 6, pp. 705–709, May 2007.

[20] A. A. Iordanidis, P. N. Kechagiopoulos, S. S. Voutetakis, A. A. Lemonidou, and I. A. Vasalos, "Autothermal sorption-enhanced steam reforming of bio-oil/biogas mixture and energy generation by fuel cells: Concept analysis and process simulation," *Int. J. Hydrogen Energy*, vol. 31, no. 8, pp. 1058–1065, Jul. 2006.

[21] Z.-G. Zhang, G. Xu, X. Chen, K. Honda, and T. Yoshida, "Process development of hydrogenous gas production for PEFC from biogas," *Fuel Process. Technol.*, vol. 85, no. 8–10, pp. 1213–1229, Jul. 2004.

[22] K. Sasaki and Y. Teraoka, "Equilibria in Fuel Cell Gases," *J. Electrochem. Soc.*, vol. 150, no. 7, p. A878, Jul. 2003.

[23] N. Q. Minh, "Ceramic Fuel Cells," *J. Am. Ceram. Soc.*, vol. 76, no. 3, pp. 563–588, Mar. 1993.

[24] J. Staniforth and K. Kendall, “Biogas powering a small tubular solid oxide fuel cell,” *J. Power Sources*, vol. 71, no. 1–2, pp. 275–277, Mar. 1998.
[25] C. M. Finnerty and R. M. Ormerod, “Internal reforming over nickel/zirconia anodes in SOFCS oparating on methane: influence of anode formulation, pre-treatment and operating conditions,” *J. Power Sources*, vol. 86, no. 1–2, pp. 390–394, Mar. 2000.
[26] A. T. Ashcroft *et al.*, “Selective oxidation of methane to synthesis gas using transition metal catalysts,” *Nature*, vol. 344, no. 6264, pp. 319–321, Mar. 1990.
[27] European Biogas Association (EBA), “EBA Statistical Report 2017 just published! - European Biogas AssociationEuropean Biogas Association,” *EBA Statistical Report*, 2017. [Online]. Available: http://european-biogas.eu/2017/12/14/eba-statistical-report-2017-published-soon/. [Accessed: 19-Jul-2018].
[28] O. US EPA, “Understanding Global Warming Potentials.” [Online]. Available: https://www.epa.gov/ghgemissions/understanding-global-warming-potentials. [Accessed: 19-Jul-2018].
[29] O. O. James, A. M. Mesubi, T. C. Ako, and S. Maity, “Increasing carbon utilization in Fischer–Tropsch synthesis using H2-deficient or CO2-rich syngas feeds,” *Fuel Process. Technol.*, vol. 91, no. 2, pp. 136–144, Feb. 2010.
[30] P. S. Roy, J. Song, K. Kim, C. S. Park, and A. S. K. Raju, “CO2 conversion to syngas through the steam-biogas reforming process,” *J. CO2 Util.*, vol. 25, pp. 275–282, May 2018.
[31] J. Xu, W. Zhou, Z. Li, J. Wang, and J. Ma, “Biogas reforming for hydrogen production over nickel and cobalt bimetallic catalysts,” *Int. J. Hydrogen Energy*, vol. 34, no. 16, pp. 6646–6654, Aug. 2009.
[32] P. S. Roy, C. S. Park, A. S. K. Raju, and K. Kim, “Steam-biogas reforming over a metal-foam-coated (Pd–Rh)/(CeZrO2–Al2O3) catalyst compared with pellet type alumina-supported Ru and Ni catalysts,” *J. CO2 Util.*, vol. 12, pp. 12–20, Dec. 2015.
[33] P. S. Roy, N.-K. Park, and K. Kim, “Metal foam-supported Pd–Rh catalyst for steam methane reforming and its application to SOFC fuel processing,” *Int. J. Hydrogen Energy*, vol. 39, no. 9, pp. 4299–4310, Mar. 2014.
[34] X. Chen, J. Jiang, K. Li, S. Tian, and F. Yan, “Energy-efficient biogas reforming process to produce syngas: The enhanced methane conversion by O2,” *Appl. Energy*, vol. 185, pp. 687–697, Jan. 2017.
[35] C. S. Lau, A. Tsolakis, and M. L. Wyszynski, “Biogas upgrade to syn-gas (H2–CO) via dry and oxidative reforming,” *Int. J. Hydrogen Energy*, vol. 36, no. 1, pp. 397–404, Jan. 2011.
[36] V. R. Choudhary and K. C. Mondal, “CO2 reforming of methane combined with steam reforming or partial oxidation of methane to syngas over NdCoO3 perovskite-type mixed metal-oxide catalyst,” *Appl. Energy*, vol. 83, no. 9, pp. 1024–1032, Sep. 2006.
[37] W.-H. Chen and S.-C. Lin, “Characterization of catalytic partial oxidation of methane with carbon dioxide utilization and excess enthalpy recovery,” *Appl. Energy*, vol. 162, pp. 1141–1152, Jan. 2016.
[38] M. Lo Faro, A. Vita, L. Pino, and A. S. Aricò, “Performance evaluation of a solid oxide fuel cell coupled to an external biogas tri-reforming process,” *Fuel Process. Technol.*, vol. 115, pp. 238–245, Nov. 2013.
[39] E. V. Kondratenko, M. Schlüter, M. Baerns, D. Linke, and M. Holena, “Developing catalytic materials for the oxidative coupling of methane through statistical analysis of literature data,” *Catal. Sci. Technol.*, vol. 5, no. 3, pp. 1668–1677, Feb. 2015.
[40] J. H. de (Jan H. Boer and P. W. (Pierce W. Selwood, *Journal of catalysis.* Academic Press.
[41] *Journal für praktische Chemie, Chemiker-Zeitung.* J.A. Barth, 1992.
[42] H. Heinemann and J. J. Carberry, *Catalysis reviews: science and engineering.* M. Dekker.
[43] L. Su *et al.*, “Creating Mesopores in ZSM-5 Zeolite by Alkali Treatment: A New Way to Enhance the Catalytic Performance of Methane Dehydroaromatization on Mo/HZSM-5 Catalysts,” *Catal. Letters*, vol. 91, no. 3/4, pp. 155–167, Dec. 2003.
[44] S. Ma, X. Guo, L. Zhao, S. Scott, and X. Bao, “Recent progress in methane dehydroaromatization: From laboratory curiosities to promising technology,” *J. Energy Chem.*, vol. 22, no. 1, pp. 1–20, Jan. 2013.

[45] D. Ma, Y. Shu, X. Han, X. Liu, Y. Xu, and X. Bao, "Mo/HMCM-22 catalysts for methane dehydroaromatization: A multinuclear MAS NMR study," *J. Phys. Chem. B*, vol. 105, no. 9, pp. 1786–1793, 2001.
[46] I. Y. Hwang *et al.*, "Biocatalytic conversion of methane to methanol as a key step for development of methane-based biorefineries," *J. Microbiol. Biotechnol.*, vol. 24, no. 12, pp. 1597–1605, 2014.
[47] I. Hwang, D. Hur, J. Lee, … C. P.-J. M., and undefined 2015, "Batch conversion of methane to methanol using Methylosinus trichosporium OB3b as biocatalyst," *researchgate.net*.
[48] A. Holmen, "Direct conversion of methane to fuels and chemicals," *Catal. Today*, vol. 142, no. 1–2, pp. 2–8, Apr. 2009.
[49] M. J. da Silva, "Synthesis of methanol from methane: Challenges and advances on the multi-step (syngas) and one-step routes (DMTM)," *Fuel Process. Technol.*, vol. 145, pp. 42–61, May 2016.
[50] S. Murcia-López *et al.*, "Controlled Photocatalytic Oxidation of Methane to Methanol through Surface Modification of Beta Zeolites," *ACS Catal.*, vol. 7, no. 4, pp. 2878–2885, Apr. 2017.
[51] M. Ravi, M. Ranocchiari, and J. A. van Bokhoven, "The Direct Catalytic Oxidation of Methane to Methanol-A Critical Assessment," *Angew. Chemie Int. Ed.*, vol. 56, no. 52, pp. 16464–16483, Dec. 2017.
[52] J. Niesner, D. Jecha, and P. Stehlik, "Biogas upgrading technologies: State of art review in european region," *Chem. Eng. Trans.*, vol. 35, no. June 2016, pp. 517–522, 2013.
[53] R. K. Sinnott, "Coulson & Richardsons Chemical Engineering Design, 4th edition," *Coulson Richardson's Chem. Eng. Ser.*, vol. 6, no. 4, p. 1055, 2005.
[54] F. Beggel, I. J. Nowik, M. Modigell, M. G. Shalygin, V. V. Teplyakov, and V. B. Zenkevitch, "A novel gas purification system for biologically produced gases," *J. Clean. Prod.*, vol. 18, pp. S43–S50, Dec. 2010.
[55] E. Ryckebosch, M. Drouillon, and H. Vervaeren, "Techniques for transformation of biogas to biomethane," *Biomass and Bioenergy*, vol. 35, no. 5, pp. 1633–1645, May 2011.
[56] M. Gupta, I. Coyle, and K. Thambimuthu, "CO 2 Capture Technologies and Opportunities in Canada " Strawman Document for CO 2 capture and Storage (CC&S) Technology Roadmap "."
[57] S. Basu, A. L. Khan, A. Cano-Odena, C. Liu, and I. F. J. Vankelecom, "Membrane-based technologies for biogas separations," *Chem. Soc. Rev.*, vol. 39, no. 2, pp. 750–768, Jan. 2010.
[58] "Transforming biogas into biomethane using membrane technology," *Renew. Sustain. Energy Rev.*, vol. 17, pp. 199–212, Jan. 2013.
[59] "Methanation of carbon dioxide by hydrogen reduction using the Sabatier process in microchannel reactors," *Chem. Eng. Sci.*, vol. 62, no. 4, pp. 1161–1170, Feb. 2007.
[60] S. Rönsch *et al.*, "Review on methanation – From fundamentals to current projects," *Fuel*, vol. 166, pp. 276–296, Feb. 2016.
[61] M. Gregoris and P. Canu, "SVILUPPO DI UN IMPIANTO SPERIMENTALE PER STUDIARE LO STEAM REFORMING DI METANO A BASSI RAPPORTI STEAM TO CARBON," 2014.
[62] G. Garbarino, P. Riani, L. Magistri, and G. Busca, "A study of the methanation of carbon dioxide on Ni/Al2O3 catalysts at atmospheric pressure," *Int. J. Hydrogen Energy*, vol. 39, no. 22, pp. 11557–11565, Jul. 2014.
[63] G. Garbarino *et al.*, "Spectroscopic characterization of Ni/Al2O3 catalytic materials for the steam reforming of renewables," *Appl. Catal. A Gen.*, vol. 452, pp. 163–173, Feb. 2013.
[64] EERC, "Hydrogen Separation Membranes: Technical Brief," no. May, 2010.
[65] E. S. Division, "Hydrogen separation membrane," *Membr. Technol.*, vol. 2000, p. 14, 2000.